Department of Metallurgy and Materials Science
Massachusetts Institute of Technology
Cambridge, Massachusetts

HIGH CONDUCTIVITY - HIGH STRENGTH COPPER ALLOYS PRODUCED FROM RAPIDLY QUENCHED POWDERS

ANNUAL REPORT

February, 1969

To:
International Copper Research Association, Inc.
1271 Avenue of the Americas
New York, New York

Department of Metallurgy and Materials Science
Massachusetts Institute of Technology
Cambridge, Massachusetts

HIGH CONDUCTIVITY - HIGH STRENGTH COPPER ALLOYS PRODUCED FROM RAPIDLY QUENCHED POWDERS

ANNUAL REPORT

February, 1969

To:
International Copper Research Association, Inc.
1271 Avenue of the Americas
New York, New York

INTRODUCTION

High strength copper conductors capable of retaining such strength after exposure at high temperatures continue to be sought on several fronts. Solid solution alloying (also second phase alloying which involves some aspects of solubility in the matrix) inevitably leads to low conductivity values; such alloys, after cold work, are also subject to significant losses of strength on exposure to temperatures above about 400 or 500 degrees C.

One of the more useful alloying approaches calls for the use of alloying elements which are soluble in the liquid phase but are essentially insoluble in the solid state. The copper-zirconium and copper-chromium alloys, with numerous modifications, have shown considerable promise. Unfortunately, the strength values due to alloying are relatively poor, and the alloys depend on high levels of cold work to achieve the desired strength values. Subsequent brazing operations lead to recovery or recrystallization with undesired loss of low temperature strength.

Several new alloy developments, coupled with processing refinements, offer considerable promise for producing high strength alloys, with excellent conductivity, but with high temperature stability very much improved over that of the copper-zirconium and copper-chromium type alloys.

Oxide dispersion strengthened copper alloys, capable of being produced by any one of several processing techniques, have been shown to possess attractive low temperature strength properties, excellent high temperature strength and high temperature stability, and suffer only a relatively small loss of conductivity. The current disadvantages of these alloys are an indicated high cost level, only fair formability, and an inadequate measure of commercial feasibility in terms of desired sections and shapes. There is, however, every reason to believe that the oxide dispersed alloy approach is a practical one, and that commercial feasibility both in terms of cost and manufacturing potential can be demonstrated through proper research and development support.

A more recent approach to this problem is based on the utilization of rapidly quenched powders, the structures of which can be controlled to an extent not possible in the recent past, but now indicated to be capable

of generating mechanical and physical properties not hitherto possible. "Splat cooling", the most rapid of the liquid metal quenching techniques, capable of achieving cooling rates of 10^7 to 10^9 degrees C per second, and "rapid quenching", capable of achieving cooling rates of 10^2 to 10^5 degrees C per second, are described briefly below to establish the basis for the current research program.

In the course of disintegrating liquid metals and alloys into fine droplets, delivering the droplets in the molten state to a suitable quenching substrate, and impacting the liquid droplets to produce relatively thin foils which stick to the substrate, it has been possible to achieve cooling rates of the order of 10^7 to 10^9 degrees C per second. Studies of these structures indicate that it is possible to accomplish one or more of the following important structural modifications:

1. Amorphous structures
2. Microcrystalline structures which are essentially amorphous
3. An exceedingly refined grain size and dendrite size such that dendrites as fine as 0.01 micron can be achieved. By contrast the dendrite size in ingot structures is anywhere between 1000 and 10,000 microns, and can in fact be significantly coarser.
4. Increased solubility of one or more solute components, varying from improvements of a few percent to complete solid solubility across the phase diagram.
5. The generation of nonequilibrium intermetallic compounds
6. Phase distribution and crystal mixtures which are not achievable in conventionally cooled systems
7. Refinement of all excess phase particles to the extent that the particles are submicron in size, and can be utilized for strengthening purposes, for example, as a dispersion.

One can easily speculate over the advantages of achieving structures such as those described above. By increasing solid solubility extensively, one can enhance aging systems, one can produce a variety of dispersion strengthened structures, and one can change the temperatures at which these precipitation phenomena normally occur. By refining the grain size one can expect significant improvements in strength, toughness, and second phase particles distribution. By refining the dendrite size significantly, one can avoid the presence of coarse second phase particles; one can disperse inclusions to the point that they are no longer damaging; one can improve both hot and cold plasticity significantly; and one may become tolerant of significantly larger amounts of both desirable and undesirable second phase particles.

From a commercial point of view, splat cooled foil particles are not desirable for subsequent solid state consolidation. Such fine foils will be reactive with the atmosphere, and would require costly protective systems until the particles are fully densified into a sufficiently pore-free body. It is likely in almost any alloy system that one can achieve major improvements in structure and properties by producing structures which can be achieved at somewhat slower cooling rates than those typical of splat cooling, but rates which are still very much more rapid than those achieved in ingot structures. If one can utilize advantageously the intermediate cooling rates, it would mean that coarser powder particles could be produced; such powders would be cheaper, easier to consolidate, easier to protect, and easier to convert into final product form. This is the area of rapidly quenched coarse powders, and is the method selected for this program to improve, by a significant margin, the copper-zirconium and copper-chromium type alloys.

EXPERIMENTAL APPROACH

To determine the response of copper-zirconium and copper-chromium alloys to quenching rate, alloys containing up to 5 weight percent of each element were prepared and splat cooled to achieve cooling rates of the order of magnitude of 10^7 to 10^9 degrees C per second. In addition, more slowly cooled, gas atomized alloys were received from a commercial source;

this permitted a measure of cooling rate on the structures of these powders. Intermediate cooling rates between these two were achieved by rapid quenching of liquid alloy droplets against a rotating stainless wheel.

Light microscopy, electron transmission microscopy, and X-ray diffraction were utilized to study the structures and to identify the phases.

RESULTS

It was found that the solid solubility of zirconium in copper can be increased significantly by utilizing quenching rates of approximately 10^8 degrees C per second. The solubility of zirconium in copper was found to increase from an equilibrium value of less than 0.1 percent to nearly 1.5 percent. The results are shown in Figure 1. X-ray diffraction studies indicate that the copper lattice is increased from 3.615 Å to about 3.630 Å as a result of the solution of 1.5 percent zirconium in copper.

Studies with the copper- chromium alloys, in the same manner, show that the equilibrium solid solubility of chromium was increased to about 2 percent.

Figure 2 shows the deviation from Vegards' law for the copper - zirconium alloys. There is a negative deviation observed above about 0.6 weight percent zirconium; the first evidence of this deviation is observed with the 2 percent zirconium alloy. These results confirm that the increased zirconium solubility approaches 2 percent zirconium. These solid solubility values are therefore the maximum achievable solubilities; but, as indicated above, practical considerations make it impractical to consider such high cooling rates. Lower cooling rates were studied.

It is of course not essential that significant increases in solubility be achieved in order to produce improved structures and properties. Provided that one can achieve cooling rates of the order of magnitude of about 10^3 to 10^5 degrees C per second, one can produce dendrites as fine as 10 microns. This fine dendritic structure would guarantee a distribution of zirconium and chromium particles of such fineness that one would expect to be able to produce alloys with considerably higher zirconium or chromium

content than is now the practice along with a desired very fine grain size. The fine dispersion of these submicron second phase particles is expected not to detract from a high level of hot and cold plasticity, will guarantee the retention of a very fine grain size on subsequent exposure at high temperatures, and will be a significant asset in achieving high strength values.

With these aims in mind, a relationship, of a preliminary nature, has been attained between average grain size and cooling rate, and is shown in Figure 3. It is expected that more points will become available to establish the slope of this curve more accurately than is now possible on the basis of the existing points. Figure 3 shows that there is a significant improvement in grain size as a result of the rapid solidification. Photomicrographs at 1000X show the change in structure with increased cooling rate in Figure 3.

In the meantime, a series of five alloys ranging from 0.14 to 0.98 percent zirconium were gas atomized, achieving cooling rates estimated to be about 10^3 to 10^4 degrees C per second. X-ray diffraction studies on these powders showed a slight increase in solid solubility of zirconium, as was expected.

These gas atomized powders are currently being exposed at temperatures between 250 and 800 degrees C in an effort to establish the minimum temperature of grain growth as well as for growth of the ultrafine zirconium particles.

Some thin film, transmission electron microscopy has been done on the splat cooled alloys. The studies indicate that for a 2 percent zirconium alloy, viewed at 35,000X, Figure 4A, the largest zirconium particles are only about 0.1 to 0.2 micron diameter. Such fine particles are expected to result in a dispersion hardening effect as well as in grain size stabilization on heating. Figure 4B shows a fine zirconium precipitate which formed as a result of heating of the fine foil under the electron beam. This precipitate results from the supersaturated condition of the splat cooled structure.

SUMMARY

It has been demonstrated that fairly large increases in solid solubility of both zirconium and chromium occur in copper as a result of splat cooling.

These structures can be decomposed to produce an exceedingly fine dispersion of the precipitated phase and should result in both improved strength (at both low and high temperatures) and much improved structural stability at very high temperatures.

At intermediate cooling rates, which can be achieved with coarser, quenched powders, increased solubility is unlikely to be important (except possibly in more complex alloys), but a fine dispersion of zirconium, chromium, and other insoluble elements is achieved. These powders, and the resultant structures, are expected to result in commercially interesting materials.

Submitted by:

Professor Nicholas J. Grant
Mr. Vinod Sarin

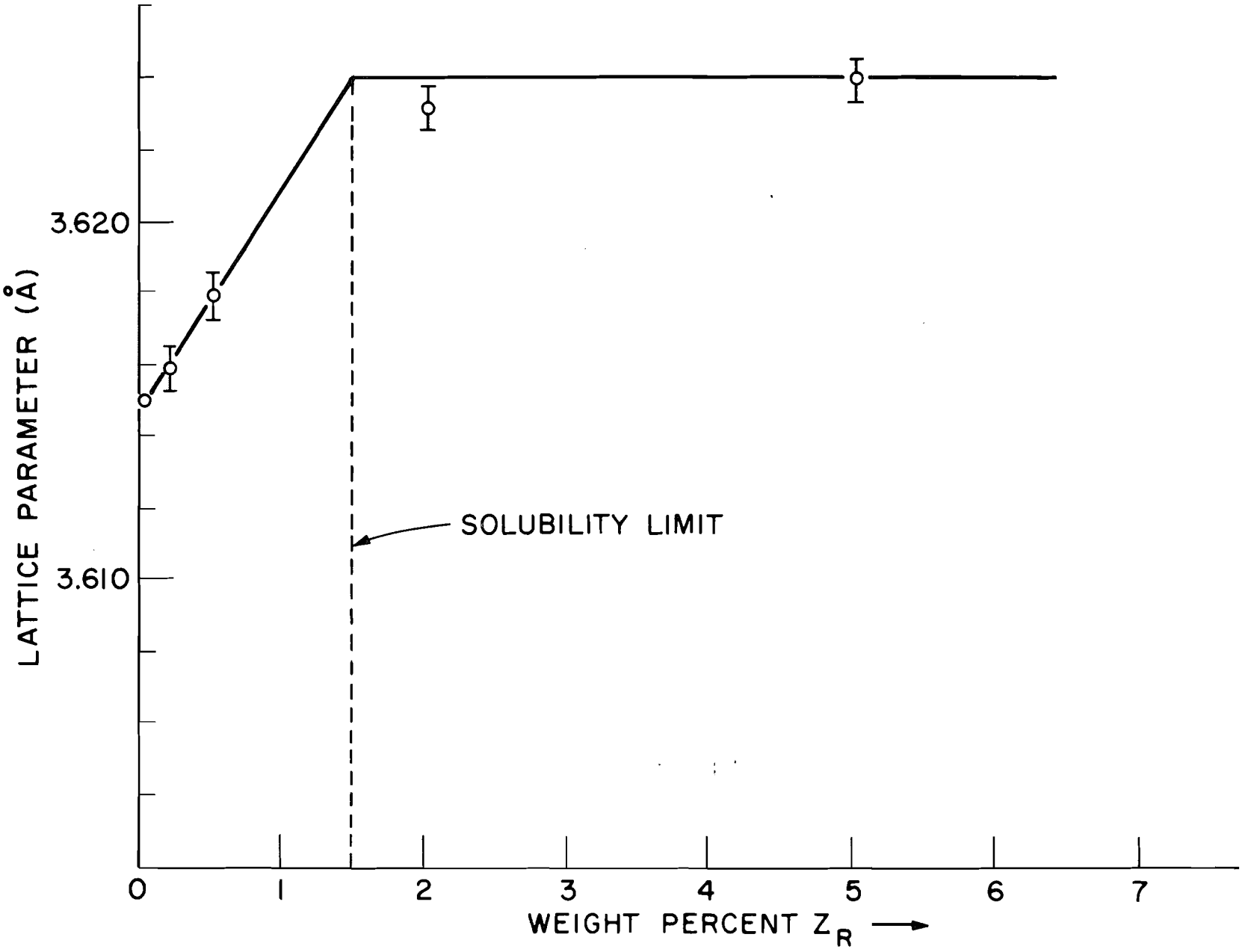

Figure 1. Solubility of zirconium in copper, in terms of lattice parameter change, as a result of cooling rates of about 10^8 degrees C/second.

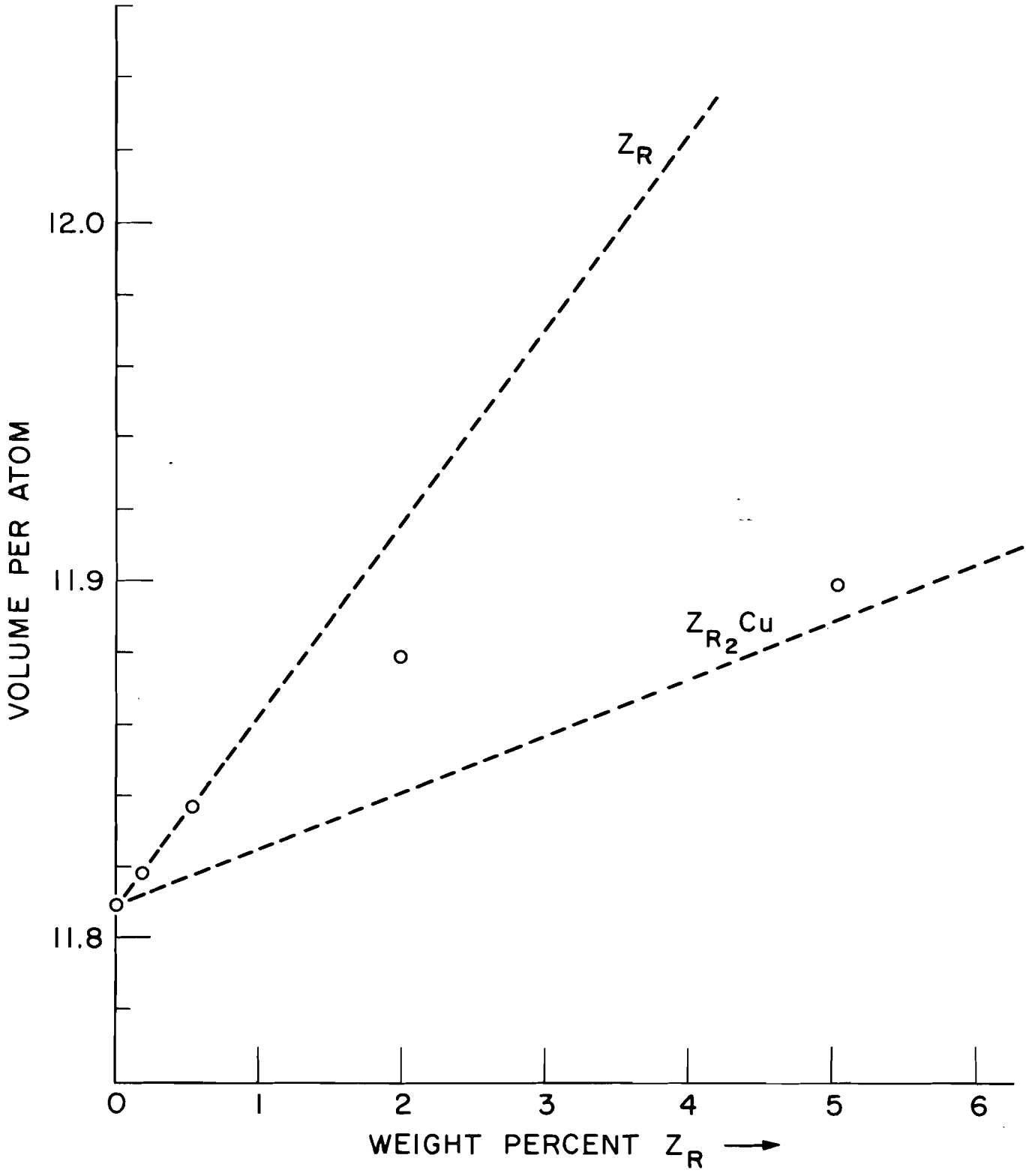

Figure 2. Deviations from Vegards' Law for splat cooled Cu-Zr alloys.

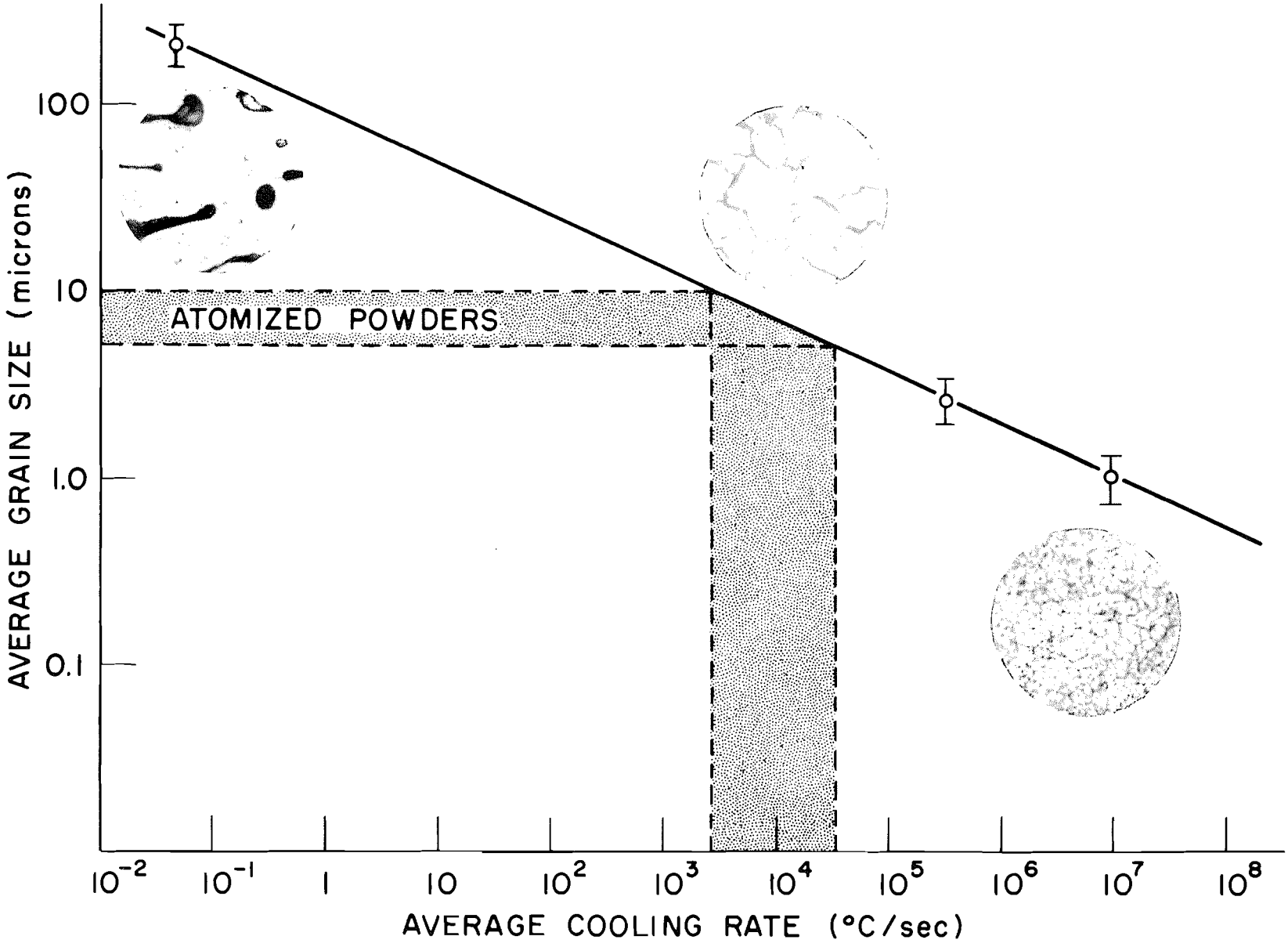

Figure 3. An approximate curve of grain size versus cooling rate for Cu-Zr alloys. Micrographs are at 1000X.

Fig. 4 a

Fig. 4 b

Figure 4. Transmission electron microscopy views of a Cu-2% Zr alloy splat cooled against a copper substrate. 35,000X.
View (a) shows some of the coarser Zr precipitates in the as-quenched condition; view (b) shows evidence of a fine Zr precipitate as a result of heating of the foil in the electron beam.

FINAL REPORT

INCRA Project No. 128C

POWDER METHODS FOR PRODUCTION OF WROUGHT HIGH STRENGTH, HIGH CONDUCTIVITY, THERMALLY STABLE COPPER BASE ALLOYS.

NOVEMBER, 1971

FINAL REPORT

INCRA Project No. 128C

POWDER METHODS FOR PRODUCTION OF WROUGHT HIGH STRENGTH, HIGH CONDUCTIVITY, THERMALLY STABLE COPPER BASE ALLOYS.

NOVEMBER, 1971

Submitted by

Professor Nicholas J. Grant
Dr. Vinod K. Sarin

Department of Metallurgy and Materials Science
Massachusetts Institute of Technology
Cambridge, Massachusetts

ABSTRACT

COPPER-ZIRCONIUM AND COPPER-ZIRCONIUM-CHROMIUM ALLOYS PRODUCED FROM RAPIDLY QUENCHED POWDERS

by

VINOD KUMAR SARIN

Submitted to the Department of Metallurgy and Materials Science on October 14th, 1971 in partial fulfillment of the requirement for the degree of Doctor of Science.

The production of alloys by means of ingot technology leads to micro and macro segregation, separation of phases and impurities, often into large, brittle particles, and coarse grain size. Alloy development is frequently restricted because of the coarseness of the structure and the resultant imposed limitations on hot and cold plasticity. One ready means of avoiding these problems is to produce the alloy in powder or pellet form; this permits attainment of high cooling rates in the liquid and solid, minimizes segregation, alters phase separation and distribution advantageously, and results in significantly finer structures. The powders utilized to produce wrought shapes may be much coarser than press-and-sinter powders, leading to important processing economies without sacrifice of structure refinement.

The alloy systems Cu-Zr and Cu-Zr-Cr were selected for the present study; these are high conductivity, high strength alloys of commercial interest. Various cooling rates (10^2 to 10^5 °C per sec.), or powder sizes, were examined to delineate the interplay between structure and properties, and to search out the most commercially feasible and economical processes. Vacuum cast alloys were steam or nitrogen atomized to produce the necessary powders. These powders were then cleaned, canned and hot extruded to produce bar stocks for evaluation and testing. A thorough examination was conducted to understand the kinetics of precipitation and various thermomechanical treatments, and their effects on room temperature and high temperature

properties.

Thermomechanical treatments were found necessary to optimize properties. Intermediate annealing temperature during a thermomechanical treatment was shown to be a major consideration in determining the room temperature and creep-rupture strength of the alloys. The combined effects of solution anneal, cold work and precipitation hardening generally yielded the best properties for both Cu-Zr and Cu-Zr-Cr alloys. Pronounced improvements in precipitation hardening obtained by the addition of chromium to Cu-Zr alloys resulted in alloys with the best overall properties.

Thesis Supervisor: Nicholas J. Grant

Director of Center
for Materials Science
and Engineering, and
Professor of Metallurgy.

TABLE OF CONTENTS

LIST OF FIGURES

LIST OF TABLES

ACKNOWLEDGEMENTS

The author wishes to express his gratitude to Professor Nicholas J. Grant his thesis advisor, without whose help this work could not have been accomplished. Professor R.M.N. Pelloux's guidance is also greatly appreciated. Thanks are also due to the International Copper Research Association for financial support, and special thanks to Dr. Schettky for his encouraging interest.

Stimulating discussions with members of the high temperature metallurgy group were helpful, during the course of this investigation. P. Keller's consistently helpful and understanding attitude is much appreciated.

The author is grateful to Elaine Wainwright for her patience, understanding and excellent typing of the final draft of the thesis. Finally, appreciation for his wife Rani's patience and assistance in proof reading, many small details, and for typing the rough draft of the thesis.

1. INTRODUCTION

High strength copper alloys, capable of retaining their strength after exposure at high temperatures continue to be sought on several fronts. Solid solution alloying (also second phase alloying which involves some aspects of solubility in the matrix) inevitably leads to low electrical conductivity; such alloys, after cold work, are also subject to significant loss of strength on exposure to temperatures above 400°C.

One of the more useful alloying techniques has been the use of elements which are soluble in the liquid phase but have very low solubility in the solid state. In this respect, copper-zirconium and copper-chromium alloys, with numerous modifications, have shown considerable promise. Unfortunately, the strength obtained due to alloying is relatively poor, and the alloys depend on high levels of cold work to achieve the desired strength values. Subsequent brazing operations lead to recovery and recrystallization with undesirable loss of low temperature strength.

Several new alloy developments coupled with processing refinements, offer considerable promise for producing high strength alloys with excellent electrical conductivity, but with temperature stability very much improved over that of the present ingot originated copper-zirconium and copper-chromium alloys.

Oxide dispersion strengthened copper alloys, capable of being

produced by any one of several processing techniques, have been shown to possess attractive low temperature strength, excellent high temperature strength and stability, and suffer only a relatively small loss of electrical conductivity. The current disadvantages of these alloys are: an indicated high cost level, only fair formability, and an inadequate measure of commercial feasibility in terms of desired section sizes and shapes.

A more recent approach is based on the utilization of techniques for the rapid quenching of alloys from the liquid state. Splat cooling, or atomization of fine liquid metal droplets, has demonstrated an ability to control structure, and therefore properties, in ways and to a degree not previously possible by alternate casting methods.

Splat cooling, the most rapid of the liquid metal quenching techniques, is capable of achieving cooling rates of 10^6 to 10^9 ^oC per sec.; certain atomization techniques are capable of cooling rates of 10^2 to 10^5 ^oC per sec.; these are being employed increasingly to control structure and therefore properties in various alloy systems. From a commercial point of view, splat cooled foils (for example, obtained with the shock tube method, with cooling rates of 10^7 to 10^9 ^oC per sec.) are not suitable for subsequent solid state consolidation. Studies on these structures indicate that it is possible to accomplish several important structural modifications, such as amporphous and microcrystalline structures, an exceedingly refined dendrite size,

vastly increased solubilities, metastable phases, refinement of excess phase particles to submicron size, and decreased grain size.

The advantages of achieving such structures can be easily documented. By extensively increasing solid solubility, enhancement of aging systems can be obtained, and a variety of dispersion strengthened structures can be produced. Refinement of grain size can significantly improve strength, toughness and second phase particle distribution. By increasing dendrite size, coarse second phase particles can be avoided; inclusions can be dispersed to a point where they are no longer damaging; both hot and cold plasticity are considerably improved; and significantly larger amounts of both desirable and undesirable second phase particles can be tolerated.

As mentioned before, fine splat foils formed through such rapid solidification rates (10^7 to 10^9 °C per sec.) are of limited commercial interest, from a practical point of view. On the other hand, somewhat slower cooling rates (10^2 to 10^5 °C per sec.), which are still very much faster than those achieved in ingot structures (10^{-3} to 10^{-1} °C per sec.), be means of selected atomization techniques, can produce powders suitable for consolidation and conversion to yield improved structures and properties.

Solidification processes are primarily responsible for segregation and phase separation. The slower the solidification process, the greater the degree of segregation and separation, the coarser the grain size, and the coarser the excess phases. This damage to struc-

ture manifests itself to a greater degree the larger the ingot or casting. Prevention or minimization of such casting faults would improve hot and cold workability, enhance mechanical properties, decrease directionality effects, permit utilization of higher alloy content, and perhaps increase the reproductibility of properties.

With the well-known advantages of fine dendrite and grain size, and the as yet not completely realized but known benefits to strength of fine particle dispersions, the technique of atomization was selected for this program. The alloy systems copper-zirconium and copper-zirconium-chromium were selected for this study; these are high conductivity, high strength alloys of commercial interest. Various cooling rates were examined to delineate the interplay between structure and properties, and to search out the most commercially feasible and economical processes. A thorough examination was conducted to understand the kinetics of solution treatments, precipitation reactions, and various thermomechanical treatments (TMT) on the extruded powders, and their effects on room temperature and high temperature properties.

The aim of the program was to produce high strength, high electrical conductivity copper alloys, which would have excellent hot and cold working capability, while exhibiting highly improved structural stability in the temperature range of 500°C to 750°C compared to present commercial alloys.

II. PHASE DIAGRAMS

A. Copper-Zirconium

Although the copper-zirconium phase diagram is reasonable well established (Figure 1a), there is still disagreement about the copper rich portion. Recently Saarivirta[2], Zwicker[3] and Showak[4] have reported the maximum limit of solubility of zirconium in copper as 0.15, 0.11 and 0.24% by weight, respectively, with a room temperature solubility between 0.01 and 0.02%. Figure 1b shows the copper-rich portion of the copper-zirconium phase diagram, after Saarivirta, based on microstructural examination. The dashed line is the result obtained by Showak, using metallographic and electrical resistivity measurements.

The first intermediate phase has been reported as Cu_3Zr[(1,3)], however, almost no data are available to substantiate this. Hansen[1] has suggested that Cu_4Zr might be more appropriate. Investigations by Donachie[5], using electron microprobe analysis supplemented by metallographic and thermal analysis, have suggested Cu_4Zr. Beck[6], using electron microscopy, established Cu_3Zr as the correct composition and reported its crystal structure to be of complex orthorhombic symmetry.

Donachie[5] reported the maximum solubility limit as 0.17% zirconium by weight. His solubility value corresponds closely to Saarivirta's (0.15%), but is substantially lower than that reported by Showak (0.24%). Donachie fixed the eutectic temperature at 970°C, which is similar to the values of 965°C reported by Hansen and 980°C reported by Saarivirta

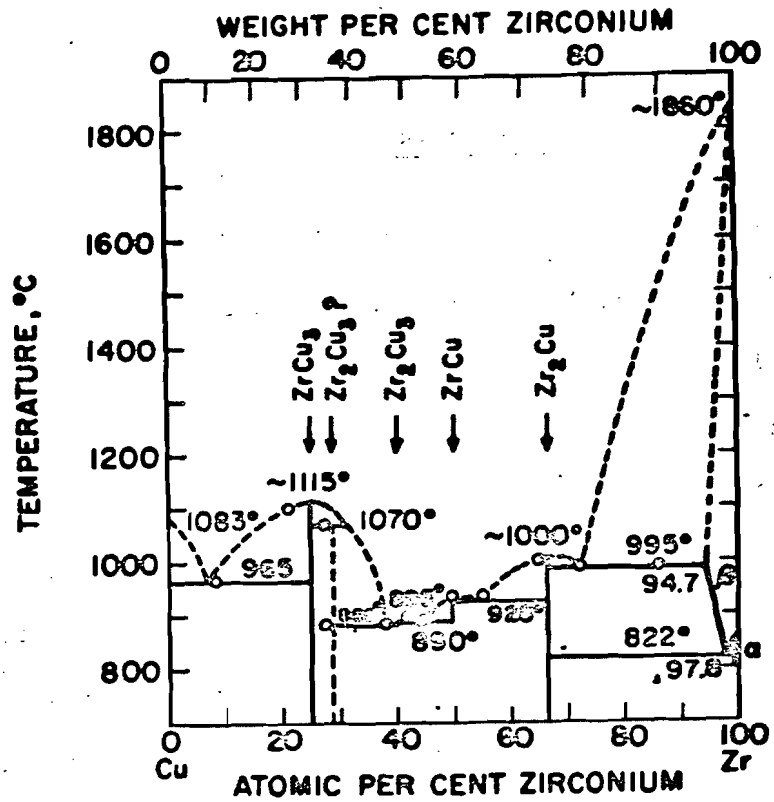

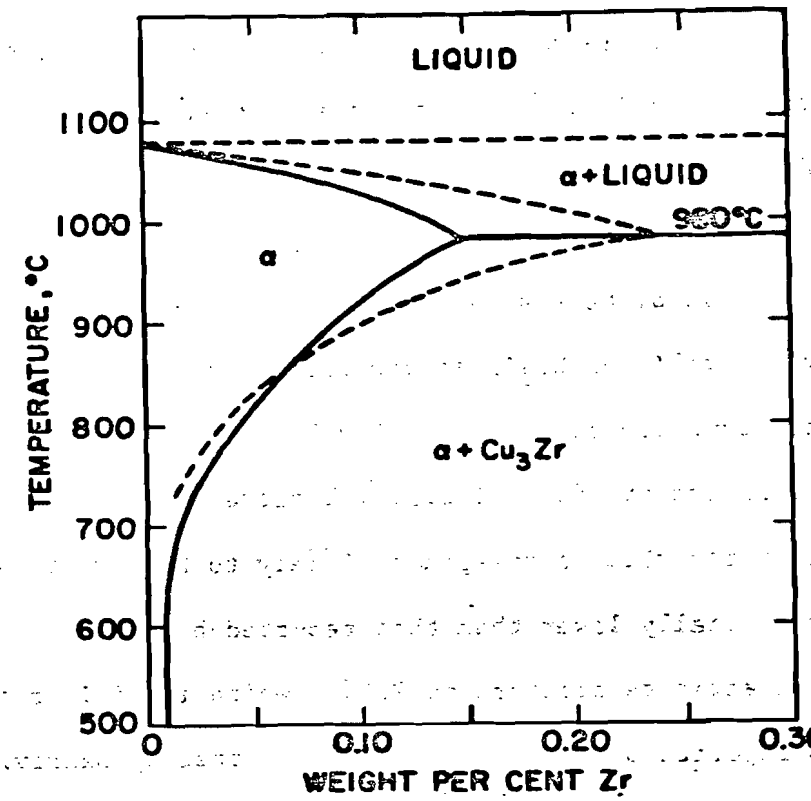

Figure 1. Phase diagrams of the binary system Cu-Zr.
(a) Cu-Zr diagram after Hansen[1]
(b) Copper rich section of Cu-Zr diagram[2,4]

and Showak. The eutectic composition has been cited by Allibone et al[7], Pogodin et al[8], and Raub et al[9], as 12.5, 12.9, and 13.7% by weight zirconium, respectively, while a microprobe trace across the eutectic lamellae by Danachie suggests an average composition of 13.5 wt. % Zr.

B. Copper-Zirconium-Chromium

Hardly any pertinent data is available on the ternary copper-zirconium-chromium phase diagram.

Zakharov et al[10,11] studied this ternary system up to 3.5% each of zirconium and chromium (Figure 2a). They found that additions of zirconium markedly increased the solubility of chromium in copper, while additions of chromium had little influence on the solubility of zirconium. The existance of a quasi-binary eutectic type system between chromium and Cr_2Zr was reported, with a solubility limit at the eutectic temperature of 1020°C corresponding to 2.3% Cr_2Zr (1.1% Cr and 1.2% Zr). All these results were obtained through microscopic examination, thermal analysis and microhardness measurements.

Mizuno's investigations[12] disagreed with the solubility limit of wt. % of Zr in the ternary system of Zakhrov et al and reported a maximum stability of 0.2%. He could not detect the presence of Cr_2Zr. Further work by Kawakatsu et al[13] (Figure 2b) also questioned the existance of Cr_2Zr. These results are a bit confusing as the presence of Cr_2Zr has been reported in the binary zirconium-chromium. Domagala

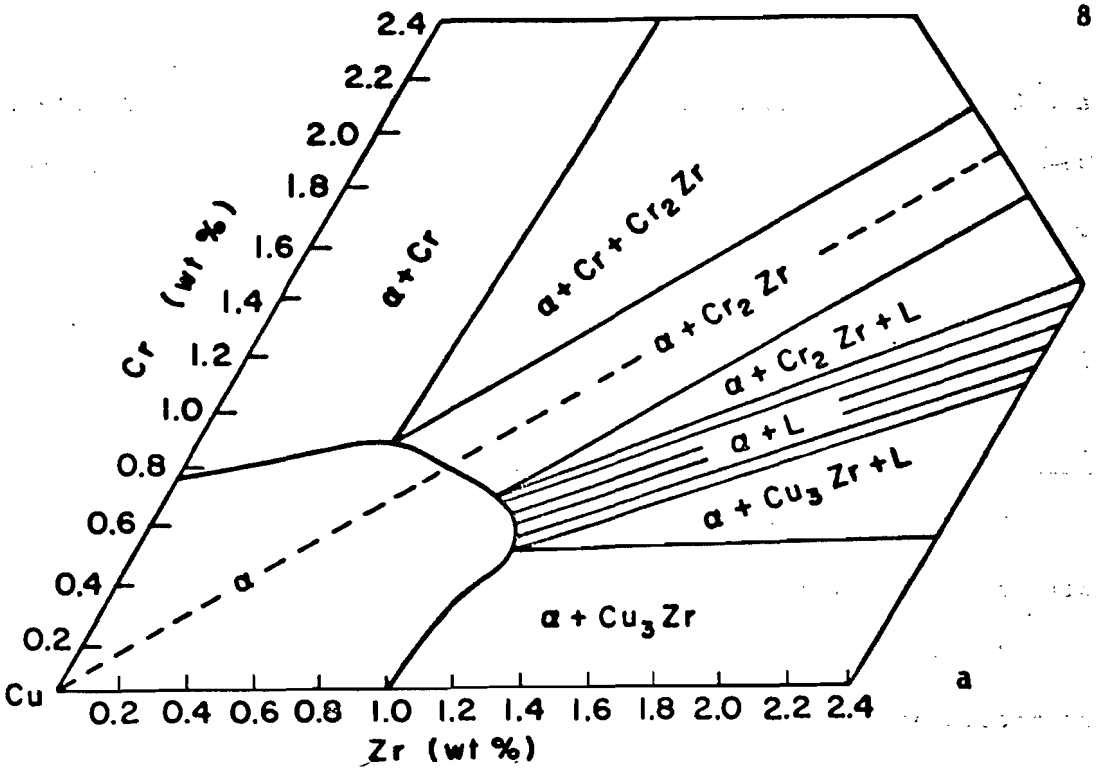

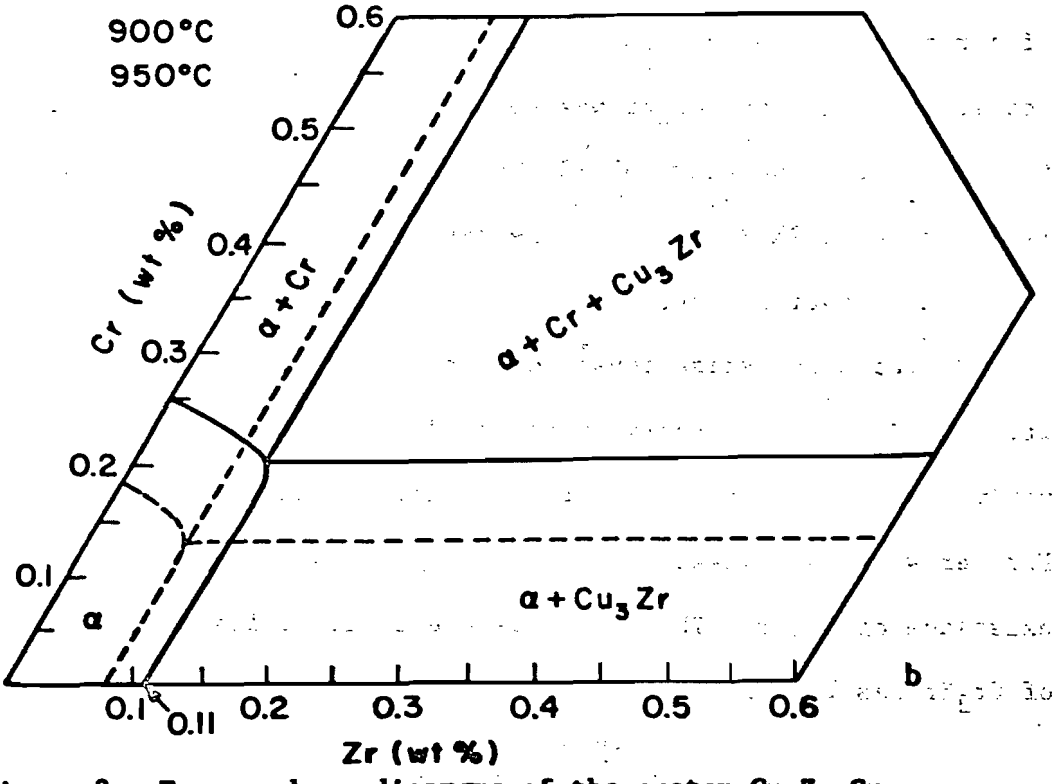

Figure 2. Tenary phase diagrams of the system Cu-Zr-Cr.
(a) The copper rich angle after Zakharov[10]
(b) The copper rich angle after Kawakatsu[13]

et al[14] reported an intermediate phase Cr_2Zr with a close packed hexagonal structure.

III. PREVIOUS WORK

A. Splat Cooling

The development of techniques for the rapid quenching of alloys from the liquid state has resulted in a unique opportunity to create new and unusual phases in various alloy systems. Although the use of high cooling rates to retain metastable phases from the melt had been investigated by Falkenhagen et al[15], a systematic examination of alloy systems in a nonequilibrium state had to await the development of the shock tube quenching technique by Duwez and co-workers[16]. Since then hundreds of investigations have been conducted; review articles by Duwez et al[17,18] and Giessen[19] extensively cover this field.

It has been found that the metastable extention of the solid solubility limit of zirconium in copper can be vastly increased by utilizing the shock tube quenching technique, with cooling rates in the range of 10^7 - 10^9 °C per sec. Studies by Ray[20] showed that the solubility of zirconium in copper could be increased from an equilibrium value of 0.01% to approximately 30 wt. % Zr, at room temperature. The results he obtained are shown in Table 1.

A measure of the unexpected stability of this supersatured solid solution was obvious, when X-ray analysis and lattice parameter measurements showed no change in structure of the splat cooled fcc "α" solid solutions (up to 20 wt. % Zr), after annealing the splat foils for one hour at 400°C. Annealing at higher temperatures for

Table 1

Phases Obtained in Splat Cooled Cu-Zr Alloys

Chemical Comp. Atomic %	Equilibrium Phases	Phases Present at R.T.	Lattice Parameter
2	Cu+Cu_3Zr	α (100% s.s.)	3.621
5	Cu+Cu_3Zr	α (100% s.s.)	3.628
7	Cu+Cu_3Zr	α (100% s.s.)	3.634
12	Cu+Cu_3Zr	α (100% s.s.)	3.64
15	Cu+Cu_3Zr	α (100% s.s.)	3.64
20	Cu+Cu_3Zr *	α (100% s.s.)	
25	Cu+Cu_3Zr *	α (100% s.s.)	

* Lattice parameters not measured owing to excessive broadening of diffraction lines.

an hour or more resulted in grain growth and subsequent decomposition to equilibrium phases. Amorphous and microcrystalline structures have been reported[20,21] for high zirconium contents (up to 35 wt. %). These would of course result in extremely homogenous and fine structures (grain and dendrite size) upon decomposition.

Dendrite arm spacing is known to be a function of the degree of supercooling[22]; and, since the extent of supercooling depends on the cooling rate, one can expect a relationship between dendrite size and cooling rate. Experimental evidence available indicates that dendrite arm spacing in cast Al alloys is influenced only by cooling rate (or "local solidification time"). Bower et al[23] plotted data obtained from a number of investigations with aluminum alloys, showing the relationship between secondary arm spacing "d" and local solidification time

"θ_f". Of the wide range of solidification rates examined, the dendrite arm spacing measurements were found to correlate linearly with "θ_f" when plotted on log-log coordinates.

$$d = 7.5\ \theta_f^{0.39}$$

This relationship was confirmed for a number of aluminum alloys over a wide range of cooling rates by Matyja et al[24]. They plotted dendrite arm spacing as a function of cooling rate, and observed a similar straight line relationship having a slope of 0.32.

B. Copper-Zirconium Alloys

No information is available in the literature with reference to the specific production of wrought copper-zirconium alloys, through powder metallurgical techniques. There have, however, been numerous investigations on such alloys produced through conventional ingot techniques.

Although early work on the copper-zirconium system had indicated that zirconium improves the resistance to softening at elevated temperatures[7,9,25], the alloy was not used to any appreciable extent until recently. As a result of increased demand for copper base alloys withstanding higher operating stresses and temperature, or capable of withstanding short times at high brazing temperatures, copper-zirconium alloys are being used more and more, and are presently commercially available[26,27].

Although zirconium additions to copper produce an age hardening effect, response to precipitation hardening (unlike copper-chromium alloys) is slight, and mechanical properties are developed primarily by

cold working[28]. Solution annealing imparts to the copper-zirconium alloys their resistance to softening, up to 550°C. However, this process results in low electrical conductivity (52-72% IACS), as zirconium goes into solution, and low temperature aging is required to precipitate the zirconium and thus bring the electrical conductivity up to 85-95% IACS[2,7,9]. The effect of aging temperature on electrical conductivity for a range of zirconium contents (0.003 to 0.23 wt. %) was studied by Saarivirta[2]. He observed that aging temperatures in the range between 500 to 600°C yielded the highest conductivity values in all cases.

Lynch[29] has very thoroughly studied the effect of various solution treatments, cold work and aging cycles on the physical and mechanical properties of alloys with 0.13 to 0.20 wt. % zirconium. He found that material which was solution annealed, quenched, cold worked, aged, and then cold worked, gave higher tensile and yield strengths as compared with material given an equivalent amount of cold reduction, but with an aging treatment as a final operation. Dooley et al[30] found that a significant increase in tensile strength, hardness and conductivity were obtained when material was given a precipitation treatment before and after cold work. This double-aging treatment was found also to effectively improve creep resistance of the material.

To obtain optimum mechanical and physical properties of copper-zirconium alloys, as determined by Saarivirta[2], it is necessary to put

0.13 to 0.15 wt. % Zr. into solid solution. This requires solution-annealing at 950 to 980°C. However, heating at these high temperatures was found to give excessive non-uniform grain growth. To avoid this, Saarivirta et al[31] selected 900°C as a practical solution-annealing temperature since annealing at this temperature puts most of the zirconium into solid-solution and does not create a serious grain growth problem. Based on the fact that solution and diffusion of zirconium occurs very rapidly between 900-980°C, Lynch[29] suggested that it is only necessary to insure complete heating to temperature, prior to quenching. Dooley et al[30] examined a wide range of solution-annealing temperatures; their results clearly indicated 825 to 875°C as the best range for solution-treatment. Both improved room temperature mechanical properties and a marked minimum in the amount and rate of creep confirmed this.

Hodge[32] reports that additions of zirconium to copper (in amounts less than 0.12%) have little effect on the softening temperature, while larger additions cause the softening temperature of the alloy, cold rolled to 50% reduction, to rise rapidly from 300°C with 0.12% zirconium, to 500°C with 0.18% zirconium. These determinations were made after half hour exposure at temperature. Saarivirta[2] disagrees with these results as he found a considerable increase in softening temperature with as low an addition as 0.003% zirconium. A maximum softening temperature of 580°C was obtained with 0.13% zirconium in this study. This suggests that zirconium contents above 0.13% have no further

effect on the softening temperature of these alloys. Mizuno[12] came to a similar conclusion working with copper alloys containing 1 to 2 wt. % Zr.

Saarivirta[33] has shown that grain size decreases rapidly with increasing zirconium content. Working with compositions ranging from 0.13 to 1.11 wt. % Zr, he found that with the higher zirconium contents (0.5 wt. % and above) grain growth was almost completely retarded even up to 950°C. This suggests the benefits of higher zirconium contents since, as mentioned before, high temperature solution-annealing, for the lower composition alloys, tends to result in excessively large and non-uniform grains.

In the higher zirconium content alloys (0.19 to 0.74%), despite undissolved particles of the intermediate phase Cu_3Zr throughout the grain and grain boundaries, the alloys did not become anisotropic; the mechanical properties remained almost the same longitudinally or transversely to the rolling direction regardless of the zirconium content[33]. However, Saarivirta found that alloys containing 1.11% zirconium had inferior cold workability compared to the other alloy compositions. It appears from these observations that the zirconium content should be at least 0.35 wt. % to obtain the desirable combination of small and uniform grain size, along with optimum mechanical and physical properties.

Sohl et al[34] studied the softening behaviour of dilute copper-zirconium alloys (with small amounts of magnesium), employing X-rays and electron microscopy. They reported that the primary factor affecting

softening was the amount of zirconium that remains in solid solution. This dissolved zirconium was believed to segregate to noncoincident grain boundaries, and hence to retard their motion. When softening occurred, certain special coincident boundaries, those satisfying the Kronberg-Wilson orientation relationship, moved preferentially.

Kronberg and Wilson[35] pointed out that for certain specific orientations a certain fraction of atoms on one side of the boundary, occupy positions which correspond with atom positions for the extended lattice from the other side. These boundaries are referred to as KW (Kronberg-Wilson) high coincidence boundaries. The highest possible coincidence is a boundary 70.5° <110>, which puts one out of three atoms in registry across it. The fact that certain lattice lines extend through the boundary suggests that such boundaries are characterized by a relatively good atomic fit. Hence, the degree of solute segregation to such a boundary can be expected to be slight, causing high mobility of such boundaries as solute atoms do not hinder their motion.

Sohl et al observed numerous instances of very straight coincidence boundaries in the softened material. Hence they state that upon initial cold work, zirconium atoms form atmospheres along the dislocation lines, thus hindering their motion and retarding any recovery or polygonization stages. If a recrystallized grain containing random boundaries was nucleated, the boundary would absorb the solute atmospheres associated with the dislocations which were removed. As the solute concentration at the boundary increases, boundary motion would become slower and

eventually cease. If a portion of the boundary was of a KW orientation, it would continue to move after the motion of the random boundaries had stopped. This phenomenon was not observed below 500°C, indicating no nucleation of recrystallized grains or that the driving force was not enough to move even KW type boundaries.

Observation of particles only after extremes of time and temperature, plus the fact that they were not found to have a large interaction with the boundaries, led them to the conclusion that particle formation was not the significant factor in retarding the softening of these dilute copper-zirconium alloys.

Suzuki et al[36] observed heterogenous precipitation of Cu_3Zr in lenticular and platelet form after aging for one hour at 400°C in copper-zirconium alloys. On aging for one hour at 500°C, which yields the maximum hardness value, a particle size between 500 and 600 Å was observed. Higher temperatures yielded extremely coarse, non-uniform and localized precipitation of Cu_3Zr. The lengthwise direction of the platelets of Cu_3Zr was found to be perpendicular to the <111> directions of the matrix and growing in the {111} planes. On the other hand, the lengthwise direction of the lenticular precipitates was parallel to the (111) faces with an incline to the (110) planes of the matrix.

Unlike Suzuki et al[36], Henmi et al[37] failed to observe any precipitation of Cu_3Zr below 500°C. After 10 seconds at 750°C no precipitates were still observed; however, particles of 0.5 and 0.1μ in diameter were observed after 10 seconds at 800 and 900°C, respecti-

vely. Since zirconium atoms are 25% larger than copper atoms, incoherent particles occur in the initial stages of precipitation, hence accounting for the absence of elastic fields in the later stages of precipitation.

C. Copper-Zirconium-Chromium Alloys

The use of a third element with zirconium appear to denote the more promising trend in the development of copper-zirconium alloys. Combinations of zirconium-chromium, zirconium-hafnium, and zirconium-arsenic have been investigated.

Tarora et al[38] first reported some results on the mechanical properties and electrical resistivity of copper-zirconium-chromium alloys but their properties were more comprehensively studied by Mizuno[12]. He found that the recrystallization termperature and precipitation hardenability of copper-chromium alloys was improved by adding small amounts of zirconium. The hardness of copper containing fairly large amounts of zirconium (1 to 2 wt. %) is improved by cold working after solution annealing, but the recrystallization temperature is not raised by the increasing amounts of zirconium; rather an overaging phenomenon starts rapidly on these alloys[2,12]. On the contrary, the copper-chromium alloys containing the same amounts of zirconium have a high strength and excellent heat resistant characteristics after heat treatment. From changes of electrical resistivity of the solution treated materials during heating and cooling from room-temperature to 700°C, Mizuno suggests an optimum composition of 0.2 - 0.6 wt. % Zr and 0.5 wt. % Cr.

Suzuki et al[39,40] studied copper-high zirconium-high chromium containing 0.73-1.46 wt. % Zr and 0.77 to 1.93 wt. % Cr. They found the temperatures of 950 and 450°C to be best suited for solution-treatment and aging, respectively. Although the electrical conductivity of these alloys is somewhat lower than that of the copper-zirconium type alloys, they found that conductivity increased remarkably by prolonged aging, affecting almost no reduction in strength. Further work by these authors[13] on alloys containing 0.5% zirconium and various amounts of chromium showed that the properties of these alloys were little affected by composition changes. They found the optimum composition of the alloys showing high strength and electrical conductivity was in the range of about 0.5 to 0.8% Zr and 0.5 to 1.2% Cr. The superior strength of the copper-zirconium-chromium alloy over the copper-zirconium and copper-chromium can be attributed to the increased solid-solubility of chromium in these alloys (Figure 2).

Studying the precipitation and recrystallization kinetics of copper-zirconium-chromium alloys, Suzuki et al[36] found that under the same aging condition, precipitation of Cu_3Zr and Cr was finer and more densely distributed than the individual precipitates in each binary (Cu-Zr and Cu-Cr). They attributed the higher strength of the ternary alloy to this. The sequence of precipitation in the ternary alloy was found to correspond to that in the binary's, with Cu_3Zr precipitating heterogeneously while Cr was found to precipitate homogeneously. No evidence of Cr_2Zr was reported. In the cold-worked state, as in the

case of copper-zirconium alloys, the precipitates of Cu_3Zr were found to stabilize the worked structure owing to preferential precipitation on cell walls.

Work by Hemmi et al[37] showed that the presence of chromium and zirconium atoms in the copper solid solution retarded the recovery, recrystallization and precipitation in copper-zirconium-chromium alloys. They felt that as recovery and recrystallization result from dislocation climb and glide, these were retarded by: 1) the apparent locking of dislocation due to the presence of chromium or zirconium, or both, and 2) the reduction in self-diffusivity of the copper in the solid-solution due to the presence of chromium, or zirconium, or both. From this retardation of recovery and recrystallization in the ternary alloy, they predicted that the diffusion coefficient of chromium, or zirconium, or both, is low.

Although hardening was obtained after aging the copper-zirconium-chromium alloys for one hour at 400°C, no precipitates were detected. Hemmi[37] felt that this may correspond to the phenomena known as "low temperature anneal hardening." On aging at 550°C, the alloy recovered, local recrystallization began, and the density of dislocations decreased, but still no precipitation occured. Recrystallization and softening were observed after two hours at 600°C. It was in this stage that they first observed preciptates. After two hours aging at 700°C, precipitate particles 0.05 to 0.5 micron in diameter were observed, selected area diffraction revealed their formation in a <112> alignment. They could

not reveal the presence of the precipitates through electron diffraction. Henmi et al assumed that recrystallization was due to subgrain coalescence, after Li[41]. Subgrain coalescence occurs by the disappearance of common boundaries into intersecting boundaries around the subgrains. Bourelier et al[42] observed that some isolated dislocations resulting from the sub-boundary decomposition migrated to outer boundaries of the new grains. The curvature in the shape of such isolated dislocations indicates the beginning stage of boundary migration. In pure copper, moving dislocations can run through the grain. Lucke et al[43] feel that the energy of disappearing boundaries which provides the motive force in subgrain coalescence, can be assumed to be very low. In copper-zirconium-chromium alloys, aged for two hours at 700°C, fine precipitation in the grains inhibits the movement of dislocations, resulting in the formation of dislocation pile-ups.

Grain growth at 700°C, especially in copper-zirconium-chromium and copper-chromium alloys, was observed to be much slower than in other copper alloys[37]. This was attributed to the high binding energy between the alloy boundaries and chromium or zirconium, or both. Henmi et al, through electron microscopy, could not fully account for changes in recrystallization in these alloys, either by precipitates or solute atoms. However, it has been suggested that solute atom clusters which are undetectable, even by electron microscopy, may be formed on the cell walls on grain boudaries and thus supress grain boundary movement[44,45,46]. As Henmi et al did not observe any precipitate particles in the sub-boun-

daries in the initial stage of aging in copper-zirconium-chromium alloy, they concluded that no solute clusters were formed on the sub-boundaries or grain boundaries in this alloy.

IV. PLAN OF WORK

The major goal of this research was to develop high electircal conductivity, high strength (both at room temperature and elevated temperature) alloys of commercial value. The technique for the production of wrought alloys through rapidly quenched powders was selected, and investigated from the following standpoints:

a. effect of various solidification rates on structure, to determine the most commercially feasible and economical range;

b. effect of initial powder size on the properties of the wrought alloys;

c. optimization of properties through cold work, thermomechanical treatments and precipitation hardening, or any combination of these.

The experimental work used to achieve the above, can be summarized briefly as follows:

A. To delineate the structure-property interplay, the following quenching conditions were examined:

1. Inert atmosphere shock tube splat cooling (10^7-10^9 °C per sec.).
2. Splat cooling in air against a rotating copper disc, and into liquid nitrogen (10^5-10^6 °C per sec.).
3. Steam atomization (10^4-10^5 °C per sec.).
4. Nitrogen gas atomization (10^2-10^4 °C per sec.).
5. Cast Ingots (10^{-2} to 10^{-1} °C per sec.).

B. Processing of powder to obtain wrought products for evaluation

of structures and properties.

1. Reduction treatments.
2. Assembly of reduced powders into air tight billets for extrusion.
3. Hot extrusion of copper billets into rods.

C. Evaluation of extruded rods.

1. a. Physical soundness; b. Chemical analysis; c. Metallographic analysis, particle extraction and analysis.
2. Room temperature tensile properties, X-ray diffraction, room temperature hardness versus annealing treatment, for each alloy.
3. Stress-rupture properties.
4. Electrical resistivity measurements.

D. Precipitation and thermomechanical treatments on the extruded rods, to obtain desired properties.

1. Investigation of several precipitation and thermomechanical treatments, and determining an optimum one.
2. Effect of several intermediate annealing temperatures during cold work, on properties of one of the alloys.
3. a. Room temperature tensile strength;
   b. Effect of annealing treatments on room temperature tensile strength.
4. Stress-rupture properties.
5. Effect of these treatments on electrical resistivity.

E. Other aspects.

1. Study of powders, in various conditions, through the SEM
2. Fracture studies on wrought material.
3. Electron-microscopy on extruded, precipitation hardened, and thermomechanically worked material.
4. Notch sensitivity tests on the copper-zirconium-chromium alloys.

V. MATERIALS AND METHODS

All powders studied and used for alloys in this investigation were made from vacuum cast ingots. Oxygen-free high-conductivity copper was used as the base material in all instances to produce the required copper-zirconium and copper-zirconium-chromium alloy powders.

A. Powder Production

1. Splat Cooling

The Duwez shock tube[16] type of apparatus was used to produce thin foil particles of several alloy compositions. The method involves the disintegration of the liquid alloy into fine droplets, delivery of the droplets in the molten state to a copper substrate, and their impact to produce thin foils. It is possible to achieve cooling rates of the order of 10^7 to 10^9 °C per sec.[47,48]. Only structure studies were performed on these foils, as their solid state consolidation is not practically feasible or commercially desirable.

2. Rotating Copper Disc

A major effort was put in the design and fabrication of a workable apparatus. It was felt that cooling rates in the range 10^5 to 10^6 °C per sec. could be obtained with this set-up. Thin cigar shaped foils were obtained on atomization of liquid droplets on the rotating copper disc. Melting was performed under a slightly reducing atmosphere (10% methane, 90% argon). Quenching of atomized molten droplets was also performed in liquid nitrogen and air. Only small amounts of material

was produced for microstructural examination purposes.

3. Steam Atomization

Powders of two compositions (0.64 and 1.07% Zr) were produced by this method with the pilot facilities at Industrial Materials Technology Inc. Supersaturated steam of low pressure is expanded through a nozzle, impinging on the round metal steam. On expansion, the steam cools, condenses, and precipitates on the atomized metallic droplets, leading to rapid quenching. Relatively coarse powders 3000 microns and below (-6 mesh) were produced through this technique.

4. Nitrogen Atomization

A series of nitrogen atomized alloy powders of both copper-zirconium (0.14 to 1.0 wt. %) and copper-zirconium (0.1 and 0.25 wt. %) chromium (0.3 and 0.33 wt. %) were commercially obtained. The technique for the production of these powders is only different from the above method in that it uses an inert gas instead of compressed steam. Two of the alloy powders obtained had a relatively coarse and wide range of particle sizes 840 microns and below (-20 mesh) whereas all the others were 149 microns and less (-100 mesh). This technique achieved cooling rates estimated to be in the range of 10^3 to 10^4 ^oC per sec.

5. Cast Ingots

Vacuum cast cylindrical ingots (2" in diameter) were metallographically examined for comparison purposes. Castings ½ inches square and 1½ inches long were made in a copper die ($2^3/4$ inches in diameter, 3 inches long). A thermocouple connected to an oscilloscope was embedded

in the middle of the cavity, to measure the solidification rate. Preliminary tensile strength measurements were made on these samples.

B. Starting Powder Composition and Size Range

1. Steam Atomized Powders

Initial powder size, and composition, of the five steam atomized powders used in this investigation is listed in Table II.

Table II

Nominal Starting Composition and Size of Steam Atomized Powders

Powder	Zr Wt %	O_2 Wt %	Cu (bal) Wt %	Powder Size Range
IMT-1	0.64	0.21	99.15	-6 to +14 mesh (3360/1190μ)
IMT-2	0.64	0.35	99.01	-35 to +100 mesh (420/149μ)
IMT-3	1.07	0.47	98.46	-20 to +35 mesh (840/420μ)
IMT-4	1.07	0.60	98.33	-35 to 100 mesh (420/149μ)

2. Nitrogen Atomized Powders

Efforts to produce relatively coarse (1000μ and above) and spherical nitrogen atomized powders were uncussessful. Table III lists the composition and size of powder used.

C. Powder Preparation

1. Reduction

It is well known that inferior high temperature properties can be obtained in materials produced by powder metallurgical techniques by the

Table III

Nominal Starting Composition and Size of Nitrogen Atomized Powders

Powder	Zr Wt %	Cr Wt %	O_2 Wt %	Cu (bal) Wt %	Powder Size Range
ZA-2	0.2	-	0.03	99.77	-100 mesh (-149μ)
ZA-3	0.37	-	0.04	99.59	-100 mesh (-149μ)
ZA-8	0.80	-	0.01	99.13	-100 mesh (-149μ)
FM-8	0.88	-	0.11	99.04	-100 mesh (-149μ)
ZA-10(a)	0.90	-	0.20	98.89	-100 mesh (-149μ)
ZA-10(b)	0.90	-	0.11	98.99	$^{-20}/_{+100}$ mesh ($^{840}/_{149\mu}$)
ZAC-1	0.10	0.32	0.04	99.54	-100 mesh (-149μ)
ZAC-2(a)	0.23	0.33	0.11	99.33	-100 mesh (-149μ)
ZAC-2(b)	0.23	0.33	0.11	99.33	$^{-20}/_{+100}$ mesh ($^{840}/_{149\mu}$)

retention of solvent metal oxides[49] in the final consolidated material. In the present case the reduction of copper-oxide was achieved through reduction with dry hydrogen. The powders were reduced in a vertical furnace with a pyrex reduction tube assembly. The tube contained a micron-fine, sealed in, fitted disc to support the powder. The assembly was first evacuated, and then flushed several times with dry hydrogen before heating. Only hydrogen with less than 0.013 volume % water vapour was used for the reduction treatment. Except for the 0.8 wt. % zirconium alloy (see Appendix 1) all alloys were reduced at 450°C for ten hours. After the reduction run, the tube was clamped off at the top and bottom and placed in a dry box (with less than 0.0018 volume % water vapour).

2. Powder Compaction

Some of the initial, fine (-100 mesh) nitrogen atomized powders were cold isostatically compacted before final consolidation. The green strength of these compacts was found to be very low, and as breakage was obtained on removal from compaction cans, cold isostatic compaction was not used for the rest of the powders. These remaining powders were merely gravity packed (Appendix 2).

For the cold isostatic compaction the reduced powder was put into a perforated aluminum can (2½ in diameter) with a latex rubber tubing fitted into it. The rubber tubing was sealed off on both sides, before removal of can from the dry box. The cans were then isostatically pressed with a pressure of 60,000 pounds. On removal of compaction cans after compaction in the dry box, two inch cylinders of the powder were obtained, which were then placed in copper cans.

The remaining powders were poured in copper cans, the inside of which had been cleaned with dilute nitric acid. The cans were machined with a copper "O" ring so that when the top was screwed on, compression of the "O" ring resulted in an air tight seal.

All the cans were then electron beam welded. They were then leak tested before extrusion.

3. Extrusion

The billet assemblies were evacuated to less than one micron static pressure, then out gassed at 450°C to the same pressure. They were then preheated at 650°C for several hours before extrusion. Extrusion ratios

of 25:1 and 30:1 were utilized. Optical and specific gravity measured showed that the extruded rods were essentially fully dense after extrusion.

D. Alloy Compositions and Fabrication Variables

Final alloy compostions after extrusion and pertinent extrusion data are listed in Tables IV and V, Appendix 2.

E. Thermomechanical Treatments

Although zirconium additions to copper yield an age-hardening effect, this is slight, and hence, mechanical properties were developed primarily by thermomechanically working the extruded alloys. Hence, all alloys were given various processing treatments in order to optimize properties, and to study the effect of these treatments on properties. All treatments are listed and designated for further reference in Table VI.

F. Evaluation of Alloys and their Properties

All the wrought materials produced from extruded powders were investigated, both in the as-extruded and thermomechanically worked conditions. The alloys were examined for the following properties:

1. Hardness

As a preliminary evaluation of the stability of the extruded alloys, the effect of annealing (one hour at temperature) on the room temperature hardness was examined. Such studies were also conducted on some alloys after 50% reduction of area. An average of at least

Table VI

Combination of Processing Treatments

Designation	Treatment
A	As-extruded, cold worked straight to desired degree of reduction at 20°C, with approximately 10% strain increments.
B	As-extruded, annealed at 300, 400, 500 or 600°C for one hour after each approximate 10% strain increment at R.T., continued to the desired degree of reduction. The last step being a strain increment.
C	As-extruded, solution treated at 980°C for 30 minutes, water quenched, followed by 50% R.A. at 20°C (with approximately 10% strain increments), then aged at 400, 450 or 500°C for 1 hour, water quenched and further reduced to desired reduction.
D	As-extruded, solution treated at 980°C for 30 minutes, water quenched, followed by 50% R.A. at 20°C (with approximately 10% increments), then aged at 500°C for 3 hours, air cooled, and further reduced to 75% R.A. (from initial diameter).
E	As-extruded, solution treated at 980°C for 30 minutes, water quenched, followed by aging at 400, 450 or 500°C for 1 hour after each approximate 10% strain increment at R.T., up to 75% R.A. The last step being a strain increment.
F	As-extruded, swaged to 50% R.A., annealed for 1 hour at 300, 400 or 500°C, then further reduced to the desired reduction.

three readings was taken in each instant.

2. Metallography

Standard metallographic techniques were employed for optical microscope examination. An acidic $FeCl_3$ etch (Appendix 3) was used in all cases. Electron microscopic investigations of both replicas and thin foils, were done using a JEM 7 unit. Thin foils were prepared by a twin jet machining apparatus (Astromet), the details of which are given in Appendix 3. Selected area diffraction and dark field techniques were also employed in splat materials, for phase identification, and size and shape determination of precipitate particles.

3. X-ray Diffraction

The splat cooled foils were scraped from the substrate and mounted on a glass slide, with a thin layer of vaseline. X-ray diffraction measurements were made with a General Electric XRD-5 diffractometer using Cu-K_α radiation. The measured diffraction angles were corrected from spectormeter, and time constant errors from calibration curves made with high purity copper powders. Precision lattice parameter measurements were made, using standard extrapolation techniques. Decomposition studies were made on some of the as-received nitrogen atomized powders, by annealing them for one hour periods at various temperatures.

Laue diffraction techniques were employed on some of the wrought alloys to determine the residual stress in the as-extruded alloys.

X-ray techniques were also employed to identify extracted oxide

particles. Bar stock was dissolved in concentrated nitric acid, to accomplish the extraction of the oxide particles.

4. Tensile Testing

Tensile properties at room temperature, and as a function of annealing temperature, were determined using an Instron tension testing machine. All tests were performed using a constant cross-head speed of 0.02 inch per minute. Load-elongation curves were recorded autographically. Both tensile and stress-rupture samples were machined with ASTM specifications. Two sizes of specimens were used:

a. ¼ - 20 threads with a gage length of 0.634 inch and a gage diameter of 0.16 inch.

b. 8 - 32 threads with a gage length of 0.50 inch and a gage diameter of 0.10 inch.

5. Stress-Rupture Testing

All stress-rupture tests were performed at constant load, using lever-type frames. Specimen temperatures were measured with a thermocouple fixed close to the center of the specimen gage length. Elongation measurements were made on dial gages, which recorded elongation on the specimen train during the test. Relative minimum creep rate data was obtained using these measurements.

6. Electrical Conductivity Measurements

A four point probe method was used to calculate the electrical conductivity. A standard OFHC copper sample was used for calibration, and relative percent IACS were obtained in all cases.

7. Notch Sensitivity Tests

Preliminary tests were performed to evaluate the notch sensitivity of the Cu-Zr-Cr alloys. The standard 0.10 inch diameter samples were notched to a root diameter of 0.09 (K_t = 3.8) and 0.08 (K_t = 5.0) inch, and then tested both at room temperature and in stress-rupture (400°C).

VI. RESULTS

A. Starting Powders

1. Splat Powders

Four alloys of Cu-Zr (approximately 10 grams) were prepared by melting the ingredients in an inert gas, non-consumable arc furnace. The buttons were inverted and remelted several times to insure homogeneity. They were then reweighed, and based upon negligible weight loss after melting, the compositions reported are considered accurate. The compositionsof the alloys investigated and the lattice parameters after splat cooling are listed in Table VII.

Table VII

Results of Splat Cooled Cu-Zr Alloys

Zr Wt. %	Cu (bal) Wt. %	Lattice Parameter Å	Atomic Vol. $(Å)^3$
0.0	100.0	3.615^{50}	11.811
0.2	99.8	3.616 *	11.819
0.5	99.5	3.618 *	11.839
2.0	98.0	3.621 *	11.879
5.0	95.0	3.625 *	11.912

* The lattice parameter measurements had an estimated error of approximately ± 0.002 Å.

The effect of composition on the lattice parameter of splat Cu-Zr is shown in Figure 3a. Atomic volume calculations for these alloys plotted against the Vegard's Law Line for the Cu-Zr system show a

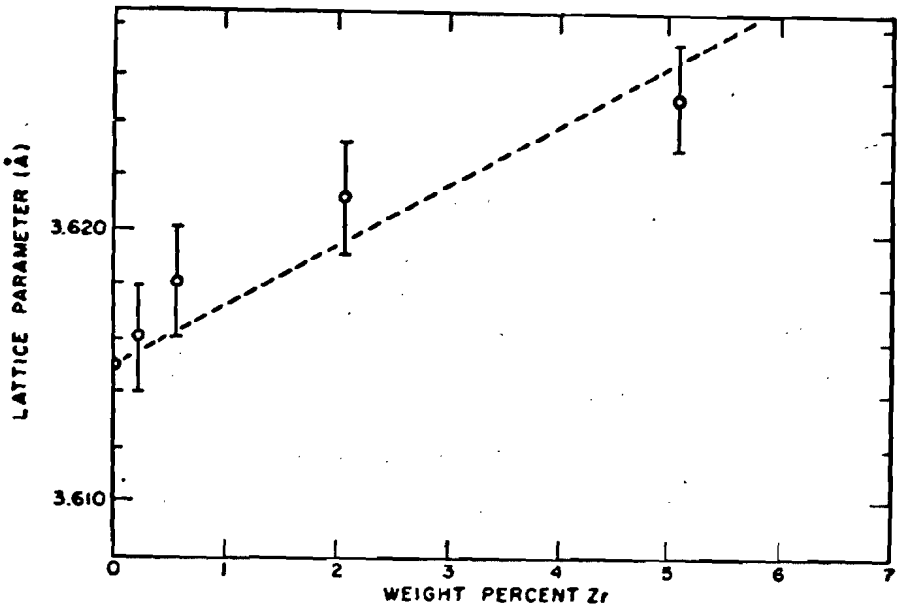

Figure 3. (a) Effect of Zr content on the lattice parameter.

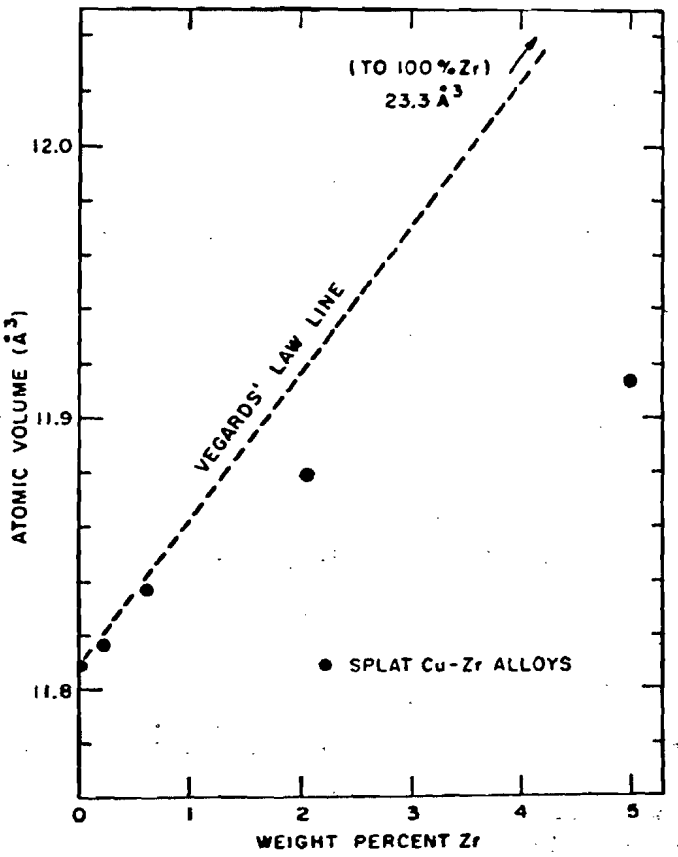

Figure 3. (b) Deviations in Vegards' Law on splating Cu-Zr.

very strong negative deviation at the higher zirconium contents (Figure 3b). This indicates a considerable reduction in the apparent atomic size of zirconium in solid solution with copper in fcc co-ordination. A broken straight line is drawn to fit the data in Figure 3a, as only the features of a fcc phase could be identified through the X-ray diffraction pattern. This would imply complete solid solubility (α phase) up to 5 wt. % zirconium, in agreement with Ray's[20] finding, but electron microscopic examination on these splats showed the presence of a fine precipitate (Figure 4) in several areas of the foils. Although these precipitates could not be identified using selected area diffraction, it is presumed that they are the intermetallic Cu_3Zr. The Bravais crystal structure of Cu_3Zr is not documented, and hence diffraction spots obtained from the precipitate could not be identified.

Two of the wrought alloy compositions, ZA-2 and ZAC-1, were also splat cooled, using the shock tube technique. Transmission electronmicroscopy on both of these alloys revealed the presence of fine precipitates with elastic strain fields associated between them and the matrix. In the case of ZAC-1, in agreement with other investigations[36,37], well defined D-lobes due to coherency between the particles (less than 100 $\mathring{A}$) and matrix were observed (Figure 5). Examination of ZA-2 in bright field showed elongated, streaky particle contrast with the precipitates not visually identifiable (Figure 6). Dark field studies (Figure 7), revealed that precipitation was occuring in patches, each patch containing several particles. The particles seemed to be globular or plate like, with an est-

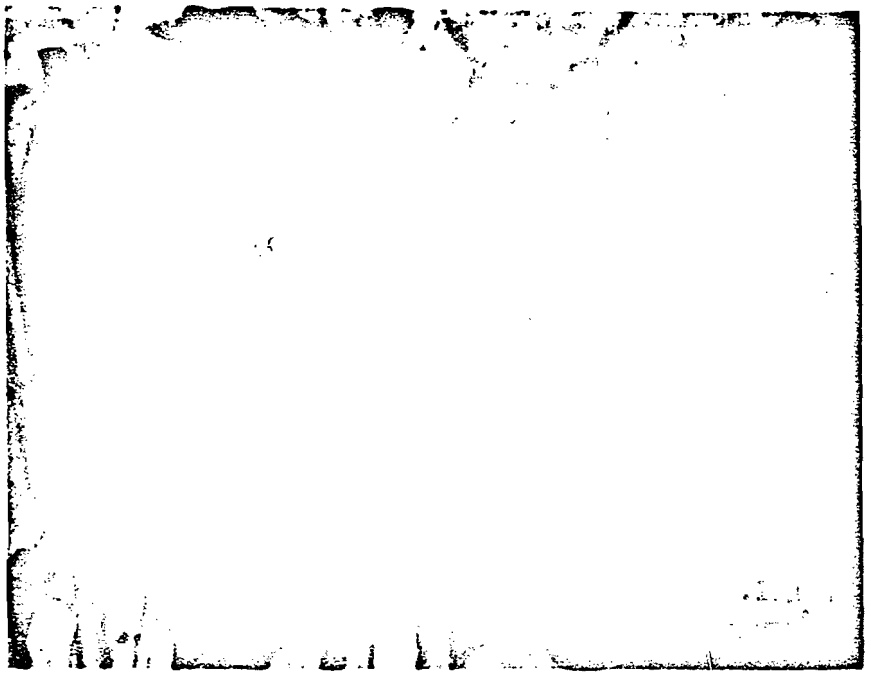

Figure 4. Transmission electron micrograph of Cu-2 wt. % Zr splat cooled alloy showing evidence of fine Cu_3Zr precipitates.

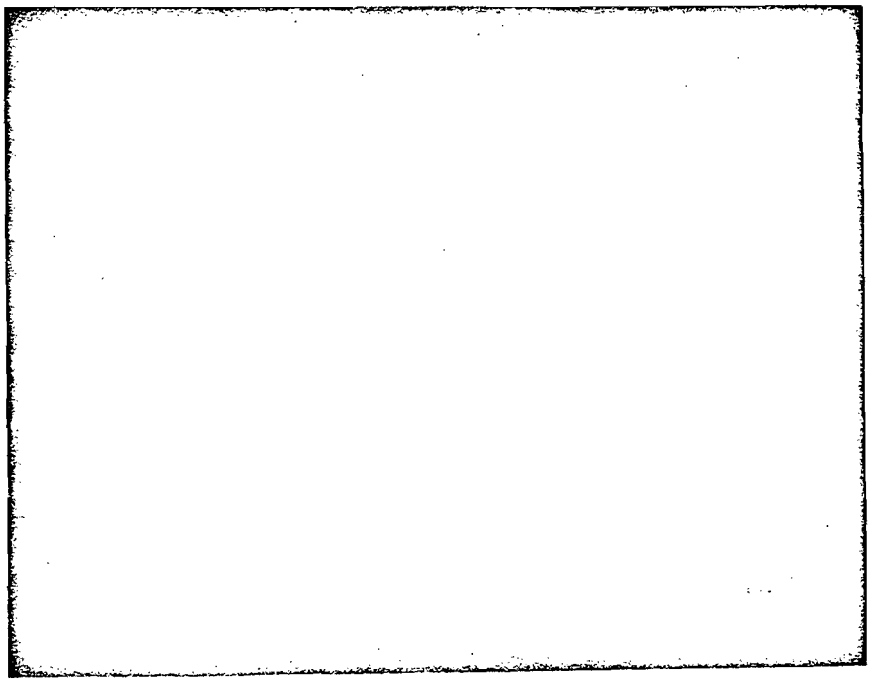

Figure 5. Transmission electron micrograph of splat foils of ZAC-1 showing D-shaped lobes around Cr precipitates (marked D).

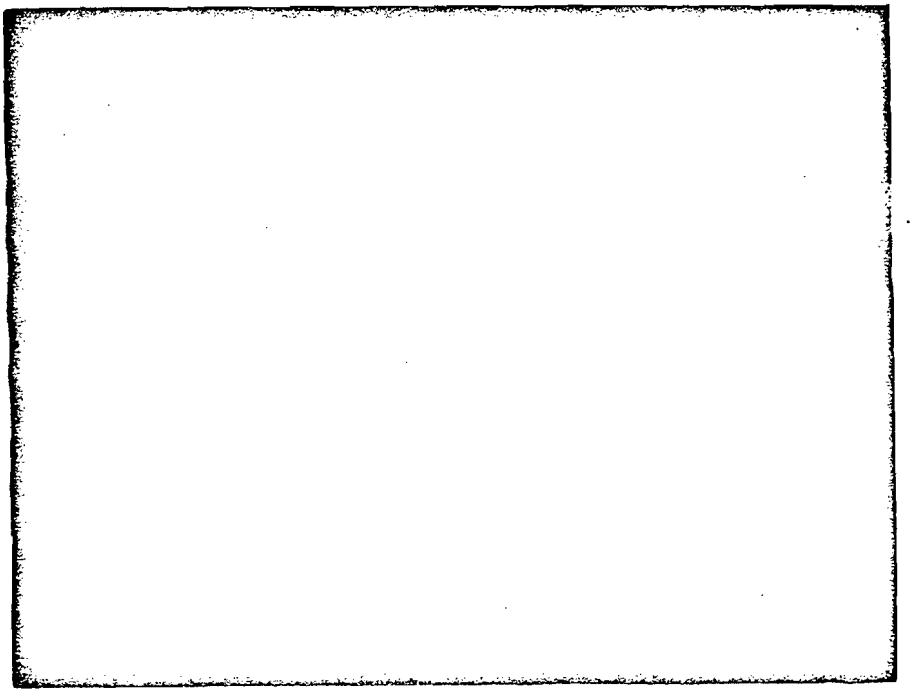

Figure 6. Elongated, streaky contrast observed in splat foils of ZA-2 alloys.

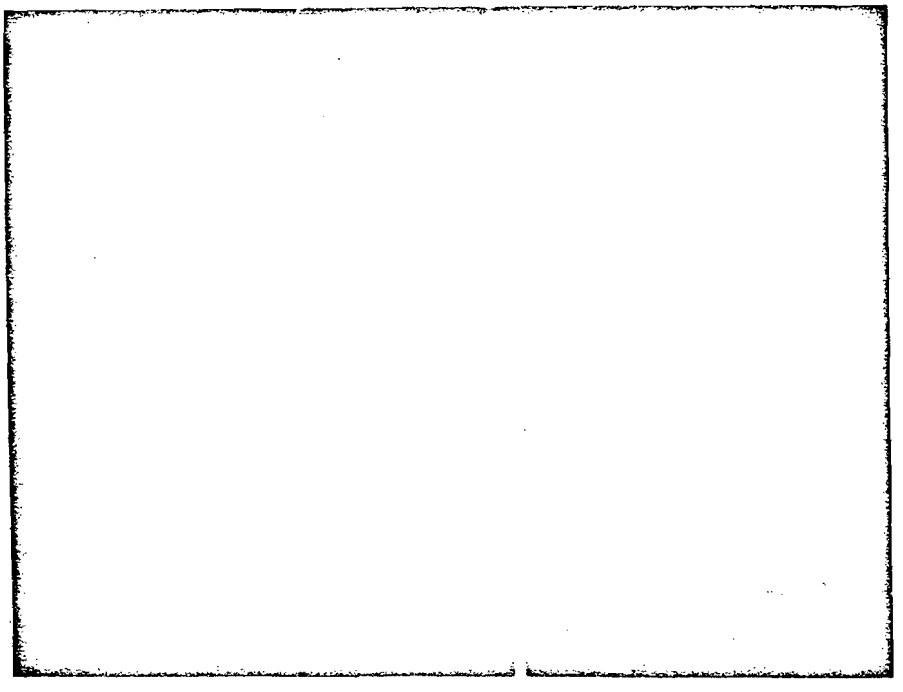

Figure 7. Dark field electron micrograph showing patchy nature of precipitation obtained in splat cooled ZA-2.

imated individual particle size of less than 200 Å.

Since both Henmi et al[37] and Suzuki et al[36] found Cu_3Zr to precipitate out incoherently, the strain fields observed (Figure 6) could be due to differential volume change between these particles and the matrix. Appendix 3 shows results obtained from selected area diffraction on these splats.

A straight line relationship between cooling rate and dendrite arm spacing was obtained for the copper-zirconium alloys (Figure 8). The slope of this line was found to be approximately 0.48, which is significantly greater than that obtained for aluminum alloys (0.32) by Matyja et al[24]. At the splat cooled end of the curve (10^7 to 10^9 °C per sec.), it was observed that dendrite arm spacing was only slightly affected by the concentration of zirconium (0.2 to 5%). This confirmed the results of Alexander et al[51] and Matyja et al[24], who also observed that the nature and concentration of the solute element only slightly affected the final dendrite arm spacing. Cooling rates reported on all other powders were obtained by measuring their dendrite sizes and then extrapolating from the straight line relationship in Figure 8.

The successful production of alloys containing a reactive element (like zirconium or chromium) is often made difficult by the affinity of this element for oxygen and other impurities. The formation of stable compounds, particularly ZrO_2, which may be desirable under certain conditions, such that the oxide size is small and its distribution homogenous, may also decrease a portion of the solute element which is required to

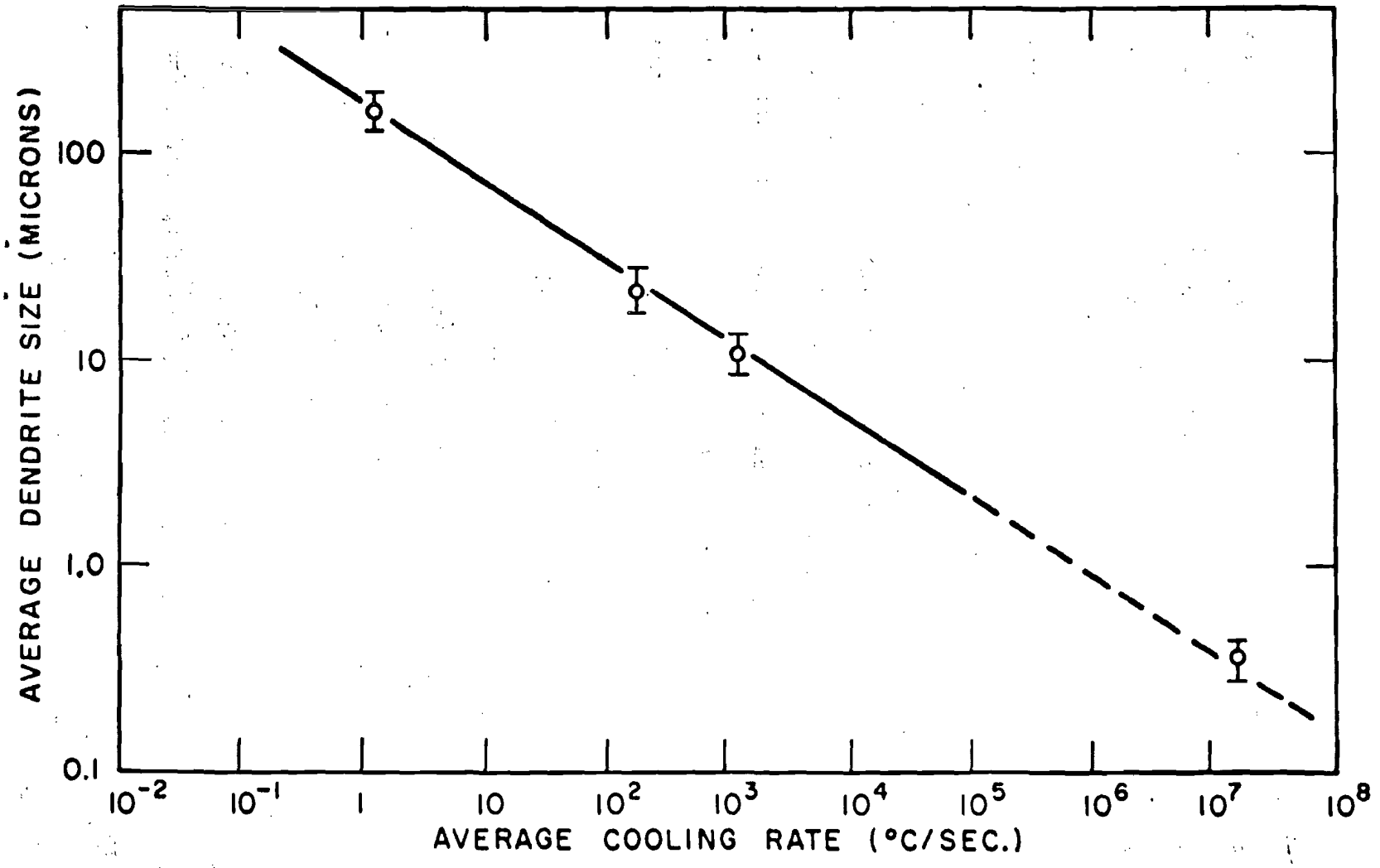

Figure 8. Variation of dendrite arm spacing as a function of cooling rate for copper-zirconium alloys.

improve properties. Powders obtained by splat cooling Cu-0.2 wt. % zirconium alloys on the rotating copper disc, yielded thin lenticular shaped particles (20 to 100 microns in width and 500 to 2000 microns long) with an oxygen content of over 0.5 wt. %. Chemical analyses and X-ray studies on extracted particles revealed a complete conversion of the Zr to ZrO_2. As less than 0.08 wt. % oxygen is required to convert all the Zr to ZrO_2, the remaining 0.42 wt. % oxygen is probably tied up as Cu_2O. Thus, owing to the lenticular powder shape and a high oxygen content, these powders were not consolidated for further study.

2. Steam Atomized Powders

Problems of oxidation, as mentioned above, were also encountered with the steam atomized powders. The oxygen content (Table VIII) on all the powders was found to be high, and a large amount of conversion of Zr to ZrO_2 was obtained during the atomization process. Table VIII shows a complete analysis of the chemical compositions of the powders after atomization. X-ray line broadening studies[52] revealed that the size of the extracted ZrO_2 particles exceeded 1000 Å, as no line broadening was obtained.

Efforts to produce coarse spherical particles were not completely successful. A mixed variety of sizes and shapes was obtained. Generally, particles below 1000μ were found to be quite spherical (Figure 9a), whereas a mixture of elongated and spherical shapes was obtained in the coarse

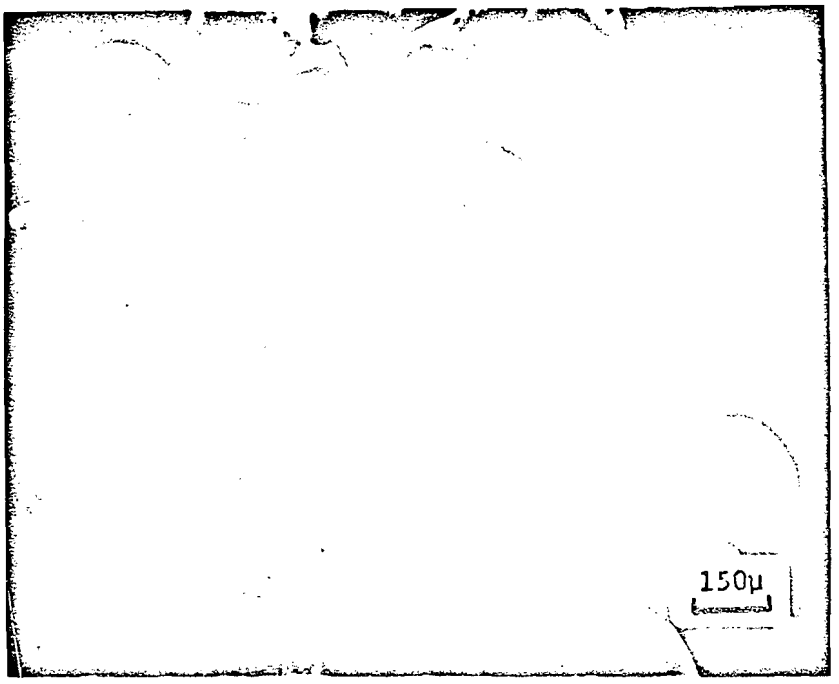

(a)

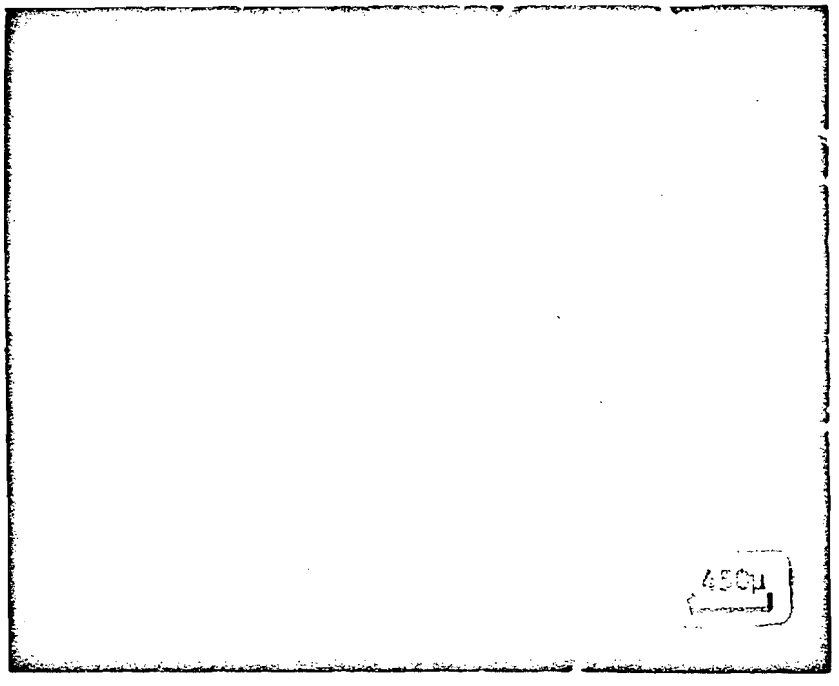

(b)

Figure 9. SEM photographs of steam atomized powders.
(a) Spherical fine (-1000μ) powder
(b) Mixed fine and coarse (elongated) powder

Table VIII

Changes in Composition (in weight pct.) Obtained After Steam Atomization

Designation	Initial[1] Zr	Final[2] Zr	O_2[2]	Measured[2] ZrO_2	Calculated[3] ZrO_2
IMT-1	0.64	0.14	0.21	0.68	0.68
IMT-2	0.64	0.03	0.35	0.55	0.80
IMT-3	1.07	0.11	0.47	0.97	1.09
IMT-4	1.07	0.06	0.60	0.96	1.37

1. Zr content present in master alloy before atomization.
2. Compositions obtained through chemical analysis on atomized powders.
3. ZrO_2 that should theoretically be present after atomization, if no loss of Zr or ZrO_2 was obtained during the atomization process.

range (1000 to 4000μ); Figure 9b shows some of the elongated particles.

Two of the more common features observed through optical metallography are shown in Figures 10a and 10b. Close to 10% of all the particles investigated showed a relatively clean dendritic morphology (Figure 10a), with no optically visible ZrO_2 particles. This type of mixture of both large and small dendrites made it difficult to estimate the cooling rate of the powders. Figure 10b reveals two features, coarse ZrO_2 particles and macroporosity, one or both of which were observed in almost all cases. As is visible, clusters of coarse ZrO_2 particles (0.5 to 1.0μ) were found to be dispersed throughout the matrix. The most undesirable feature of the holes is the entrapment of oxygen, causing formation of Cu_2O inside the particle instead of only on the surface.

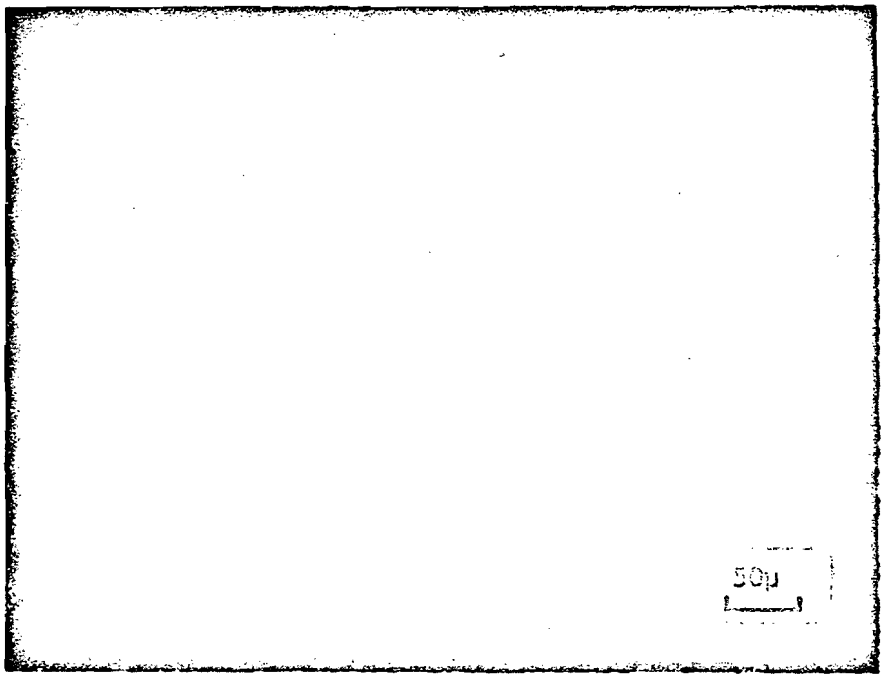

(a)

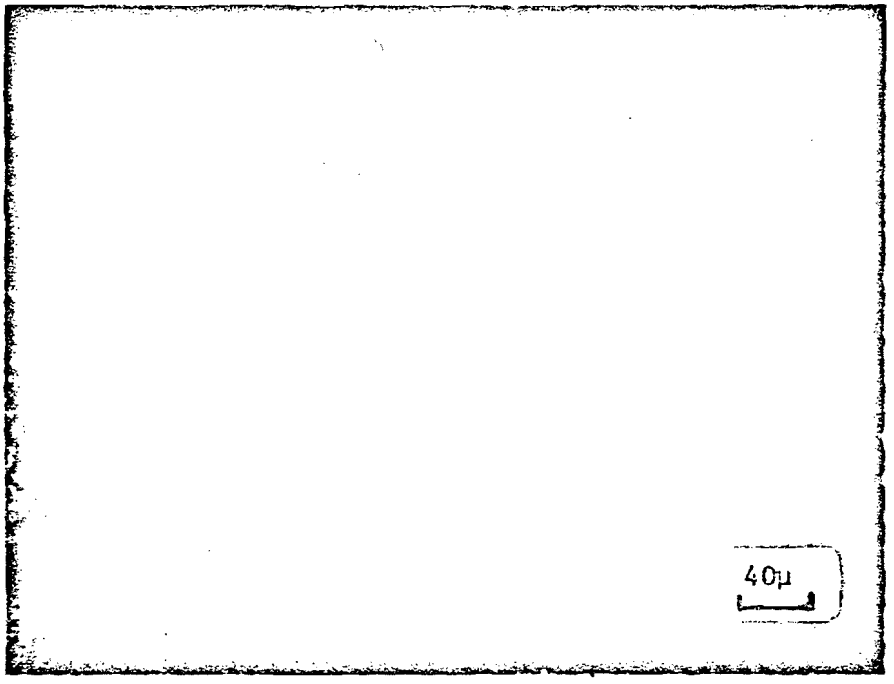

(b)

Figure 10. Optical micrographs of steam atomized powders (IMT-3)

(a) Mixed (large and small) dendritic morphology

(b) Micrograph showing clusters of coarse ZrO_2 and porosity observed in most particles

This internal oxide is probably a major contributor to the high levels of oxygen obtained in these powders (Table VIII).

3. Nitrogen Atomized Powders

All attempts to obtain coarse (larger than 1000μ) spherical powders resulted in flaky foils very similar to those obtained by splat cooling against a rotating copper disc; hence only powders less than 1000μ in size were used (Table III). In the relatively coarser range powders (840 to 149μ), the particles were lenticular shaped (Figure 11a), whereas the fine powders (less than 149μ) were quite spherical (Figure 11b). The dendrite morphology in both cases was very well defined and identical for all powder in their respective size range (Figure 12a and 12b). The cooling rate for the coarser range was calculated to be approximately 10^3 °C per sec., while that for the finer powder was around 10^4 °C per sec. Preliminary X-ray studies on some of these atomized powders showed no definite trends as to increased solid solubility in the atomized powders, or subsequent decomposition of the atomized structure on annealing up to 700°C.

4. Cast Ingots

A preliminary investigation on the effect of dendrite size on room temperature tensile strength of cast Cu-0.64 wt. % zirconium was made. Table IX shows the results obtained.

The finer dendrite size castings (10 and 14μ) were found to have substantially superior yield strength values, as would be expected.

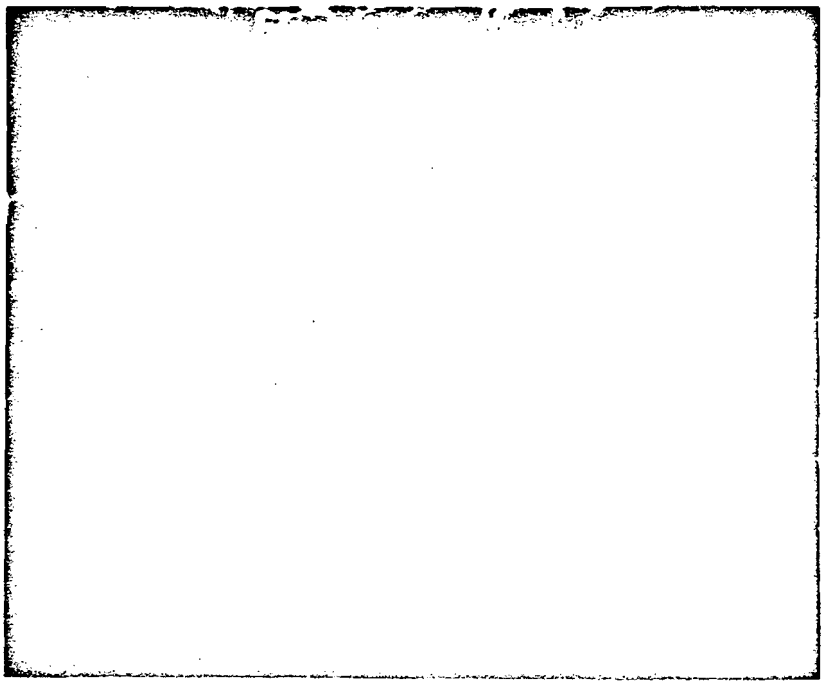

(a)

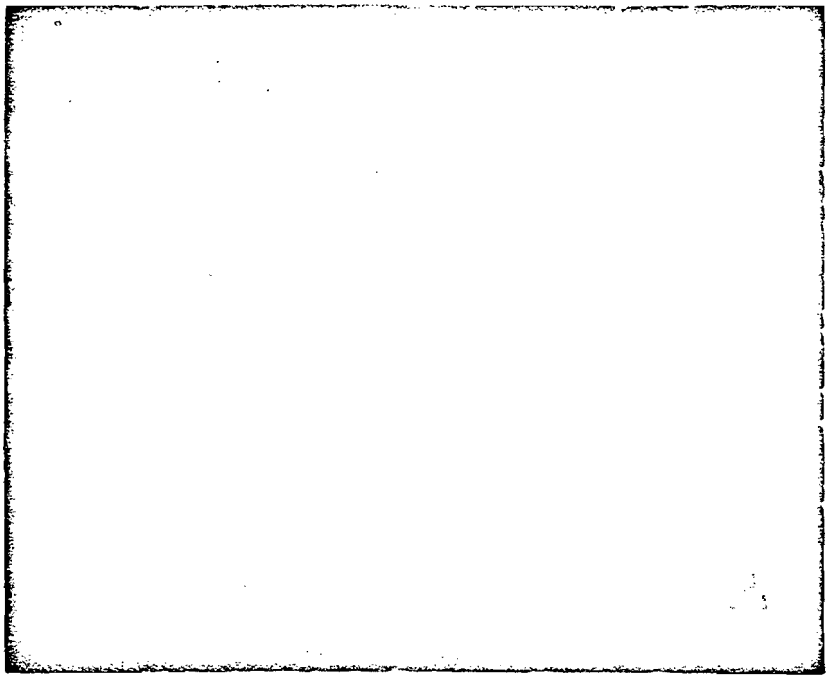

(b)

Figure 11. SEM micrographs of nitrogen atomized powders.
(a) -20/+100 (840/149μ) lenticular shaped particles
(b) -100 mesh (149μ) spherical powder

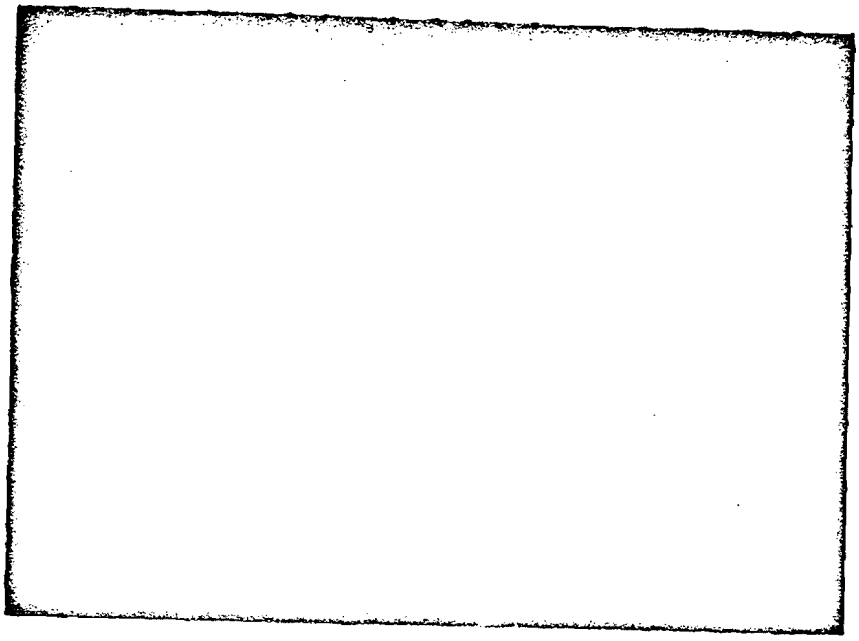

(a)

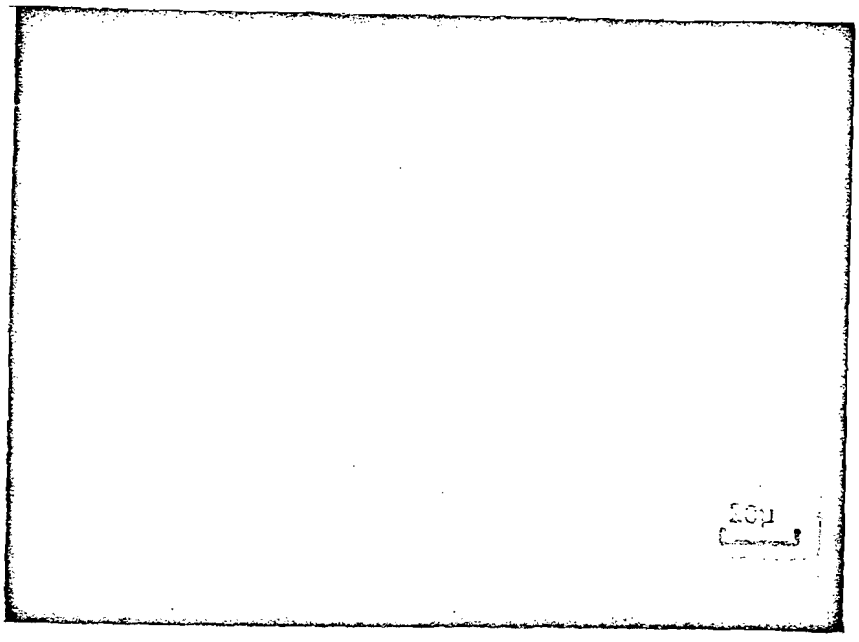

(b)

Figure 12. Photomicrographs of nitrogen atomized powder.
(a) -840 to +149μ powder (12μ D.A.S., 10^3 °C/sec.)
(b) -100μ size range powder (6μ D.A.S., 10^4 °C/sec.)

Table IX

Effect of Dendrite Size on R.T. Tensile Properties

Type*	Average[1] D.A.S.μ	Cooling Rate °C/sec.	Y.S. (psi)	U.T.S. (psi)	Elong. (%)	R.A. (%)
A	10	$2x10^3$	18,000	30,000	11.0	31
B	14	$3x10^2$	23,000	33,000	17.0	74
C	120	$8x10^{-1}$	12,300	32,000	25.0	11

* A. Cast in copper mold immersed in liquid N_2
B. Cast in copper mold immersed in water
C. Vacuum cast (2" dia.) ingot

1. Dendrite arm spacing measured using Hilliard Circle[53,54] (Appendix 3).

Their tensile strength and especially elongation values were unusually low. Optical microscopy showed no porosity in any of the castings, and hence the low strength values could not be attributed to this. Fracture studies using the SEM showed dendritic separation in the "A" samples (Figure 13a), while a ductile fracture with visible shear zones was observed in the "B" type material (Figure 13b). The vacuum cast material "C" showed a predominantly ductile type of fracture surface.

An opticle micrograph of the "A" type material (Figure 14a) showed an almost continuous film of the intermetallic Cu_3Zr enveloping the dendrites and grain boundaries. This is caused by the rejection of the eutectic to the dendritic boundaries during the solidification process. Grain boundaries seem to be composed of a chain of dendrites which compensate the misfit between the dendritic orientations of the two neighboring grains. Fracture, which seems to start in a ductile mode (as was observed

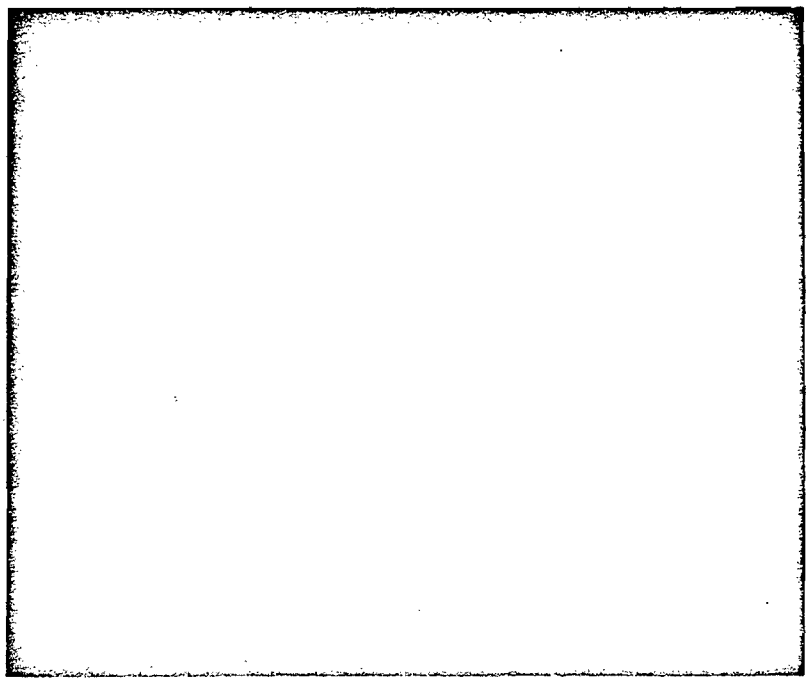

(a)

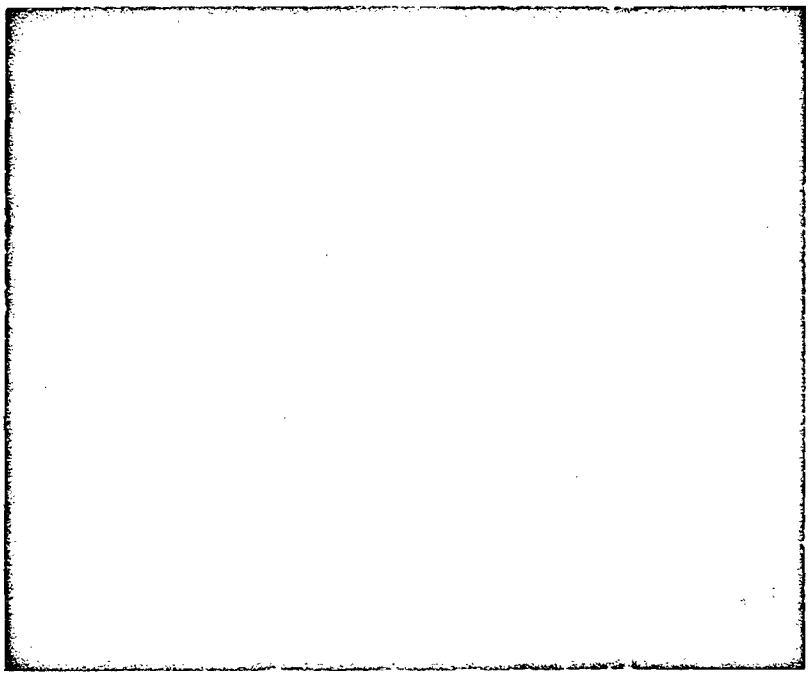

(b)

Figure 14. Rapidly solidified Cu-0.64% Zr alloy.

(a) Optical micrograph showing dendritic grain boundary
(b) Dendritic separation along grain boundaries

along the lip of the fracture surface), suddenly gives way to brittle separation along grain boundaries (Figure 14b). The low strength values obtained in this material were attributed to this fracture behaviour.

5. Powder Characterization

Table X lists all pertinent information on powders studied in this investigation.

B. Powder Preparation

1. Reduction

Surface oxide (Cu_2O) on all powders was reduced with dry hydrogen before final consolidation. All data pertaining to this treatment, and various other studies on the oxygen content of these powders, are given in Appendix 1.

All the steam atomized powders showed a substantial decrease in oxygen content after reduction (Appendix 1). Since almost a complete conversion of Zr to ZrO_2 (Table VIII) was obtained during atomization, this loss of weight of oxygen was attributed to the reduction of Cu_2O. Owing to the porous nature of the powders (Figure 10b), reduction of Cu_2O was obtained inside these holes. The eventual release of built-up steam pressure in these holes, during reduction, caused rupture in the powders. In Figure 15, deep crack formation is evident around the hole, in which the dendrite structure is also visible. Such cracks were observed in all these powders (in almost all particles examined) after the reduction cycle.

Table X

Powder Characterization

Powder Prep. Technique	Powder Size(μ)	Powder Shape	Measured D.A.S.(μ)	Calculated Cooling Rate (°C/sec.)
Shock tube splats		Powdery foils	<0.5	10^7 to 10^9
Splat against copper disc	20–100 thick 50–2000 long	Flakes	1 to 3	10^5 to 10^6
Atomized into liquid N_2	Less than 200	Spherical	3 to 4	$5x10^4$ to 10^5
Steam Atomized (fine)	+840/-149	Mostly Spherical	--	10^4 to 10^5*
Steam Atomized (coarse)	+3360/-1190	Elongates Spherical	--	10^2 to 10^4*
Nitrogen gas Atomized (fine)	-149	Spherical	6	10^4
Nitrogen gas Atomized(coarse)	+840/-114	Lenticular	12	10^3
Cast Ingot	2" dia.		120	10^{-2}

* Rough estimates owing to unhomogenous dendritic structure of these powders

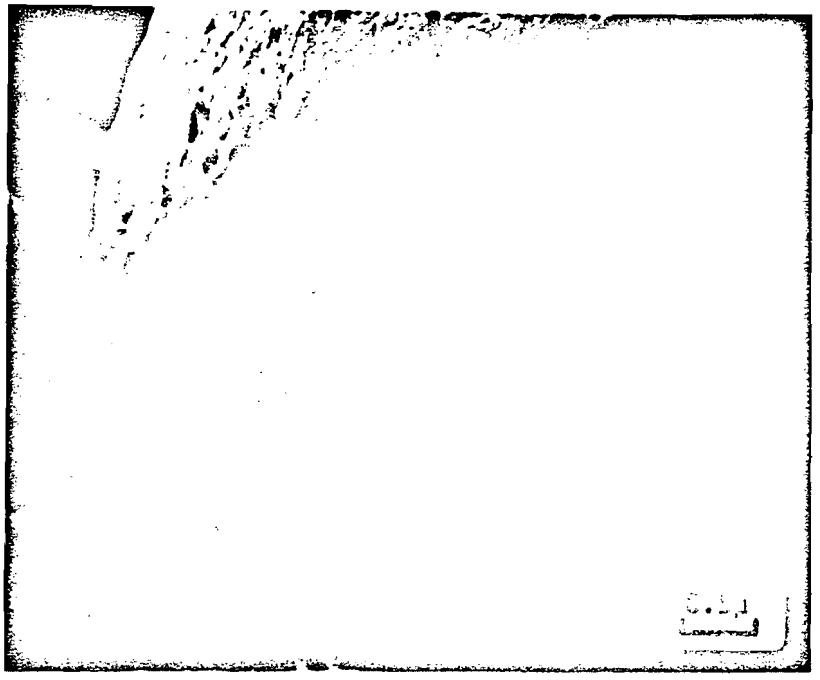

Figure 15. Crack formation obtained during the reduction cycle in the steam atomized powders.

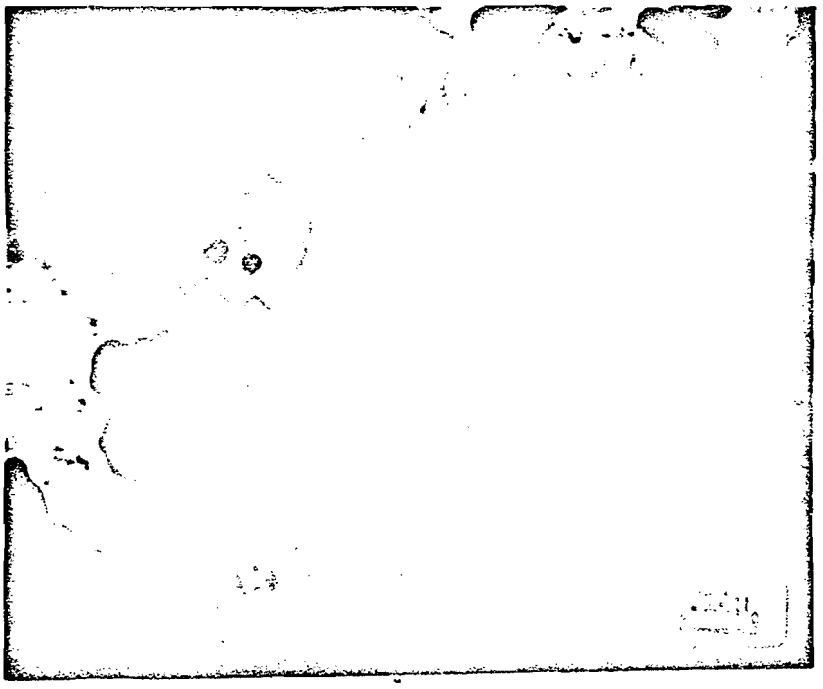

Figure 16. Wrought ZA-8 alloy showing coarse agglomeration of ZrO_2 particles throughout the matrix.

Chemical analyses on the high zirconium content nitrogen atomized powders (i.e., ZA-8, FM-8) revealed that after reduction (Appendix 1) the oxygen content was either unchanged or a slight increase was obtained. Initially this was attributed to various systematic errors in the chemical analyses, and pick up of oxygen on the reduced surface of the powder during the chemical analysis. The reduced powder (with a large surface area to volume ratio) had to be weighed in air, before the analysis. This pick up of oxygen is evident in the ZA-10 and ZAC-2 powders (Appendix 1). For example in ZAC-2a the as-atomized powder had 0.11 wt. % oxygen, after reduction chemical analyses showed the presence of 0.10 wt. % oxygen, but extruded powder (the wrought alloy) only had 0.07 wt. % oxygen. As the consolidated powder was not exposed to air after reduction, the oxygen content of the reduced powder is assumed (as is probable) to be 0.07 wt. % oxygen. In the case of ZA-8 it was found that reduction at 450°C resulted in a substantial increase in the oxygen content (0.92 wt. % oxygen), hence a temperature of 300°C was used, which resulted in 0.075 wt. % oxygen after a six hour cycle.

Transmission electron microscopy on ZA-8 showed the presence of huge agglomerated particles in the alloy (Figure 16). As the particles were opaque to the electron beam, selected area diffraction could not be used to reveal their identity. X-ray analysis on extracted particles positively identified them to be ZrO_2. Most of these particles seemed to be agglomerated around the original powder boundaries. It seemed that

flow action obtained during consolidation caused the ZrO_2 particles at the surface of the powder to coalesce.

These powders (ZA-8 and FM-8) were then examined in the as-atomized, acid cleaned and reduced condition on the SEM. The surface of the atomized powder (Figure 17a) was found to be clean with several powder particles showing a dendritic structure on their surface. The acid cleaning, with dilute nitric acid, further brought out the dendritic morphology on the surface of the powders. On the reduced surface, nonconducting particles (less than 2μ in size) were observed (Figure 17b). The presence of such particles, after reduction, was also observed on the surface of the higher zirconium content(IMT-3 and 4) powders. SEM spectographic analysis on these particles did not offer any conclusive evidence as to their identity, although in some cases a much higher concentration of zirconium in the particles than in the matrix was observed. Chemical analysis (Table XI) on these powders, before and after reduction showed conclusively that ZrO_2 was being formed during reduction.

Table XI

Chemical Analyses (weight pct.) Before and After Reduction

Powder	Before Reduction			After Reduction		
	O_2	Zr	ZrO_2	O_2	Zr	ZrO_2
ZA-8 (0.8 Zr)	0.07	0.73	0.10	0.08	0.57	0.31
FM-8 (0.88 Zr)	0.11	0.63	0.27	0.11	0.54	0.44

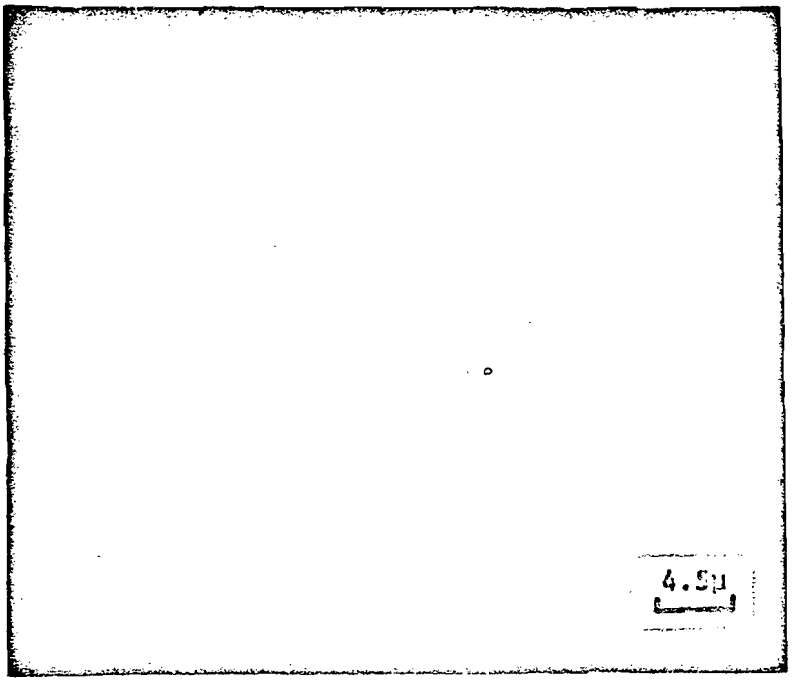

(a)

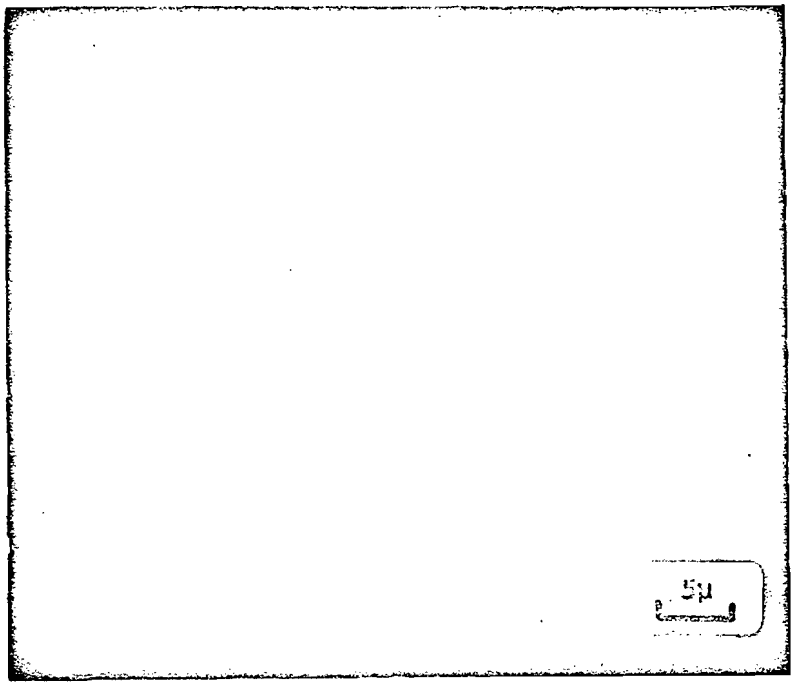

(b)

Figure 17. SEM photographs of nitrogen atomized powders.
(a) Surface of as-atomized powder showing a dendritic structure
(b) ZrO_2 particles visible on the surface of these powders after the reduction treatment

The thermodynamics of reduction can be appraised by considering the following reactions:

$$Cu_2O + H_2 = 2Cu + H_2O \quad (1)$$
$$2Cu_2O + Zr = ZrO_2 + 4Cu \quad (2)$$
$$Zr + 2H_2O = ZrO_2 + 2H_2 \quad (3)$$

Essentially selective oxidation of Zr to ZrO_2 is being obtained from oxygen available from the Cu_2O and H_2O. Similar observations have been made on atomized nickel powders, after an internal oxidation cycle[55].

Further insight as to the kinetics of this reaction can be obtained from Figure 17b. It can be clearly seen that the ZrO_2 particles are preferentially formed at the dendritic boundaries with very few and relatively fine particles being visible on the matrix. This can be attributed to the two following reasons:

1. Rejection of Cu_3Zr (eutectic) at the dendritic boundaries during solidification of the powder particles[56].

2. For the temperature range of the reduction treatment (300-500°C) it is known[57] that the coefficient of diffusion on the surface (D_s) is greater than in the dendrite and grain boundaries (D_b) which in turn is greater than in the matrix (D_m) or $D_s > D_b > D_m$.

Therefore, it can be safely assumed that formation of ZrO_2 is mainly obtained at the surface of the powder during reduction, as the temperature (450°C) is too low and the time (10 hours) too short to obtain any substantial volume diffusion of either oxygen (whose solubility in copper at

450°C is almost zero) into the matrix, or of zirconium to the surface.

2. Powder Compaction

As mentioned before (Chapter V), only some of the initial powders were cold isostatically compressed before extrusion. Owing to their low green strength, accurate density measurements were impossible to obtain (as breakage occurred during weighing, etc.). As these powders (-149μ) upon gravity packing had a relative density of 61 to 65% of that of pure copper (8.93 grm./cm.^{3}), the isostatic compacts were assumed to have been around 65 to 70% of theoretical density. Appendix 2 tabulates compaction densities of all the powders before extrusion.

3. Extrusion

As preliminary specific gravity and optical microscopy studied indicated that all the extrusions were essentially fully dense, accurate specific gravity values were not obtained.

C. Extruded Alloys

1. Alloys from Steam Atomized Powders

Optical metallography on these alloys revealed the characteristic fiber-stringer structure indicative of materials made through powder metallurgical techniques[58,59]. The unhomogenous distribution of coarse (0.5 to 1.0μ) ZrO_2 particles in the powders (Figure 10b) resulted in severe localized stringers oriented in the direction of extrusion (Figure 18a). Some areas between these stringers, owing to a very low

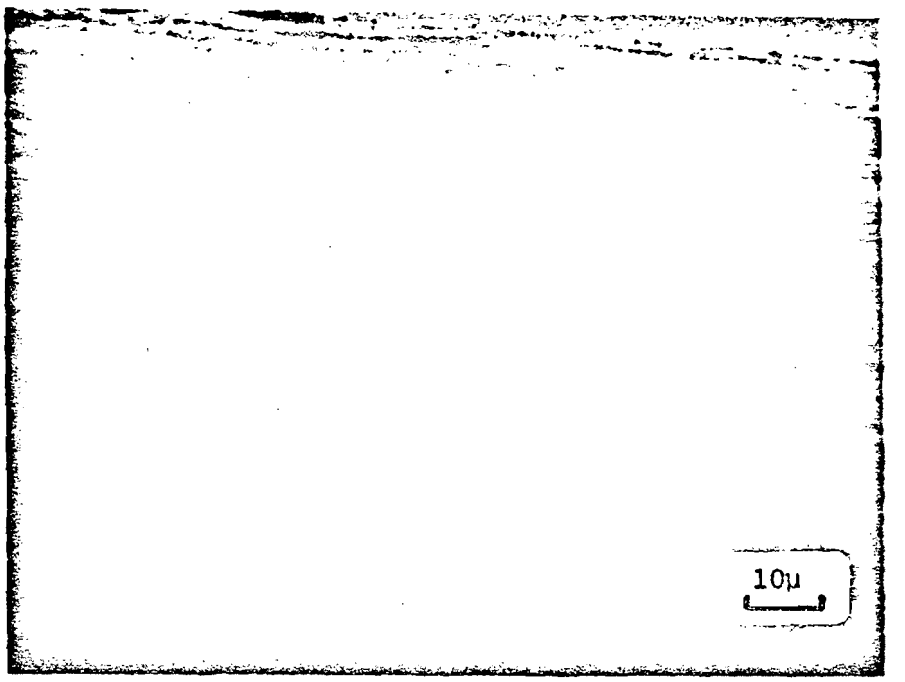

(a)

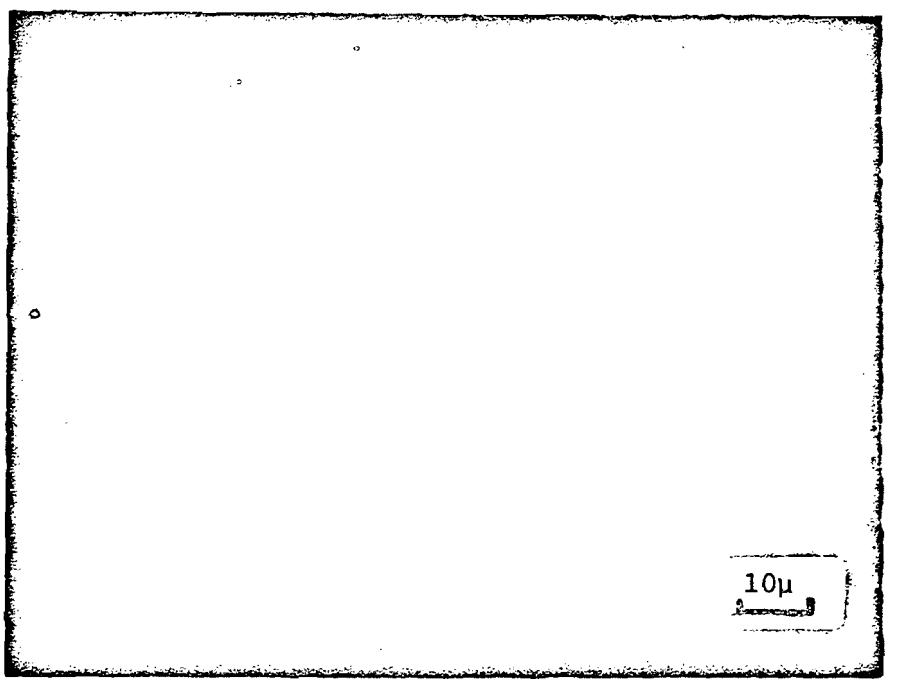

(b)

Figure 18. Typical microstructures observed of extruded steam atomized powders.

(a) Longitudinal section showing localized oxide stringers
(b) Transverse section with clusters of ZrO_2

volume fraction of dispersoid, show localized recrystallization. Figure 18b shows a transverse section typical of all these alloys; a grain size in the range of 5-15μ was measured. Localized clusters of ZrO_2 were observed in all the extrusions. Grain size in the recrystallized patches between the oxide stringers, in the longitudinal direction (Figure 18a), was of the same magnitude as that observed in the transverse direction, but stringer size and distribution could not be generalized owing to their unhomogenous nature. Laue diffraction studies on all the extrusions revealed the absence of extensive cold work since the K_α doublet could be resolved in all cases. Hence it was assumed that all the alloys were in a recovered state in the as-extruded condition.

As a preliminary evaluation of the stability of the extruded alloys, the effect of annealing (one hour at temperature) on the room temperature hardness was examined. The results obtained are presented in Figure 19. In each case 500°C is the limit of stability, as large decreases in the hardness values are obtained on annealing beyond this temperature. As the alloys are in a recovered state in the extruded condition, this drop in hardness is attributed to recrystallization. Optical metallography revealed the occurence of grain growth at 550°C.

Relatively poor room temperature tensile strength values were obtained for these alloys (Table XII). This is attributed to the almost complete conversion of Zr to ZrO_2 (Table VIII), and its large size and distribution in the alloys. The recovered condition of the alloys probably also contributed to their lower strength values. The higher strength values

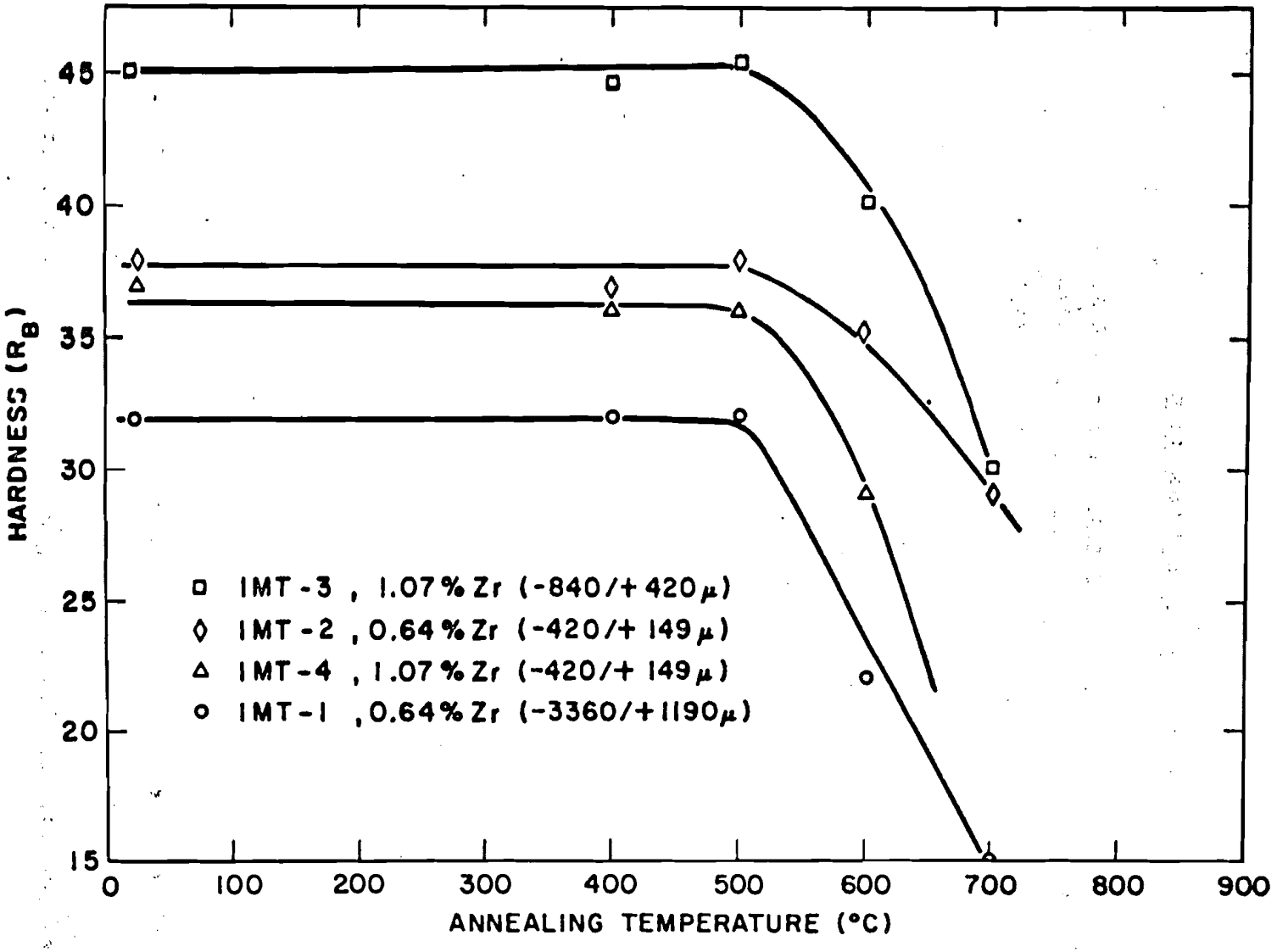

Figure 19. Hardness at 20°C as a function of annealing temperature (1 hr. at temp.) of extruded steam atomized powders.

Table XII

Tensile Properties of Steam Atomized Powders in the As-Extruded Condition

Alloy	Y.S. (0.2%) Offset (psi)	U.T.S. (psi)	Elong. (%)	R.A. (%)
IMT-1	26,000	38,500	31.6	55.2
IMT-2	25,000	35,000	32.0	71.0
IMT-3	45,000	47,500	23.3	30.0
IMT-4	28,000	37,000	25.4	31.2

obtained for IMT-1 and IMT-3 can be related to the greater availability of unoxidized zirconium in the initial powders (Table VIII). The ductility values in all cases seem to be good, with the higher zirconium content alloys (IMT-3 and 4) having the lower values, as would be expected.

Unfortunately none of these alloys could be further cold worked. Upon as little as 5% strain, cracking was obtained along the stringer boundaries. Concentration of coarse ZrO_2 agglomerated at these boundaries makes them extremely weak in the transverse direction, causing delamination upon cold work. All these alloys could be hot worked (over 400°C), but since preliminary results showed no appreciable improvement in room temperature properties up to 50% reduction of area, this was abandoned. The lack of response of these alloys to hot work is presumed to be due to dynamic recovery[60,61] obtained during the hot working process. Dislocation annihilation[62,63] through climb, which can occur at these temperatures (400°C), probably caused dynamic recovery during the hot working

process.

Stress-rupture tests were performed on all steam atomized alloys in the as-extruded condition at 400°C in air. Figure 20 shows a plot of initial stress versus time to rupture (all the data are listed in Appendix 6). Although all alloys show the characteristic shallow slopes of oxide dispersed materials, their strength values are poor. No appreciable improvement in stress-rupture strength values was obtained upon hot working these alloys. For example, hot working IMT-3 at 400°C to 50% R.A. increased the 100 hour rupture life to 19,000 psi, as compared to 18,500 psi in the as-extruded condition. Intergranular fracture was observed in each case, with extensive void formation at stringer-grain interfaces.

One of the objectives in this series of alloys was to investigate the effect of initial powder size (Table II), and hence of cooling rate on the properties of the final wrought product. Owing to the lack of a well defined dendritic morphology in these powders, accurate cooling rates could not be calculated, but it was assumed that the coarser powders had a slower cooling rate. In both room temperature (Table XII) and high temperature (Figure 20), strength and stability studies (Figure 19), IMT-3 840 to 420μ powder size was found to be the most stable. In the case of the lower zirconium content alloys, again the coarser initial powder (IMT-1, powder size 3360 to 1190μ) resulted in superior strength, both in tensile and stress-rupture, over its counterpart (IMT-2, powder size 420 to 149μ). Although this observable trend of coarser powders yielding superior properties is interesting, since they would result in important

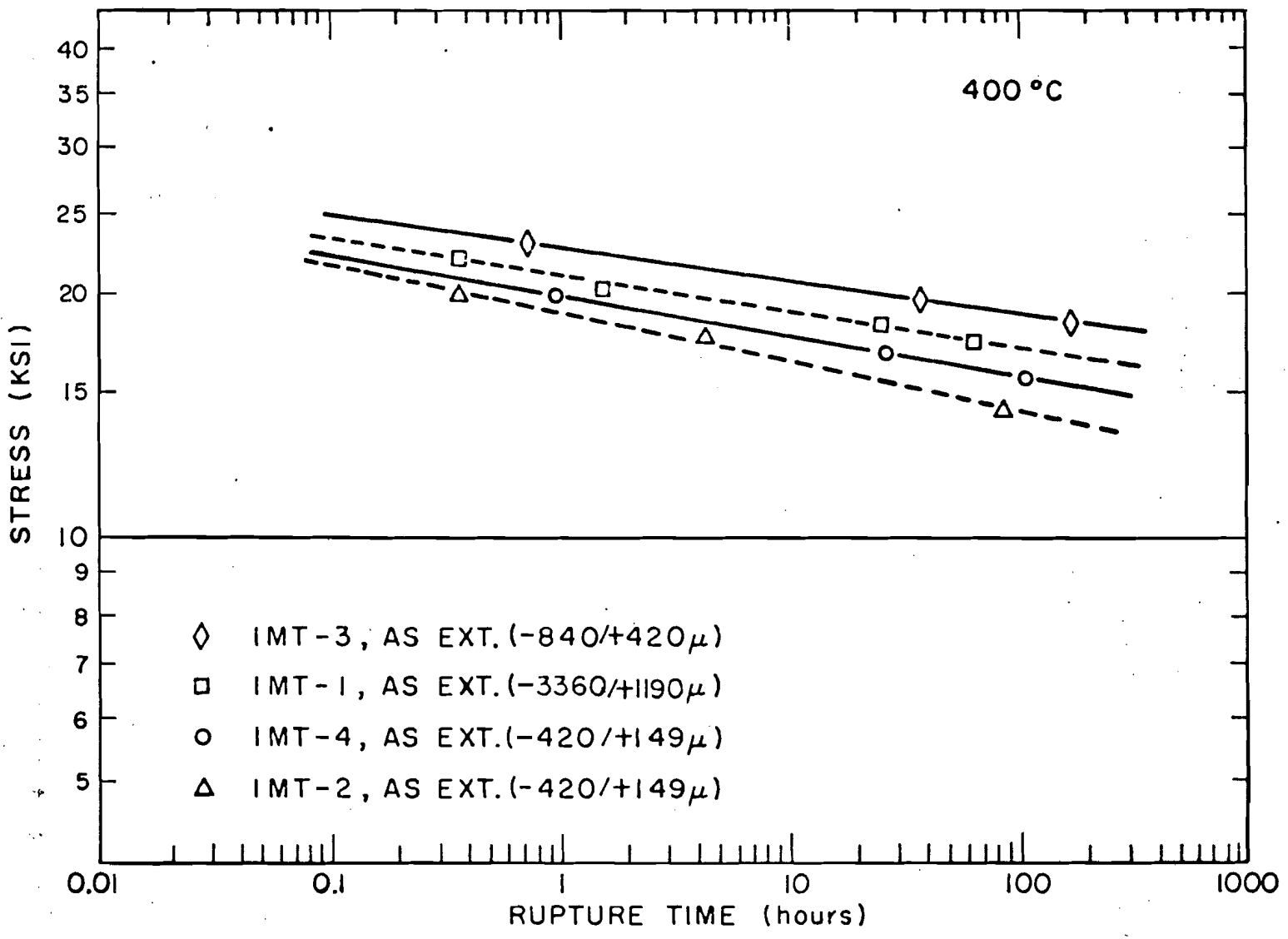

Figure 20. Log stress versus log rupture time plot of the extruded steam atomized powders.

processing economics, it is not an entirely fair analysis owing to variation in Zr, ZrO_2 (Table VIII) and oxygen (Appendix 1) in all cases.

2. Alloys made from Nitrogen Atomized Powders

The powders were atomized in two batches, in one case five pound lots of fine (-149μ) powder were made (ZA-2, 3, 8 and ZAC-1), while in the second case, seventy five pound heats were made to obtain a spectrum of powder sizes (FM-8, ZA-10 and ZAC-2). As mentioned earlier, only powders of less than 1000μ in size were used (Table V), because the coarser size powders were always obtained as flaky foils. The oxygen contents of these alloys varied from 0.03 to 0.12 wt. % (Table V). This relatively high oxygen content is due to the atomization process. If it is assumed that all the oxygen is tied up with zirconium to form ZrO_2, then these alloys contain 0.12 to 0.44 wt. % ZrO_2 (Table XIII). The presence of ZrO_2 was confirmed by X-ray and chemical analysis.

Optical metallography on ZA-2, 3, 8, FM-8 and ZAC-1 revealed that all these alloys had a very fine grain size range of 2-6μ in the transverse direction, with characteristic elongated grains oriented in the direction of extrusion in the longitudinal sections. Figures 21a and b show photomicrographs of typical longitudinal and transverse sections observed for the fine batch of powders (this also includes the fine -149μ size FM-8 powder). Although optical metallography gave a generalized view of the grain boundaries (Figure 21) owing to the fineness of the structure, no information as to distribution and nature of the dispersoid, or of grain morphology could be obtained. In spite of this, in

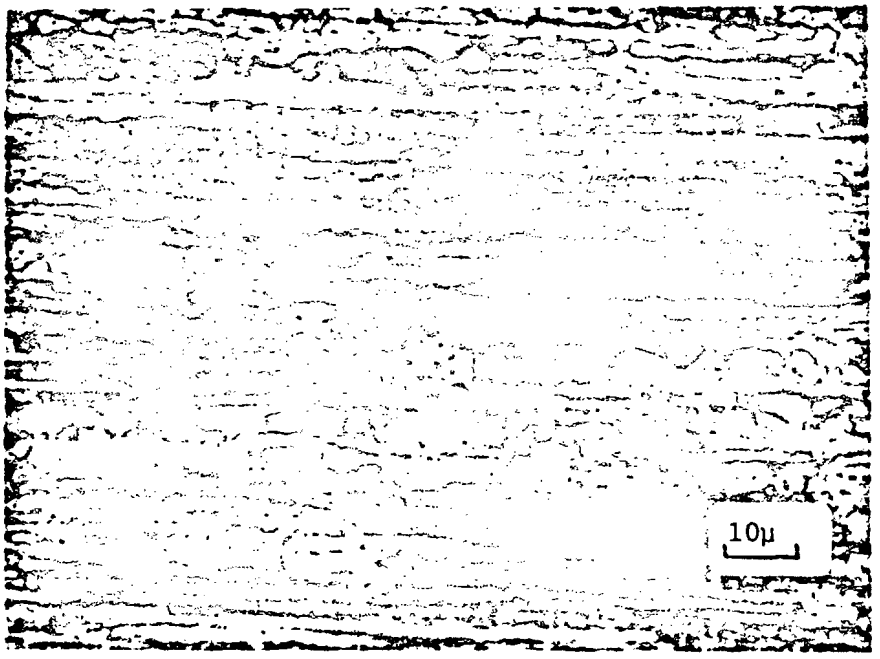

(a)

(b)

Figure 21. Typical microstructures observed for nitrogen atomized powders.
(a) Longitudinal section
(b) Transverse section

Table XIII

Estimated* Final Alloy Compositions of the Nitrogen Atomized Alloys

Alloy	O_2 Wt. %	Zr Wt. %	ZrO_2 Wt. %	Cr Wt. %	Cu(bal) Wt. %
ZA-2	0.03	0.11	0.12	---	99.77
ZA-3	0.03	0.28	0.12	---	99.60
ZA-8**	0.08	0.57	0.31	---	99.13
FM-8**	0.11	0.54	0.44	--	99.02
ZA-10(a)	0.09	0.64	0.35	--	99.01
ZA-10(b)	0.08	0.67	0.31	--	99.02
ZAC-1	0.04	--	0.14	0.32	99.54
ZAC-2(a)	0.07	0.03	0.27	0.33	99.37
ZAC-2(b)	0.07	0.03	0.27	0.33	99.37

* Assumes all the oxygen in the alloys is combined with Zr to form ZrO_2; this permits calculation of the wt. % ZrO_2 present.

** Chemical Analyses agreed with estimated values.

the higher zirconium content alloys (FM-8 and ZA-8), clusters of agglomerated ZrO_2 were observable throughout the matrix.

Transmission electron microscopy proved this to be true, as massive clusters of coarse ZrO_2 were observed in ZA-8 (Figure 16) and FM-8. The accurate size of these particles was hard to measure owing to their agglomerated nature, but measurements on the reduced powders (Figure 17b) and electron micrographs revealed their average size to be approximately 0.5μ with a measured range of 2 to 0.1μ. The ZrO_2 particles were found

to be fairly spherical in nature as is evident from Figure 17b. Examination of the lower zirconium content alloys (ZA-2 and ZA-3), or the ternary Cu-Zr-Cr alloy (ZAC-1), showed no evidence of such clustering, although some coarse particles (1 to 0.1μ) were generally observed, mostly at the grain boundaries in all of these alloys (Figures 22 and 23). As mentioned earlier, all the coarse particles were found to be too thick for selected area diffraction, but ZrO_2 diffraction spots were identified in all the alloys, from generalized diffraction patterns on the matrix. Some such indexed patterns are given in Appendix 3.

Figure 22 shows a transverse view of ZAC-1. Particularly noteworthy is the fine and well defined grain structure. Grain size measurements[53] on electron micrographs of several of these alloys compared favorably with the results obtained through optical metallography. Electron diffraction (Appendix 3) positively revealed the presence of both ZrO_2 and chromium in ZAC-1. The few relatively coarse particles (0.5 to 0.1μ) are assumed to be ZrO_2 formed during the reduction process, while the fine (less than 0.1μ) homogenously dispersed particles are probably a mixture of chromium precipitates and ZrO_2 (formed during the atomization process). Examination of the longitudinal sections of this alloy revealed several areas free from elongated grains (in the direction of extrusion). Well defined equiaxed grains were visible, showing the presence of localized recrystallization. A transverse section of ZA-2 is shown in Figure 23. Again a fine and homogenous dispersion of particles is observed. A positive identification as to the nature of the particles was impossible. Electron diffraction pos-

itively identified the presence of ZrO_2 (Appendix 3). No unidentifiable spots (as were observed in splat cooled material, Appendix 3) were obtained in the wrought alloy. The particles observed in Figure 23 can be broadly separated into two distinct size ranges. Relatively coarse (0.5 to 0.1μ) particles, which are probably ZrO_2 formed originally on the surfaces of the powders during reduction, and fine (less than 0.1μ) homogenously dispersed particles which are considered to be a mixture of ZrO_2 (formed during atomization) and the intermetallic Cu_3Zr.

Except for ZA-2 (which was extruded at a temperature 50°C lower than the other alloys) the K_α doublets could be resolved from the Laue diffraction patterns on all the other extrusions. In the case of ZA-2, slight line broadening was observed, signifying the presence of cold work. Transmission electron microscopy revealed the presence of some dislocations in all the as-extruded structures (Figures 16, 22, 23 and 28), with ZA-2 containing the highest dislocation density. Most of the grains observed in ZA-2 were relatively free of dislocations, the dislocations visible in the large grain (Figure 23) seem to be pinned by particles which apparently impeded their motion. A dislocation network forming a subgrain boundary between two grain boundaries can also be observed. All these features indicate that ZA-2 is in a partially recovered state. Due to the lower dislocation density and the resolution of the K_α doublet on the Laue diffraction patterns, all the other alloys are presumed to be in an almost completely recovered state in the as-extruded condition. Therefore, it is felt that stored energy due to extrusion did not contribute to any great

extent to the mechanical properties of any of these alloys.

Two extrusions (one from -149μ and the other from -840 to +149μ size powders) were made of each of the alloys, ZA-10 and ZAC-2, from the second batch (75 lb heats) of powders. This was done to investigate the effect of dendrite size in the powders (and hence cooling rate) on properties of consolidated wrought products. Unfortunately, owing to undesirable powder shapes and oxygen contents, a wider spectrum of powder sizes could not be examined.

All alloys possessed the characteristic fibre-stringer structure so often indicative of wrought products obtained through powder metallurgical techniques. Figure 24 shows optical micrographs of typical structures observed in all these alloys. The concentration of ZrO_2 at stringer boundaries is clearly visible (Figure 24a). Particularly noteworthy is the distribution of the ZrO_2 dispersoid around original particle boundaries in the transverse direction (Figure 24b). This almost continuous film of oxide outlining the particle boundaries is believed to have been formed from ZrO_2 particles obtained on the surface of the powders during the reduction reaction. The reason for its continuous nature, rather than the clustering obtained in FM-8 and ZA-8, is conceivably due to the higher oxygen content of these powders in the as-atomized condition (Table III). Laue-diffraction studies on these alloys showed the absence of cold work in the as-extruded condition.

All the alloys have a very fine grain size (5-10μ) in the transverse direction. Since only two dendritic sizes, 6 and 12μ with approximate

Figure 22. Transmission electron micrograph of ZAC-1 showing fine and well defined grain structure.

Figure 23. Electron micrograph of ZA-2 showing particle distribution and size range obtained in the extruded condition.

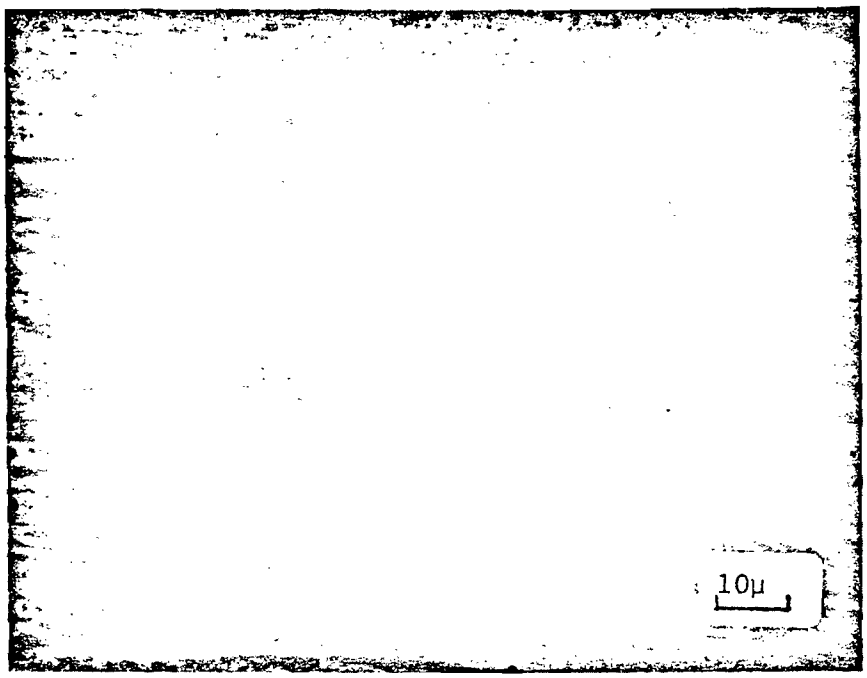

(a)

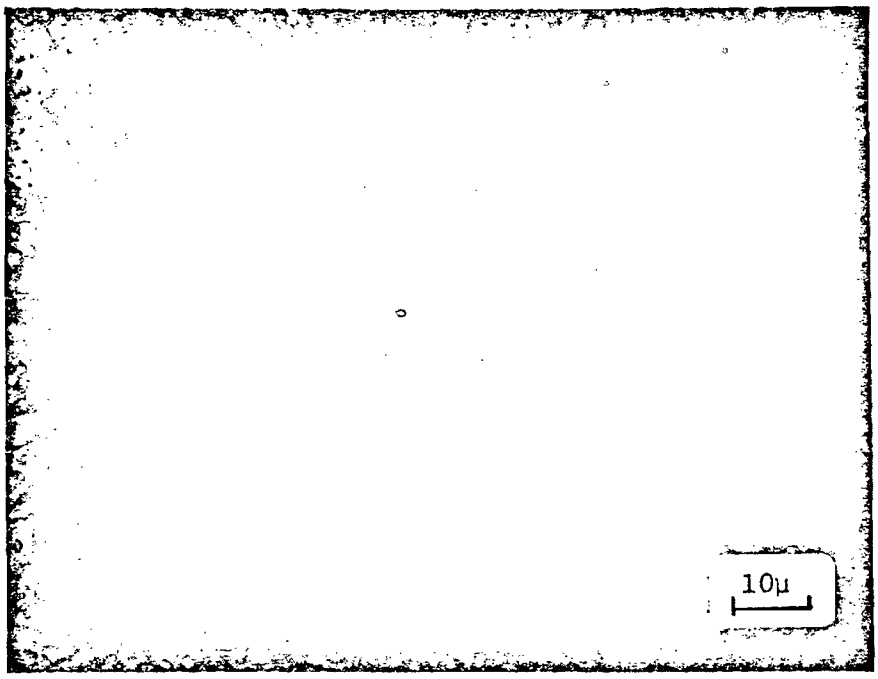

(b)

Figure 24. Typical microstructures observed for coarse (840/149μ) nitrogen atomized powders.
(a) Showing ZrO_2 stringers (longitudinal section)
(b) ZrO_2 outlining particle boundaries (transverse section)

cooling rates of 10^4 and 10^3 °C per sec. respectively, were examined in this instance, no generalized conclusions as to the influence of initial powder size (or cooling rate) on the final structure can be drawn. But for the two cooling rates examined, there seems to be no correlation between final grain sizes of the wrought products and the initial dendrite size of the powders. As a direct correlation exists between structure and properties, the use of coarser powder within a certain spectrum of cooling rates would mean important processing economics without sacrifice of structure refinement.

As a preliminary evaluation of the stability of these alloys, the effect of one hour anneals on the room temperature hardness was examined. The results obtained are shown in Figure 25 and Figure 26. In both figures a comparison between a commercial ingot cast alloy (Cu-0.22 wt. % Zr) and the wrought alloys extruded in the present instance is made. It can be seen clearly that all the alloys made through powder techniques are more stable above 600°C. This is attributed to refinement in structure (Table XIV) obtained through this technique, and the presence of ZrO_2 in all the alloys. Optical metallography revealed the occurence of grain growth immediately after softening (600-700°C). For example, in ZA-2, the first signs of grain growth were observed around 600°C. At 700°C the average grain size was calculated to be 8μ (average starting grain size was around 3μ). Annealing twins were clearly visible throughout the structures, with a few localized areas where no discernable change in grain size was visible. At 800°C the average grain size was around 10μ with the measured range

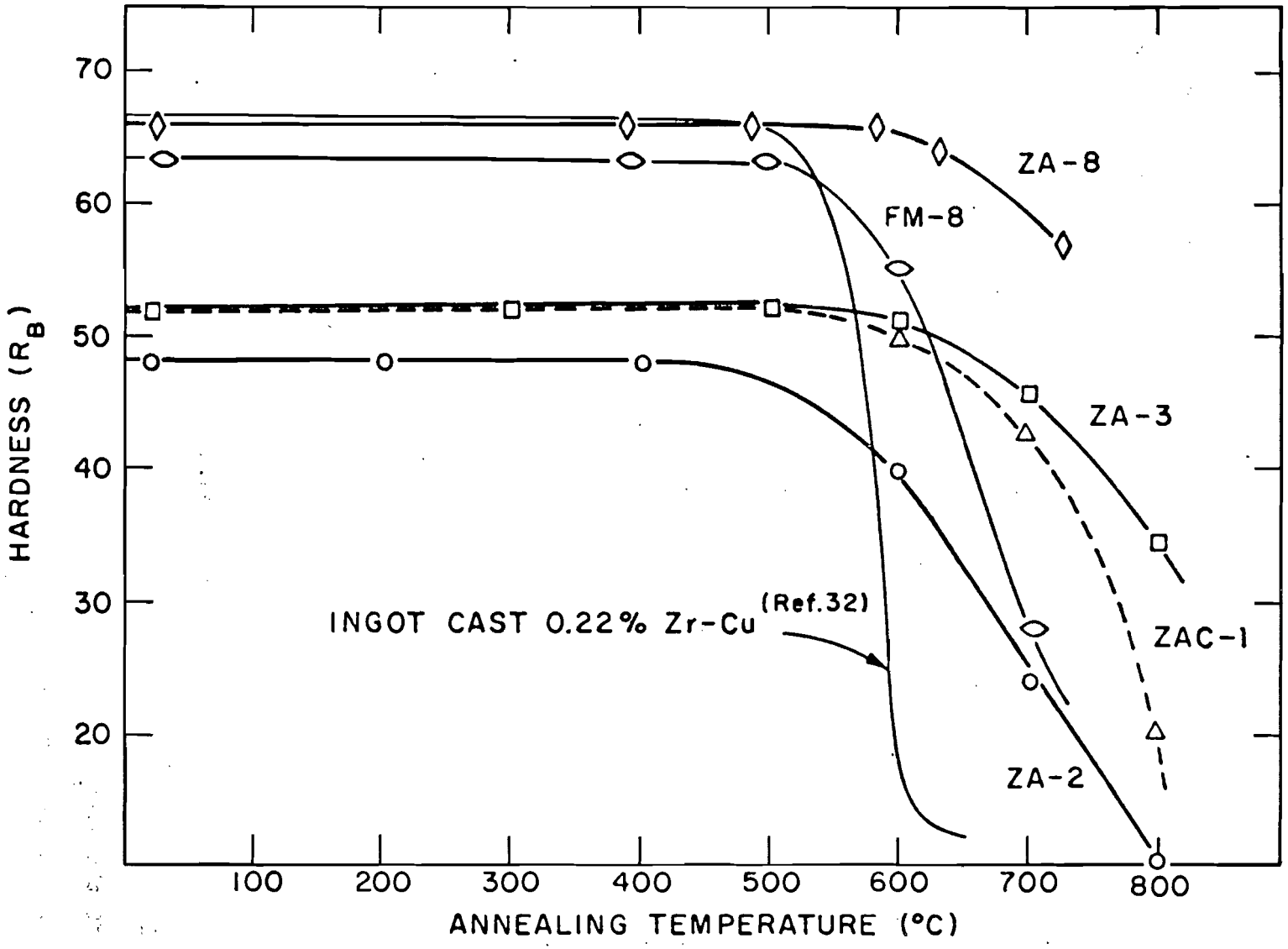

Figure 25. Hardness at 20°C as a function of annealing temperature (1 hr. at temp.) of as-extruded fine (-149μ) nitrogen atomized powders.

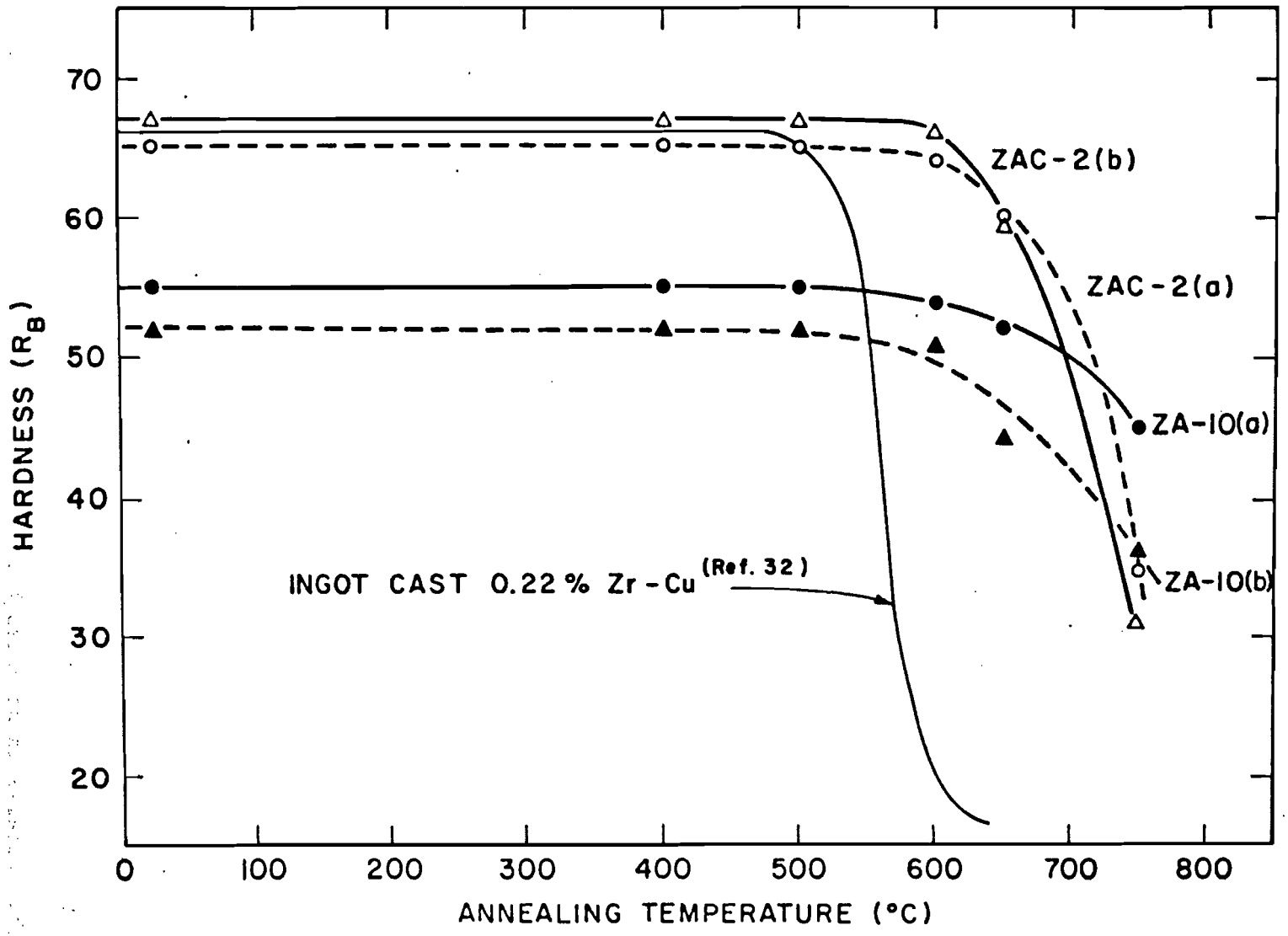

Figure 26. Hardness at 20°C as a function of annealing temperatures (1 hr. at temp.) of as-extruded coarse (-840/+149μ) nitrogen atomized powders.

varying from 3 to 15μ. The effectiveness of the ZrO_2 to prevent grain growth in these alloys is evident from these results.

Table XIV summarizes the properties of all these alloys in the as-extruded condition. These alloys show superior strength and ductility values compared to alloys of similar composition cast through conventional ingot techniques[33] (See Table XIII for compositions). Although a direct comparison between the elongation and the reduction of area values can not be made owing to different sample gage lengths, it can be seen that the cast alloys have much poorer ductility values. The increased strength and ductility values in these alloys are associated with the fine grain size, fine and homogenous dispersion of phases, and the absence of general segregation patterns.

Although zirconium additions to copper produce an age-hardening effect, response to precipitation hardening is slight and the mechanical properties are developed primarily by thermomechanical treatments. The ZAC series of alloys utilize a third element, chromium, but in spite of a pronounced strengthening on precipitation, the alloys still have to be cold worked to achieve optimum strength values.

As would be expected, a decrease in the softening temperature occurs after the alloys had been cold worked. Figure 27 shows the effect of one hour anneals on the hardness of ZA-2 and ZA-8 after 50% reduction of area compared to the as-extruded state. It is particularly noteworthy that unlike the as-extruded material, the alloys in the cold worked state show a slight decrease in hardness between room temperature and 400°C owing to

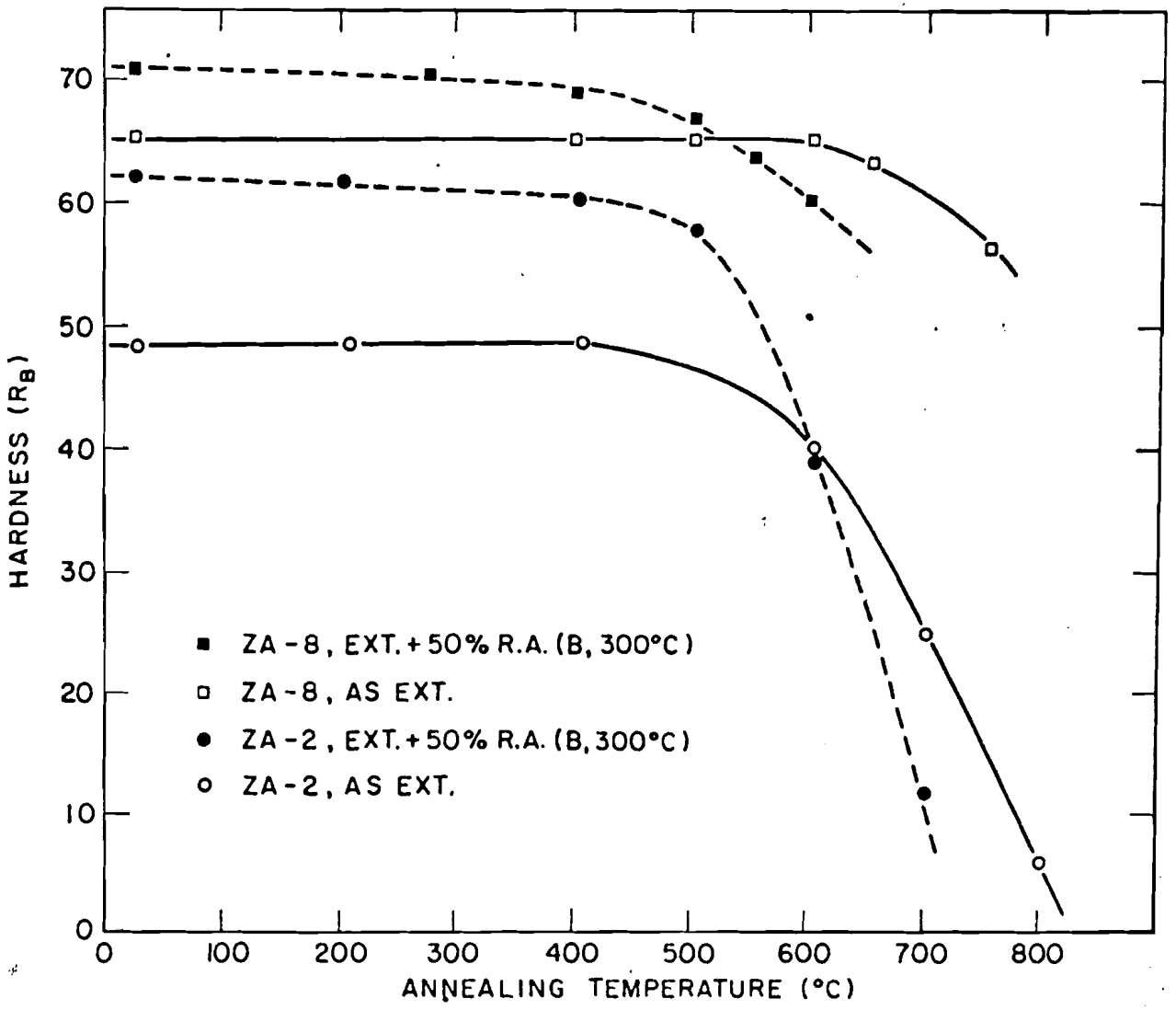

Figure 27. Hardness at 20°C as a function of annealing temperatures of as-extruded and cold worked (50% R.A.) ZA-8 and ZA-2.

Table XIV

Properties of As-Extruded Cu-Zr and Cu-Zr-Cr Alloys

Alloy	G.S. (μ)	Hard. (R_B)	Y.S. (psi)	U.T.S. (psi)	Elong.[1] (%)	R.A. (%)	Elec. Cond. (% IACS)
ZA-2	2-4	48	28,000	37,000	34.0	84.5	94.6
ZA-3	2-4	52	25,000	37,000	34.0	88.0	92.0
ZA-8	3-5	65	47,000	60,500	30.5	65.6	91.2
FM-8	4-6	63	37,000	50,000	34.4	80.5	90.6
ZA-10(a)	3-6	55	34,000	51,000	34.0	65.0	92.0
ZA-10(b)	4-6	53	35,000	50,500	27.5	63.0	92.5
ZAC-1	2-5	52	35,000	37,000	22.6	86.5	82.6
ZAC-2(a)	3-6	65	46,500	60,500	21.0	52.0	89.2
ZAC-2(b)	4-6	68	46,000	62,500	20.0	53.0	90.3
AMZIRC*	---	42	19,000	37,000	19.0	--	90.0
0.19% Zr**	---	--	45,800	45,500	06.0	--	--
0.40% Zr**	---	--	46,900	47,8000	05.0	--	--
0.74% Zr**	---	--	45,800	49,800	05.0	--	--

1. % Elong. on 0.634" gage length in extruded alloys and 2" gage length in cast material.

* 0.15% Zr, solution annealed at 980°C, aged 1 hour at 500°C[2].

** Experimental ingot type alloys produced by M.J. Saarivirta[33]. Material solution annealed at 900°C and quenched, cold rolled 25%.

recovery. This further affirms previous observations regarding the recovered nature of the alloys in the extruded condition. An average grain size around 1μ was measured after a 50% reduction which grew to around 9μ after a one hour anneal at 750°C. A further refinement in grain size to approximately 0.5μ was obtained upon a 75% reduction of area, while swaging ZA-2 to 90% reduction of area gave an estimated grain size in the

range of 0.3 to 0.2μ.

A standard solution annealing cycle of 980°C for thirty minutes was utilized for all the alloys. Owing to the fine and homogenous distribution of the precipitates in the as-extruded condition (Figure 28), it was felt that a short solution anneal time (30 minutes) would not only prevent extensive grain growth[29,31] but would be sufficient to obtain complete solid solution. This was observed to be the case through both optical and electron microscopy. The presence of several undissolved particles was observed in each case (Figure 29); based on analytical and X-ray results, these particles are assumed to be ZrO_2. This is quite probable, since all the alloys contain a substantial amount of ZrO_2 (Table XIII). This solution annealing treatment on ZAC-1 resulted in an average grain size of 10μ with an observed size range between 5 to 20μ.

Figure 30 shows the effect of one hour aging treatments on the hardness values of solution annealed ZAC series of alloys. The pronounced response to precipitation hardening of these alloys is evident, with peak hardness being obtained around 500°C in all cases. Almost identical behaviour is observable for ZAC-2(a) and ZAC-2(b) with the coarser powder alloy having slightly lower hardness values. The higher hardness values obtained in the ZAC-2 alloys are due to the presence of almost twice as much ZrO_2 (Table XIII). In spite of this, ZAC-1 is relatively more stable at the higher temperatures. This superior stability is attributed largely to the more effective retardation of grain growth

Figure 28. Electron micrograph showing the presence of very fine precipitates in the as-extruded structure of ZAC-1.

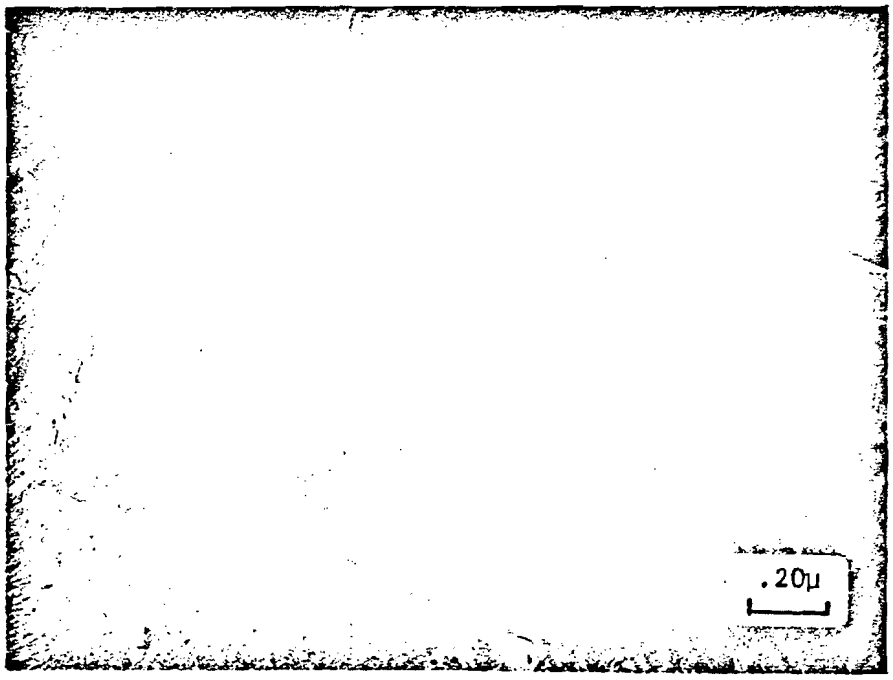

Figure 29. Replication electron photomicrograph of ZAC-1 after a solution anneal (980°C, 30 min.) showing the presence of undissolved ZrO_2 particles.

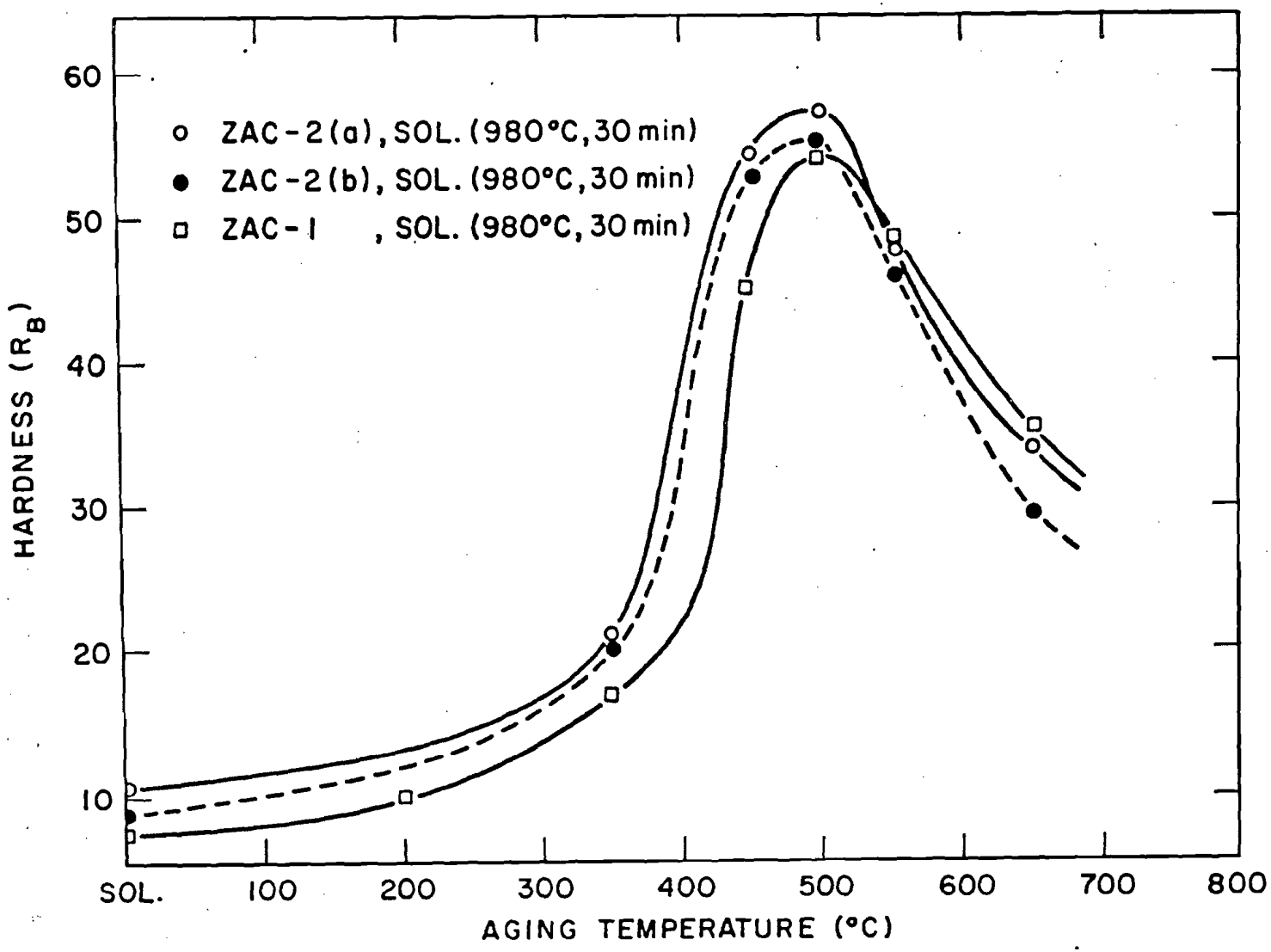

Figure 30. Hardness at 20°C after one hour aging of solution-annealed Cu-Zr-Cr alloys.

in ZAC-1 owing to its homogenous distribution of oxide in comparison to the agglomerated oxide at the particle boundaries in the ZAC-2 series of alloys. The effect of prolonged aging at 400, 450 and 500°C on hardness of ZAC-1 and ZAC-2(a), in the solutionized condition, and of ZAC-2(a) in the sol. + 50% R.A. condition, is shown in Figure 31. The most noteworthy features of these curves are:

a. The stabilization of hardness after the initial drop beyond peak hardness.

b. The maintainence of increased hardness in ZAC-2(a) due to cold work, even after 35 hours at 500°C.

c. The smaller hardness drop from peak to plateau in ZAC-1 at all temperatures.

Several similar characteristics between these curves and those obtained for the binary Cu-Cr alloys[65 to 69] are observed. Among the most significant are temperature (one hour aging time) to obtain peak hardness (around 500°C), and the decrease in peak hardness and time required to obtain it, with increasing temperature. The most striking difference in these alloys is the stabilization of hardness at all temperatures after the initial drop. This leveling in the hardness is believed to be due to the dispersion of ZrO_2 oxide in these alloys, and its effective retardation of extensive grain growth during prolonged aging cycles. At 400°C, no further drop in hardness was observed in any of the alloys even after a 50 hour aging cycle.

Laue diffraction studies revealed the complete recrystallization on the flat portion of these curves (Figure 31). Continuous spotty Debye rings signifying fine grain size were obtained, even after a 35

hour exposure at 500°C. This infers the retardation of grain growth after the initial hardness drop caused by recrystallization and precipitate coarsening. Grain size measurements, using optical metallography indicated ZAC-2(a) to have an average grain range size of 10-15μ after an aging cycle of 35 hours at 500°C, whereas the same cycle resulted in an average grain size range of 8-12μ at 400°C.

Figure 32 confirms the poor response of the copper-zirconium alloys to precipitate hardening. Again, as was the case with ZAC-2(a) and (b), the coarser powder alloy ZA-10(b) shows inferior strength than its counterpart ZA-10(a) made from the finer powder size range. As the grain sizes of the two alloys are comparable, this difference in hardness is probably caused by the difference in size and distribution of the continuous oxide film outlining the original particle boundaries (Figure 24). An unexplainable feature in Figure 32 is the sluggishness of ZA-3 to obtain peak hardness. All other alloys show a peak hardness at 500°C, in agreement with Saarivirta[2] but ZA-3 attains its peak hardness at 550°C. The effect of one hour aging at various temperatures on material cold worked to 50% reduction of area after solution treating (980°C, 30 minutes) is shown in Figure 33. The substantial drop in hardness obtained at 500°C, in all the alloys, is due to recrystallization. Again, the poor response to precipitation hardening of the copper-zirconium alloys (ZA-10 and ZA-8) is evident.

In order to optimize the strengths of these alloys, various combinations of precipitation hardening and thermomechanical work were

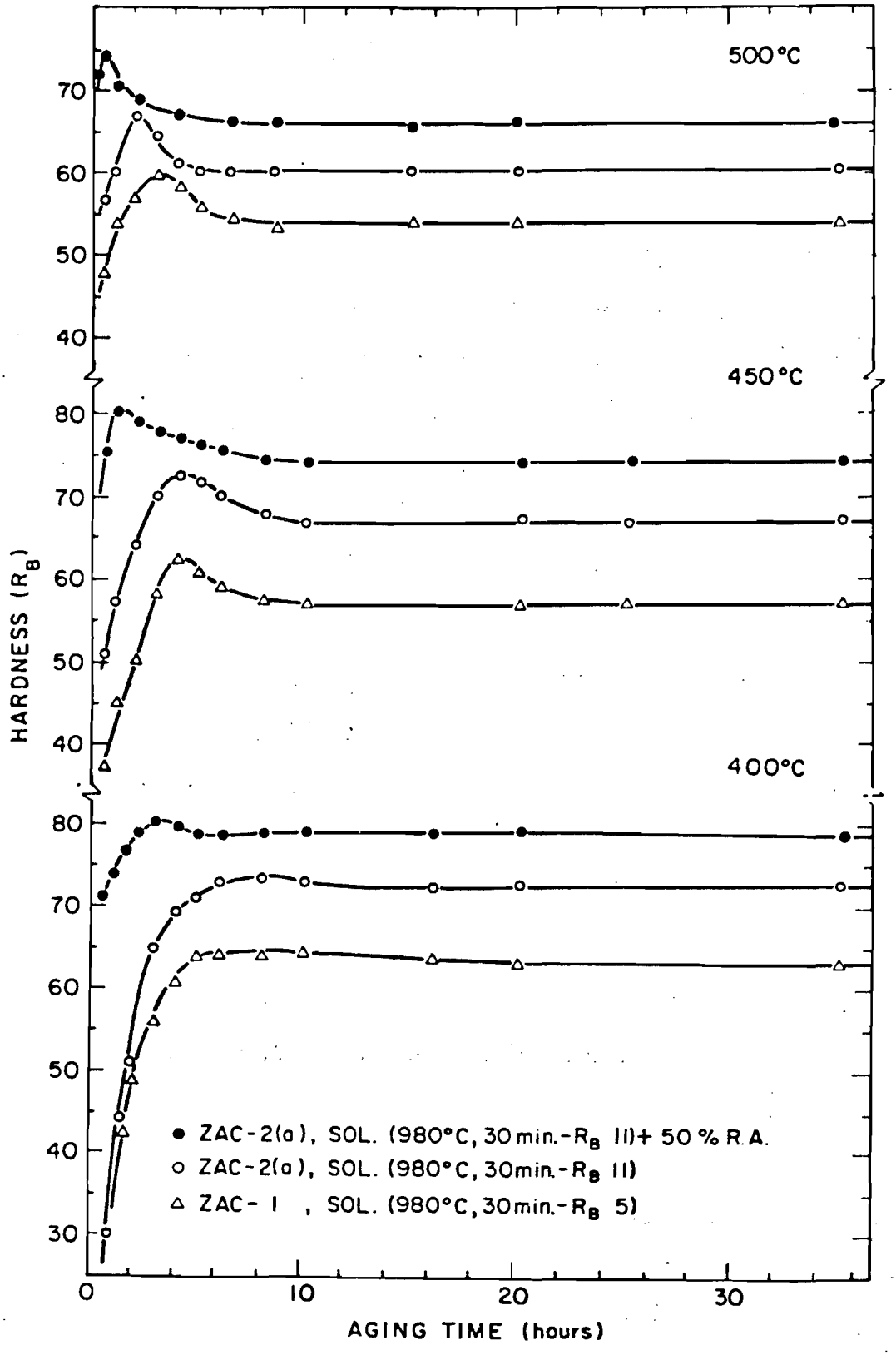

Figure 31. The effect of prolonged aging on the room temperature hardness values of ZAC-1 and ZAC-2(a).

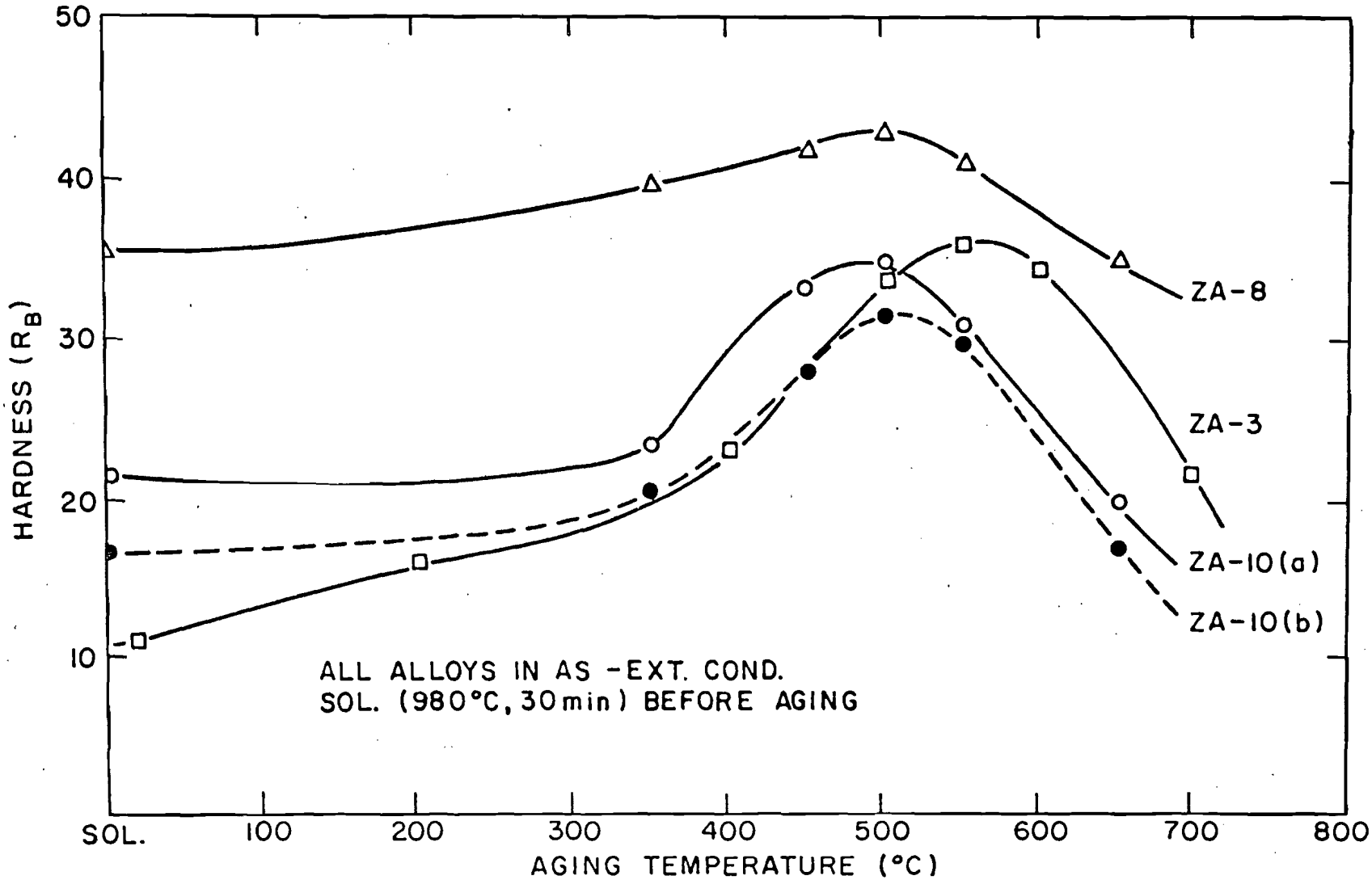

Figure 32. Hardness at 20°C after one hour aging of extruded plus solution annealed Cu-Zr alloys.

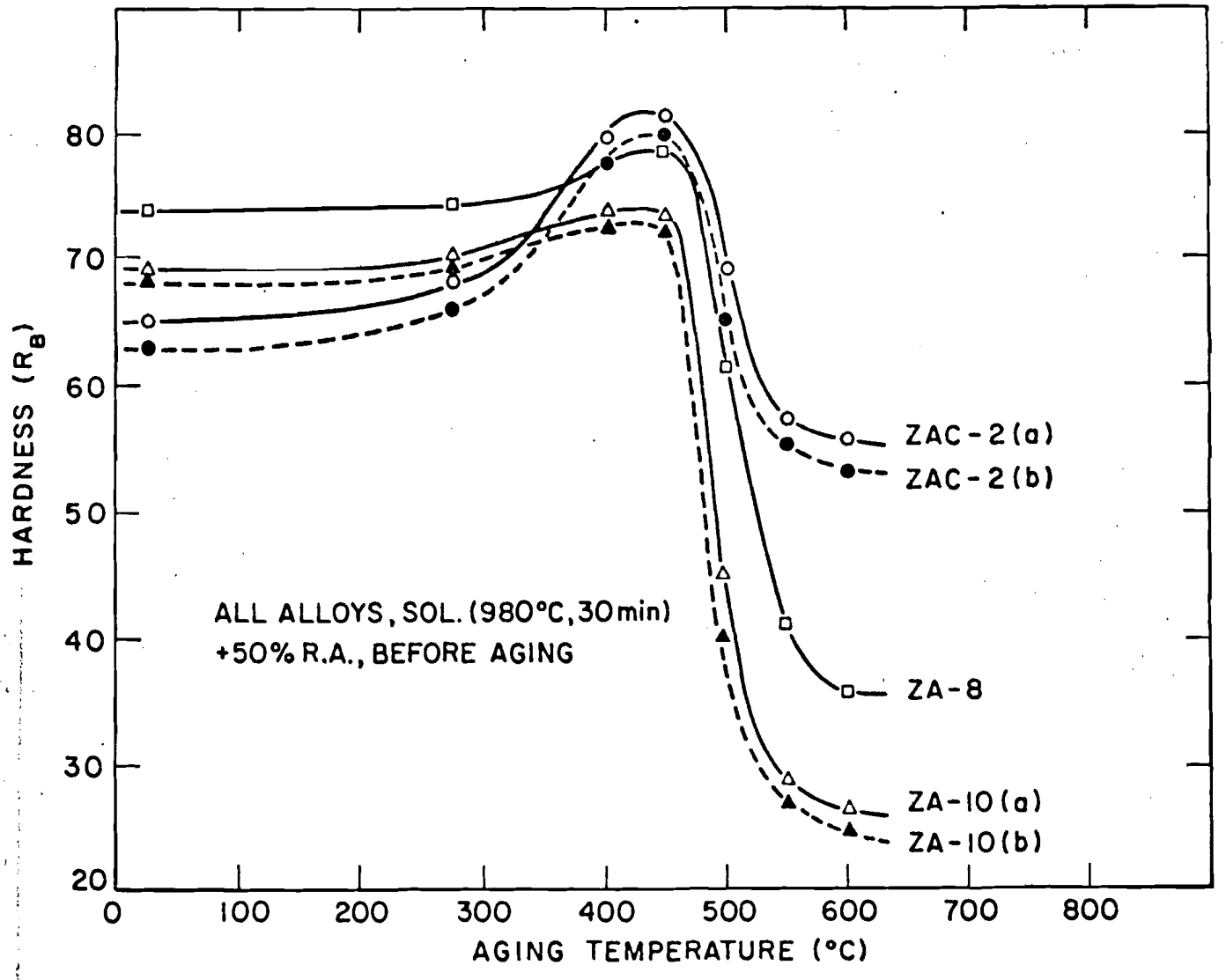

Figure 33. Effect of aging on room temperature hardness of solution annealed plus cold worked (50% R.A.) alloys.

utilized. The effect of cold work in increasing both room and high temperature properties is well established and has been experimentally confirmed by several investigations[70 to 75] in several alloy systems. In spite of this, the mechanism of strengthening is still controversial and poorly defined. Some of the factors contributing to the resultant strengthening are believed to be an improved distribution of dispersed phase and the development of fibrous structure[70,75], further densification of starting material[76], an apparent decrease in interparticle spacing[88] and stabilization of the substructure through intermediate annealing treatments[75].

Cold work introduces dislocations, which rearrange themselves into low angle boundaries (minimum energy configuration) during the annealing cycle. Essentially, the annealing cycle recovers the material of excess dislocations, thus helping the material to take more cold work. The number of dislocations introduced by the cold work step should be minimal in order to avoid the formation of recrystallization nuclii. The sub-boundaries (or dislocations if no cell formation is obtained) introduced by the TMT are then stabilized by the pinning action of the dispersoid. Hence, the annealing temperature (which should be below the recrystallization temperature of the material) and the amount of cold work introduced in each step, play an important role on the resultant properties during a TMT. With this in mind, several thermomechanical treatments were investigated (Table VI).

The variation in hardness obtained in ZA-8 owing to repeated cold

work and annealing cycles (Table VII) is shown in Figure 34. Figure 35 illustrates a similar effect on ZAC-2(a) after a solution anneal. A comparison between the two figures shows some obvious difference. In the case of ZA-8, it is evident that all the strengthening is obtained during the swaging cycle, while the annealing treatment just relieves the material of some stored energy. The drop in hardness, except in the last stages of TMT, is almost identical for each annealing cycle. In the case of ZAC-2(a), strengthening is obtained in the initial stages of the TMT (Figure 35) from both cold work and intermediate annealing (because of precipitation hardening).

The effect of cold work on the hardness of ZA-8 is shown in Figure 36. The hardness measurements were made after each swaging cycle. In the TMT with no intermediate anneals ("A" Table VI), softening due to excessive cold work is evident after about 60% reduction of area. ZA-8 cold worked to 50% R.A. (with no intermediate anneals) was found to have a yield strength of 67,500 and a tensile strength of 69,000 psi, whereas material cold worked to 75% R.A. under the same conditions had a yield strength of 63,000 and tensile strength of 68,000 psi (Appendix 5). The difference in yield strength values is indicative of slight softening.

Room temperature strength values (Table XV) obtained from ZA-8, correlate with the drop in hardness obtained upon increasing the intermediate annealing temperature (Figure 36). It is evident from Table XV that an intermediate annealing temperature of 300°C yields optimum

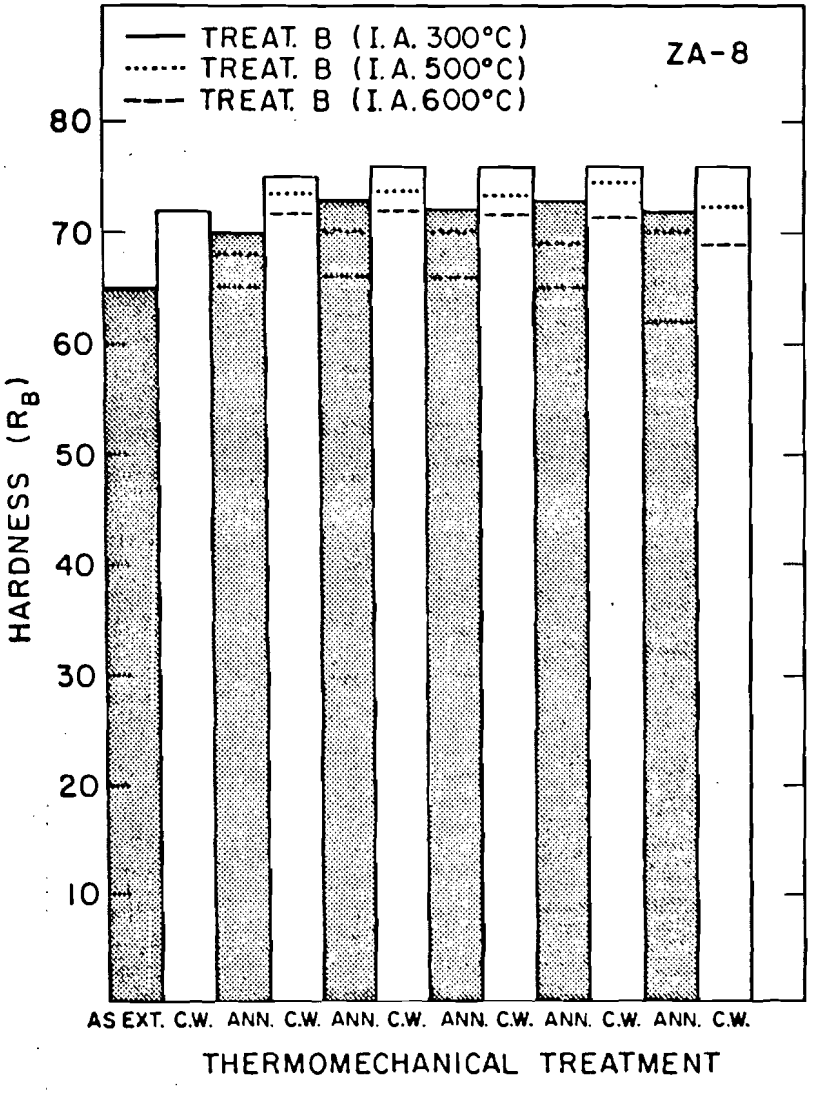

Figure 34. Hardness at 20°C during the TMT (B).

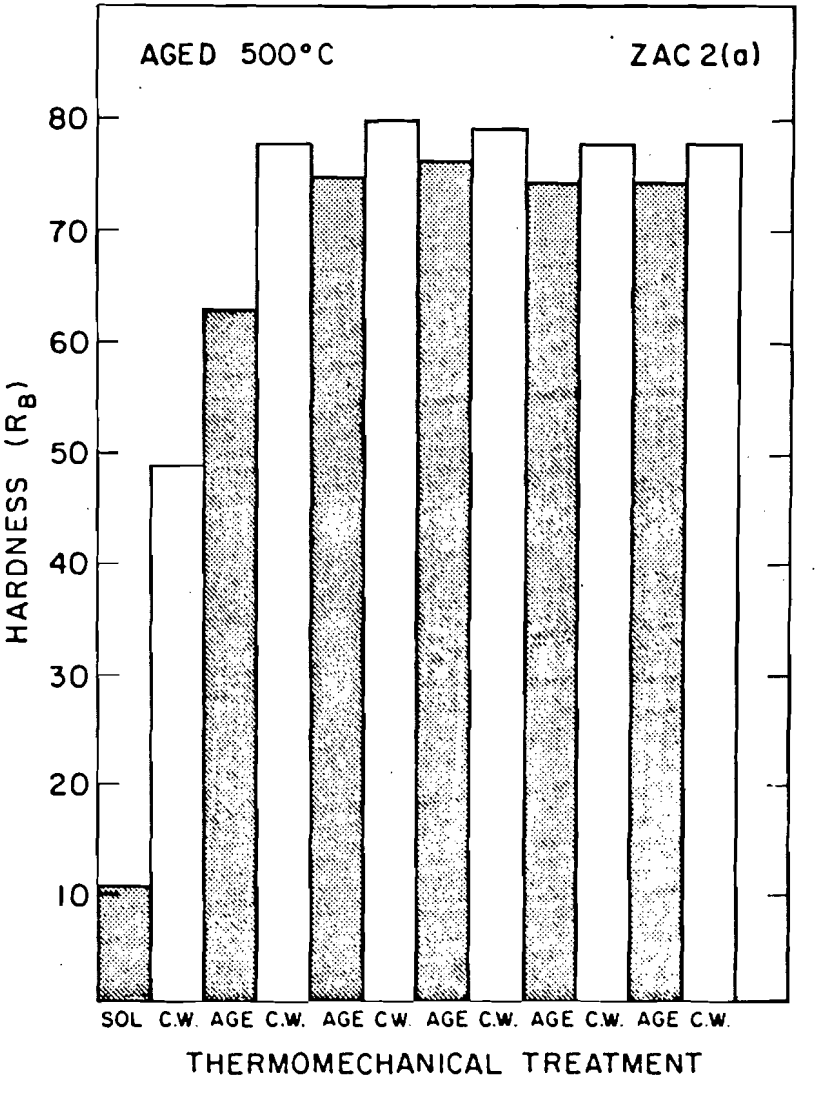

Figure 35. Hardness at 20°C during the TMT (C).

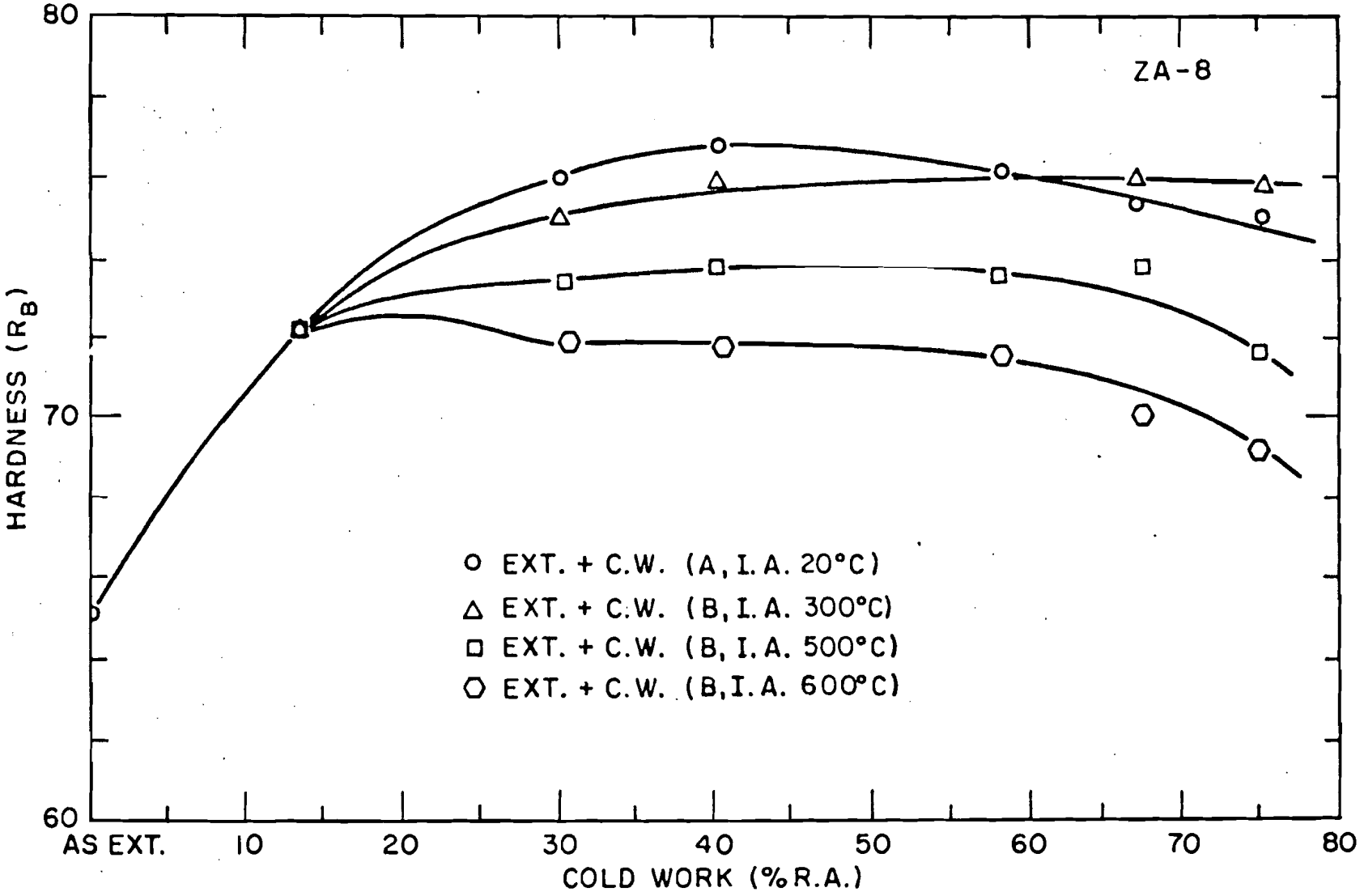

Figure 36. The effect of intermediate annealing temperature on room temperature hardness during a TMT.

Table XV

Effect of Intermediate Annealing Temperature on Tensile Strength of ZA-8

Treatment Designation	Y.S. (psi)	U.T.S. (psi)	Elong. (%)	R.A. (%)	Elec. Cond. (% IACS)
Ext + 75% R.A. (A, 20°C)	63,500	68,000	15.5%	70.0	88.1
Ext + 75% R.A. (B, 300°C)	69,000	76,000	18.0	78.0	88.5
Ext + 75% R.A. (B, 400°C)	63,000	68,000	18.8	74.0	88.9
Ext + 75% R.A. (B, 500°C)	61,000	67,000	19.0	78.0	90.5
Ext + 75% R.A. (B, 600°C)	59,000	66,000	20.2	76.0	88.4

strength values for ZA-8. The final grain size measured[53] using optical metallography was found to be approximately the same in all cases.

Figure 37 shows the effect of cold work (% R.A.) on the ultimate tensile strength values of ZA-2, 3 and 8; the yield strength values (Appendix 5) for all the alloys followed a similar trend and hence are not plotted in this figure. All other pertinent data related to this figure are tabulated in Appendix 5. No experimental evidence as to the reason for the sudden increase in strength after 60% R.A. in ZA-8 was found. ZA-2 and 3 show the expected leveling off of strength with increased cold work. Preliminary quantative X-ray studies on ZA-2 revealed that in the extruded condition the percentage of [111] component of the duplex fiber texture [111] + [100] was predominant. Upon further cold work, after 50% R.A., a gradual change was observed until, at 90% R.A., the predominance of the [100] fiber texture was evident. If it is assumed that a small difference in the zirconium (0.11 wt. % Zr in

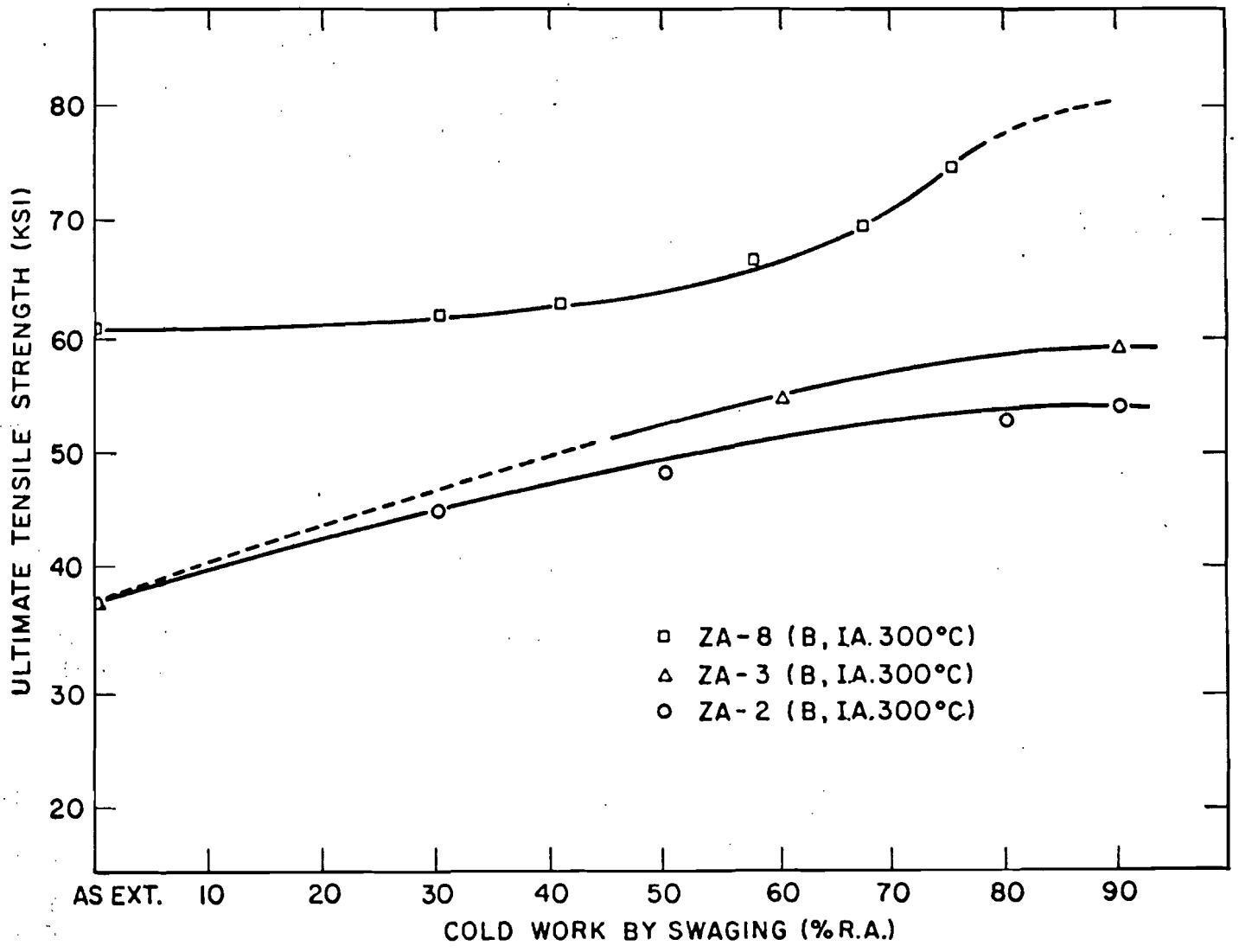

Figure 37. Effect of cold work (% R.A.) on room temperature tensile strength values.

ZA-2 and 0.54% Zr in ZA-8) does not drastically change the stacking fault energy in these alloys[77,78], then similar crystallographic changes as in ZA-2 should occur in ZA-8 upon cold work. If this is the case, then according to Hosford et al[79] a decrease in strength should be observed in these alloys upon cold work after 50% R.A., because they state that in a cubic structure, a wire with [111] or [110] fiber texture should be 50% stronger than one with a [100] texture. Hence it is felt, although this is not usually observed in copper[80], that twinning is causing reorientation out of [111] into [511][81]. Since [100] is near [511], perhaps the amount of material that appears to be in the [100] position is actually the amount that has undergone first-order mechanical twinning. No experimental evidence to confirm this was obtained.

An added strengthening factor is obtained on thermomechanically working solution annealed Cu-Zr-Cr alloys. In the initial stages of swaging, strengthening is obtained even during the annealing cycle because of an aging effect (Figure 35). Figure 38 illustrates the effect of both the swaging and annealing (1 hour at 500°C) cycles on the hardness values of ZAC-2(a). The complimentary strengthening effect obtained on repeated swaging and annealing (or aging) is evident on comparison of hardness values obtained during the TMT (Figure 38) and upon aging solution-annealed ZAC-2(a) (Figure 31).

Table XVI illustrates the difference in room temperature properties obtained through some of the TMTs investigated. A complete tabulation

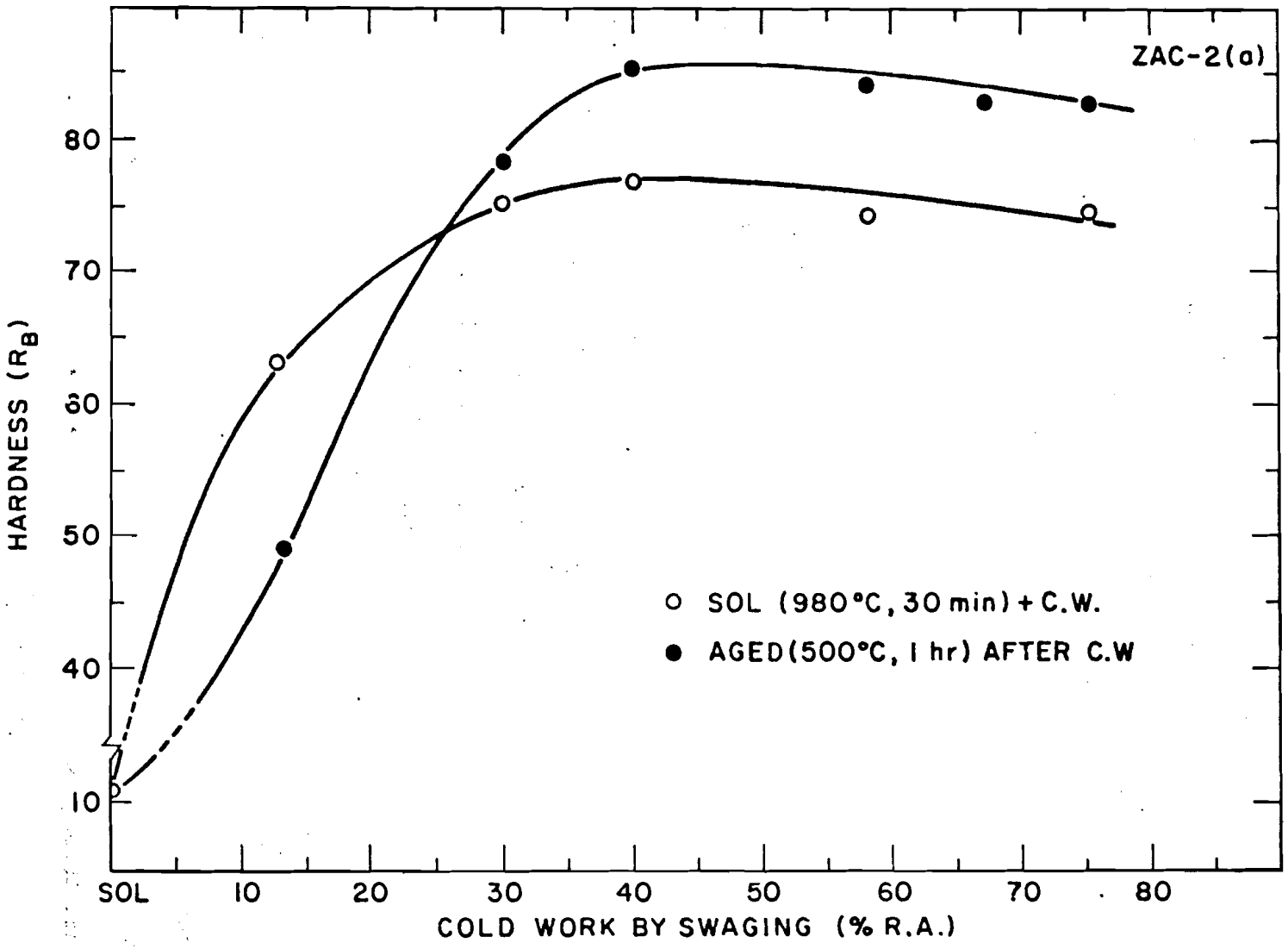

Figure 38. Hardness values (at 20°C) obtained during cyclic cold work and aging.

Table XVI

Effect of Various TMTs on Room Temperature Tensile Strength

Alloy & Condition	Y.S. (psi)	U.T.S. (psi)	Elong. (%)	R.A. (%)	Elec. Cond. (% IACS)
ZA-2					
90% R.A. (B, I.A. 300°C)	47,000	53,000	17.61	90.5	91.6
90% R.A. (C, Aged 450°C)	57,000	58,000	16.60	90.5	88.1
ZAC-1					
90% R.A. (B, I.A. 300°C)	50,500	51,500	14.0	89.0	80.1
75% R.A. (C, Aged 450°C)	73,000	76,000	14.0	85.0	85.0
75% R.A. (E, I.A. 500°C)	63,000	71.200	17.8	85.0	--
75% R.A. (D, Aged 500°C)	63,000	66,000	14.6	85.0	85.8
ZAC-2(a)					
75% R.A. (C, Aged 450°C)	77,000	80,500	11.8	60.0	--
75% R.A. (E, I.A. 400°C)	82,000	84,000	13.0	60.0	79.2
75% R.A. (E, I.A. 450°C)	84,500	86,000	13.2	72.0	81.2
75% R.A. (E, I.A. 500°C)	71,000	74,000	10.0	75.0	85.4

* See Table VI for complete information regarding the various TMTs.

of all tensile data for all the treatments investigated is given in Appendix 5. It is evident from this table that a pronounced response to precipitation and to various TMTs is obtained in these alloys. For both ZAC-1 and ZAC-2(a) cyclic swaging and annealing (or aging) of solution annealed material yields superior room temperature strength values without any loss of ductility, compared to a cold work (50% R.A.) age, cold work cycle. The effect of different intermediate aging temperatures is demonstrated in the case of ZAC-2(a), with 450°C yielding maximum strength values. It is particularly noteworthy that some of the TMTs result in a substantial increase in strength without any appreciable loss in ductility (elongation and reduction of area) values.

To simulate the effect of various brazing cycles on these alloys, their resistance to softening on short time (½ and 1 hour) elevated temperature exposures was investigated (Figures 39,40,41,42,43). Figure 39 shows the effect of prior deformation on the recrystallization temperature of ZA-2. Although a substantial increase in strength is obtained on cold working over 50% R.A., it is evident that all of it is lost after a half hour exposure over 500°C. Almost identical room temperature tensile strength values are obtained after exposure over 800°C, this is attributed to effective retardation of grain growth by the ZrO_2 dispersoid. The improvement in elongation obtained through annealing is also illustrated by Figure 39. The reduction of area (Appendix 5) values did not show any substantial change with these annealing treatments. The effect of intermediate annealing temperature during the TMT

on the softening behaviour of ZA-8 is shown in Figure 40. In spite of the higher strength levels obtained with the lower I.A. temperatures after the TMT, a half hour exposure above 650°C yields almost identical strength values for all the TMTs. Figure 40 also shows the effect of these annealing treatments on the elongation values of ZA-8. Again, the reduction of area values seem to be relatively insensitive to these exposures (Appendix 6). As is evident in both Figures 39 and 40, the Cu-Zr alloys show a typical recrystallization drop, with the further drop in room temperature strength, owing to grain growth being prevented by the ZrO_2 dispersion.

The effect of a short time elevated temperature exposure on the Cu-Zr-Cr alloys is shown in Figures 41 and 42. It is evident from these figures that neither aging temperature (Figure 41) nor different TMTs (Figure 42) have any substantial effect on the response of these alloys to short time elevated temperature exposures. A particularly noteworthy feature is the two drops obtained in strength values, especially in ZAC-2(a) (Figure 41). The first drop (400°C) can be associated with recrystallization while the second (600°C) is assumed to be caused by coarsing of the precipitate and its redissolution into solid solution. The effect of exposure time on the room temperature tensile strength values is shown in Figure 43. All other pertinent data on these tests are tabulated in Appendix 5.

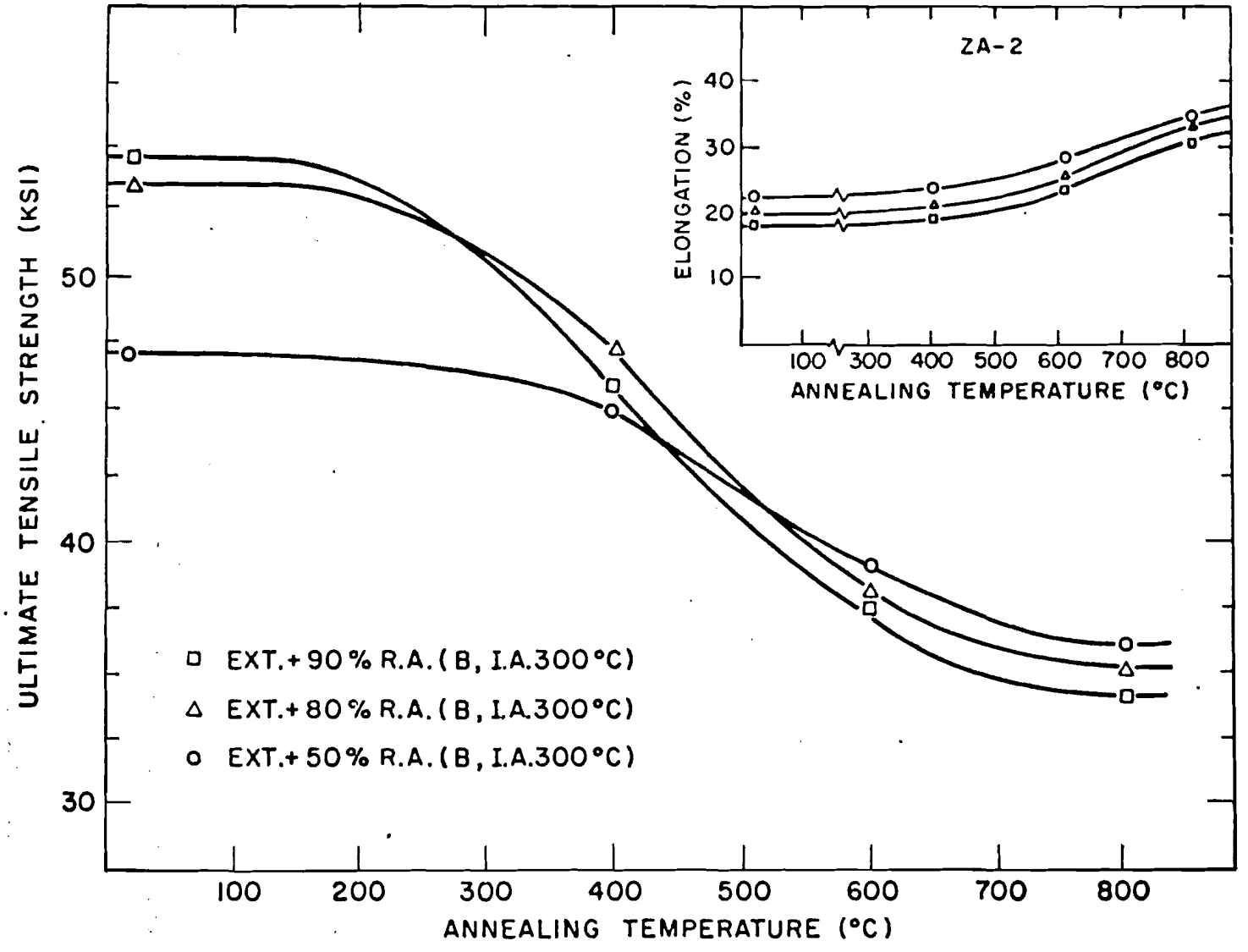

Figure 39. The effect of degree of cold work on stability of ZA-2 on short time (1 hr.) elevated temperature exposures.

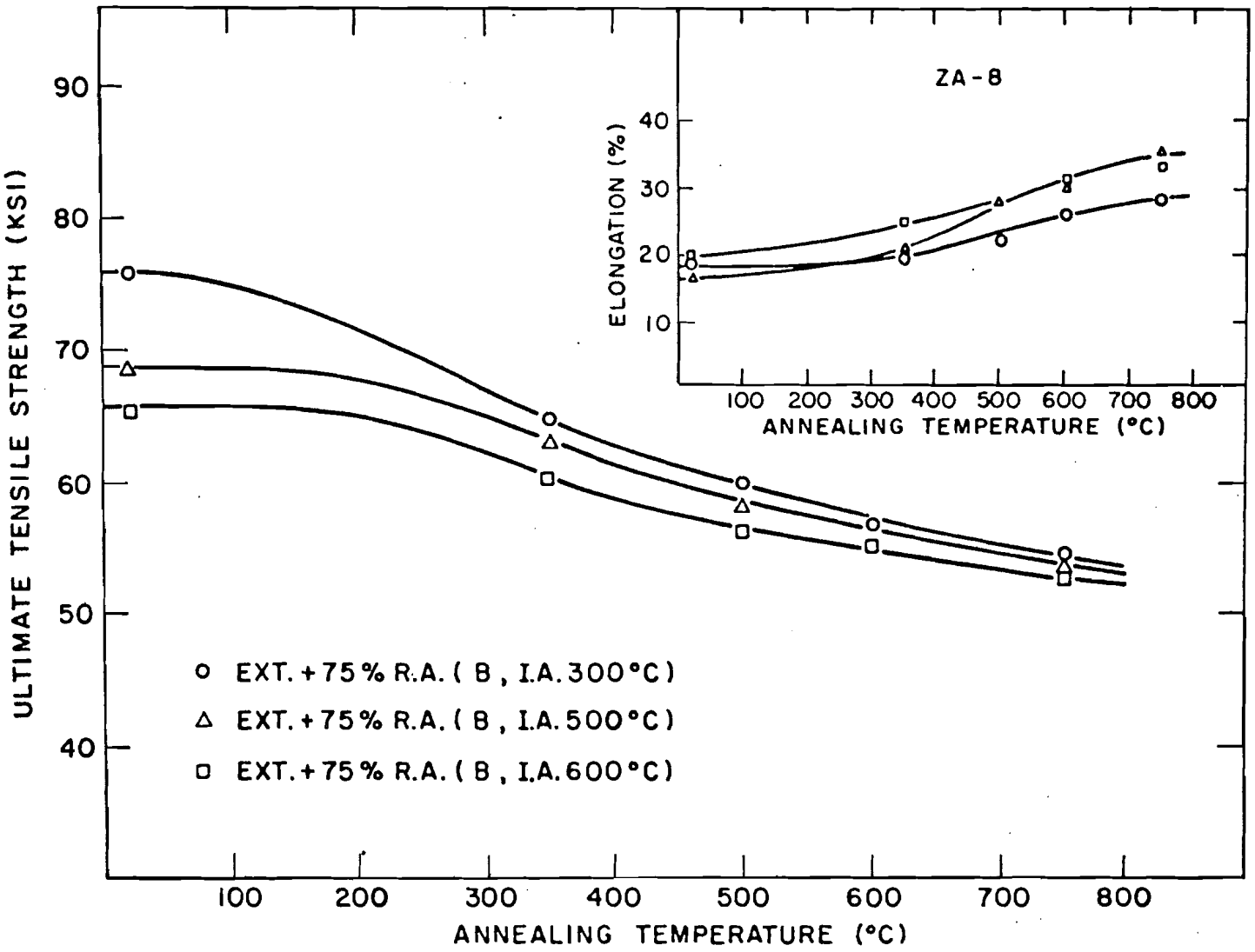

Figure 40. The effect of intermediate annealing temperature on room temperature tensile strength values after ½ hour anneals.

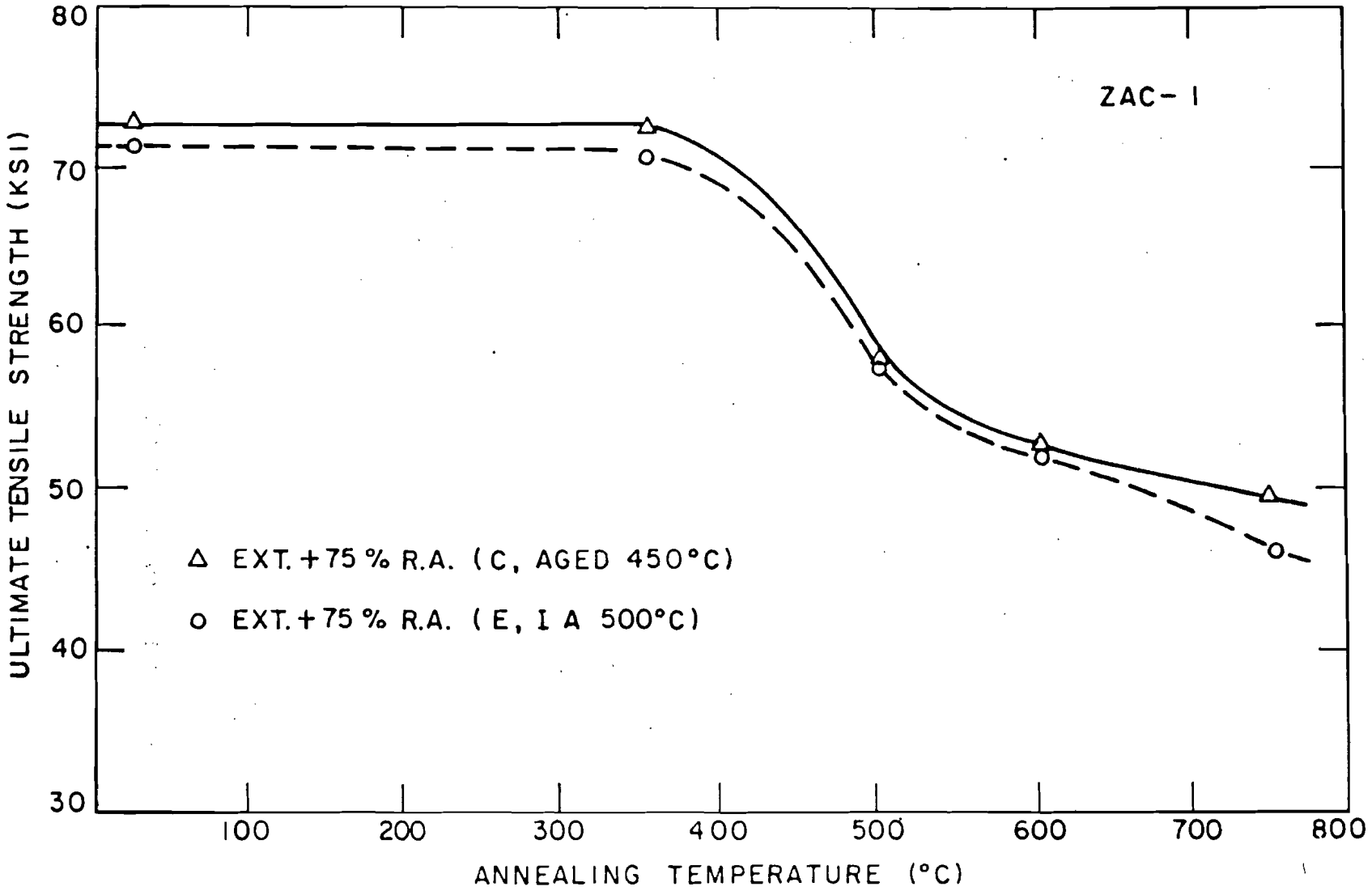

Figure 41. The effect of different aging temperatures on the room temperature tensile strength of ZAC-1 after half hour anneals.

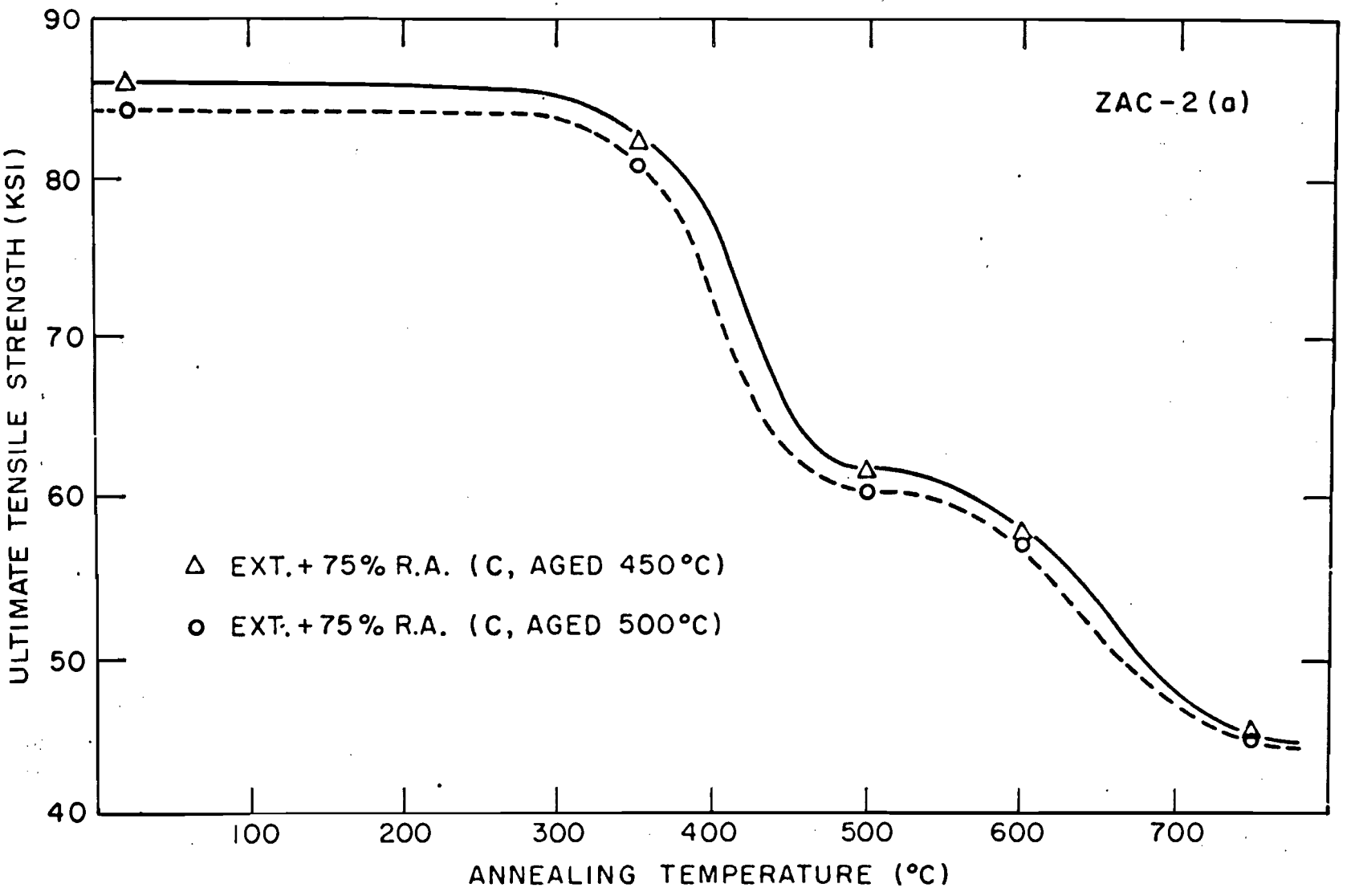

Figure 42. The effect of different aging temperatures on the room temperature tensile strength of ZAC-2(a) after ½ hour anneals.

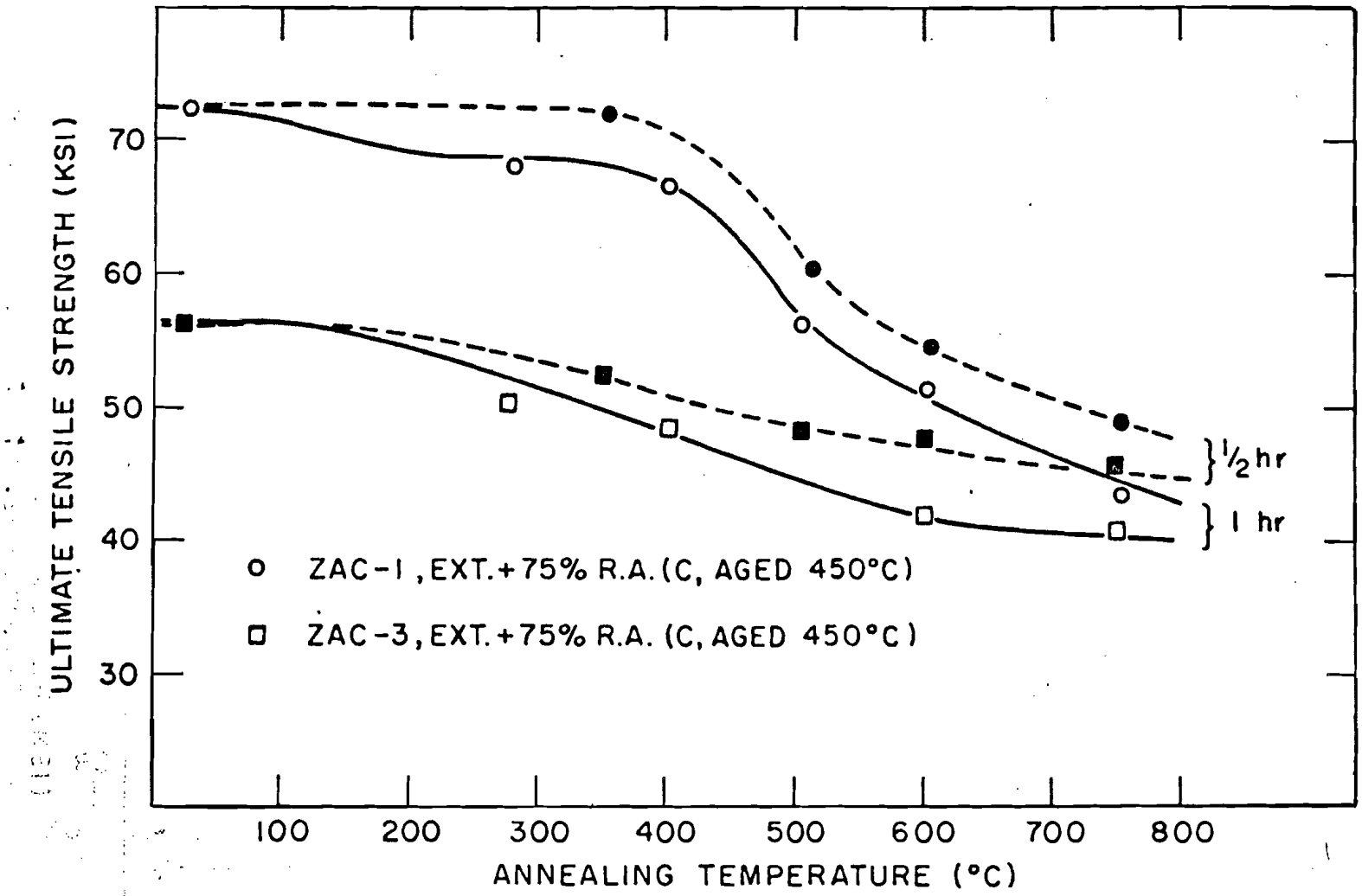

Figure 43. The effect of exposure time on the room temperature tensile strength values ZAC-1 and ZA-3.

As is evident from Appendix 5, all these alloys have excellent ductility. Examination of the tensile fracture surfaces of both extruded and cold worked alloys revealed typical ductile fractures. Figure 44a shows a SEM view of the fracture surface obtained in ZA-8 in the as-extruded condition. Clear evidence of huge cavities obtained from the agglomerated ZrO_2 clusters is visible. In comparison, Figure 44b shows the fracture surface of ZA-8 after 90% R.A. The smaller dimple size observed in this case is due to resultant finer interparticle spacing obtained through the swaging treatment. SEM examination of the fracture surfaces showed a direct relationship between the volume fraction of oxide particles and the number of dimples obtained[89]. This can be seen on comparison of Figure 44a to Figure 45a. The fracture surface of ZAC-1 (Figure 45b) reveals the presence of grain boundaries. Although grain boundaries were observed on the fracture surfaces of both the Cu-Zr and Cu-Zr-Cr alloys, they were more predominant in the Cu-Zr-Cr alloys.

The effect of TMT on the stress-rupture life of these alloys was investigated extensively. The results obtained were used as a major criterion to determine their high temperature stability. All tests were performed in air. A few samples which were used for fracture studies, were ruptured in a 20% hydrogen, 80% argon mixture to minimize oxidation of the fracture surface. All pertinent data on these tests are tabulated in Appendix 5.

Figure 46 shows the initial stress versus time to rupture plot for

(a)

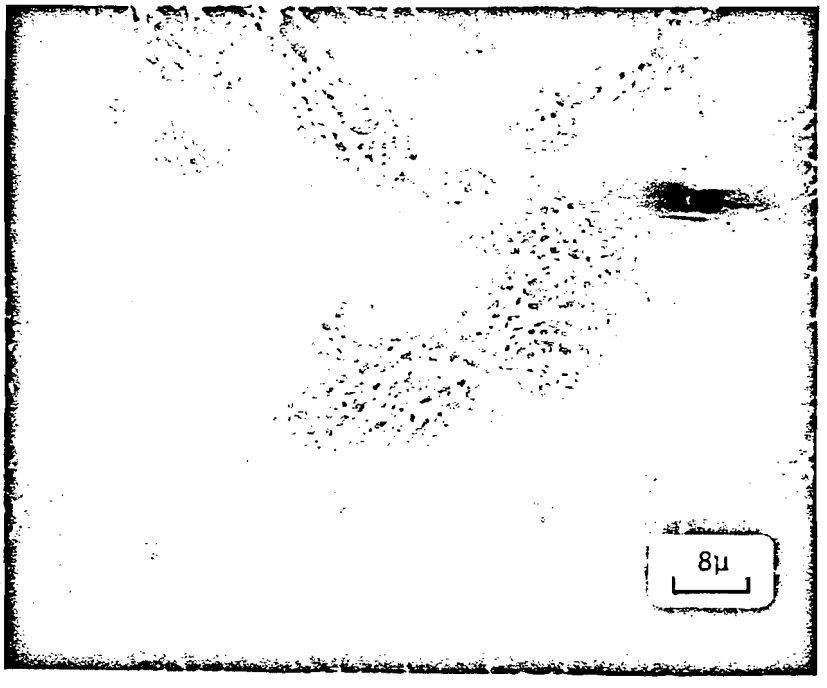

(b)

Figure 44. SEM of fracture surfaces of room temperature tension tested ZA-8.

(a) As-extruded
(b) Ext. + 90% R.A.

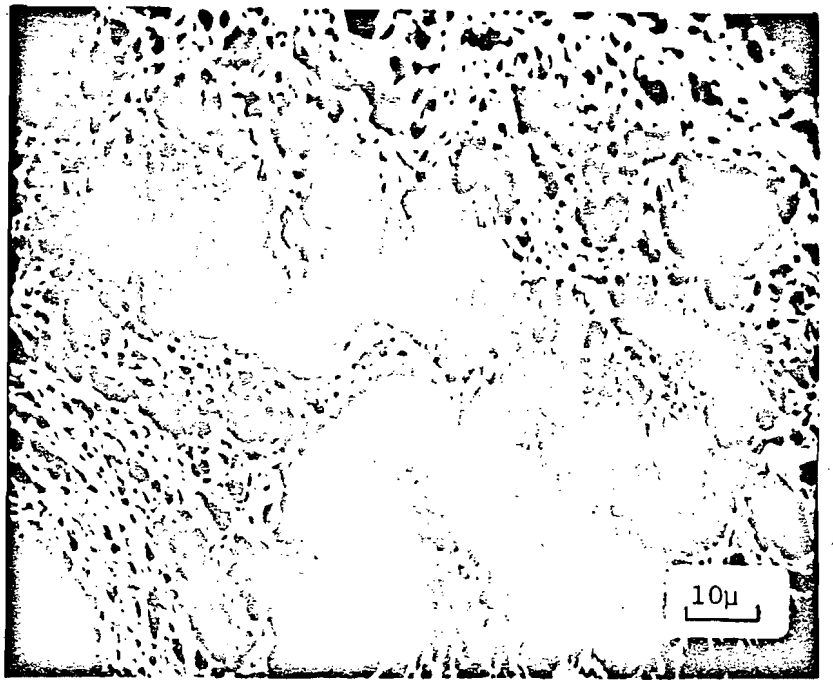

(a)

(b)

Figure 45. SEM of fracture surfaces of room temperature tension tested alloys.

(a) ZA-3, as-extruded
(b) ZAC-1, as-extruded

some of the TMTs studied on ZA-2. As is evident, a substantial increase in rupture life is obtained through cold work. The difference in slope between 450°C and 650°C is attributed to the difference in the activation energy for creep at these two temperatures[82]. It is assumed that at 450°C (approx. 0.4 T_m) the activation energy for creep is less than that for self-diffusion and hence the rate controlling process is believed to be associated with cross slip of screw dislocations[83]. At 650°C (0.6 T_m), the most likely controlling mechanisms are dislocation climb[84] and grain boundary sliding[85]. Although the combination of precipitation hardening and cold work (C; Aged 450°C) yields the strongest material at 450°C, its effectiveness is substantially decreased at 650°C. Figure 47 shows the effect of cold work on the 100 hours stress-rupture life of ZA-2. It is evident that at both 400 and 650°C cold work increases the rupture life. The stress required for rupture in 100 hours in ZA-2 at 450°C increased from 15,000 psi in the as-extruded condition to 19,800 psi after 90% R.A. A similar trend was observed at 650°C where the stress for 100 hour rupture life increased from 3,600 psi (for a 50% R.A. cycle) to 6,200 psi after a 90% R.A. TMT. A further increase to 22,000 psi was obtained at 450°C owing to precipitation hardening (C, Aged 450°C). Hence it seems that through an effective TMT, both room temperature (Fig.37) and high temperature (Fig.47) strength values of the extruded allowys can be substantially improved. Similar

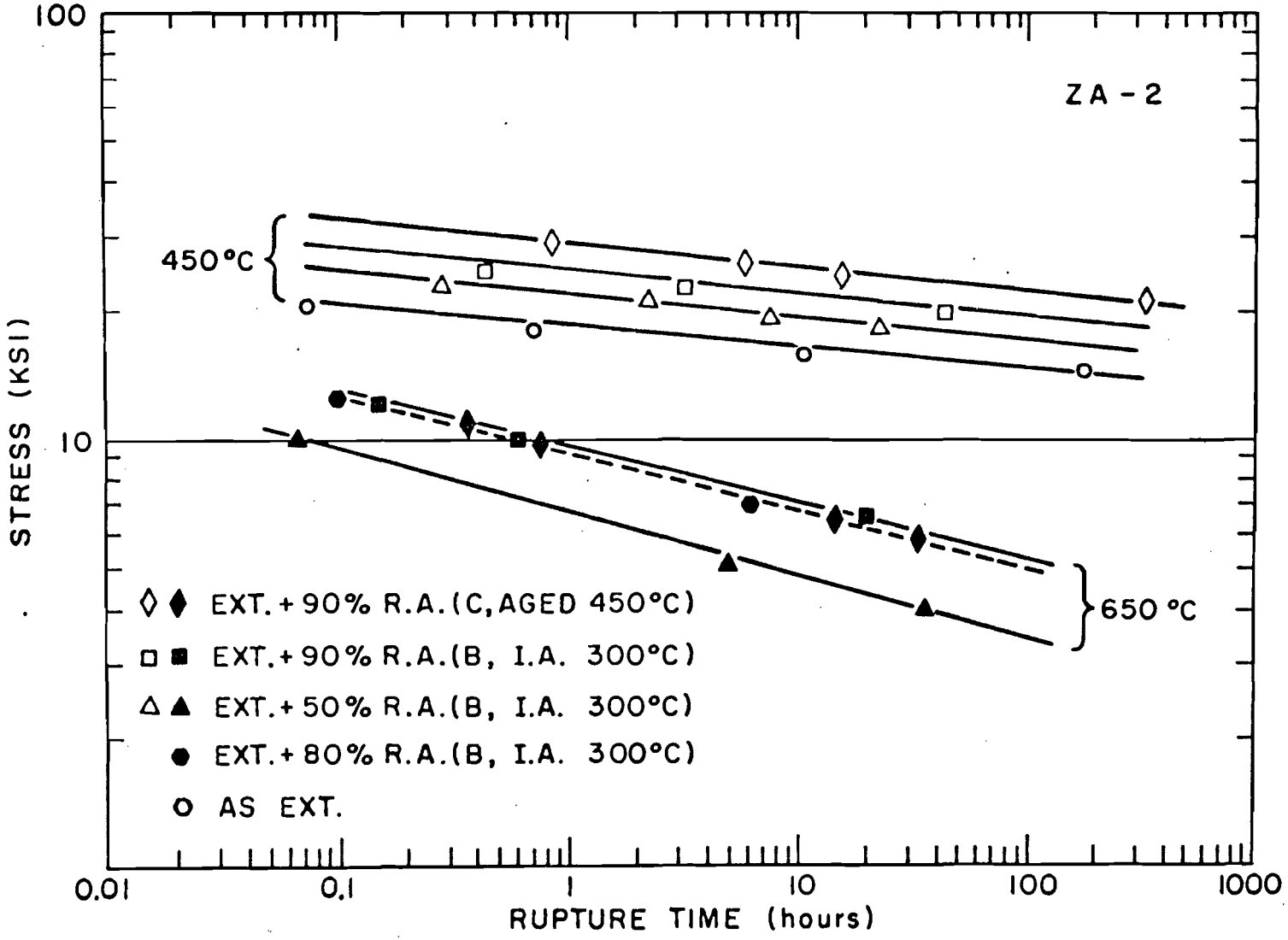

Figure 46. Log stress versus log rupture time plot of ZA-2

results were obtained for ZA-3 (Figure 48). In this case at 400°C, the stress for 100 rupture life increased from 16,000 psi to 23,000 psi after a 90% R.A. TMT (B, 300°C). A further increase to 27,000 psi was obtained after a 75% R.A. plus precipitation hardening treatment (C, Aged 450°C).

The effect of intermediate annealing (I.A.) temperature on the creep rupture properties of ZA-8 and FM-8 was investigated (Figures 49 and 50). Two types of TMTs were used, in the case of FM-8, the F designated treatment (50% R.A.; 1 hr. anneal; further C.W. to 90% R.A.) was studied, while the B designated treatment (1 hr. anneal after every approx. 10% R.A. cycle) was used for ZA-8. To prevent cluttering of data, both the figures do not show all the treatments investigated, but all relevant data are tabulated in Appendix 6, and Table XVII lists the stress required for rupture in 100 hours for the various TMTs.

The effect of intermediate annealing temperature on the 1, 10 and 100 hour rupture lives of ZA-8 is shown in Figure 51. It is evident from both Table XVII and Figure 51 that a substantial increase in the stress-rupture life can be obtained by using an appropriate I.A. temperature. A similar effect of I.A. temperature on the room temperature tensile properties of ZA-8 can also be seen (Table XV). The reason for the high stress values obtained for treatment A (No I.A.) at 650°C for 1 and 10 hour rupture life (Figure 51) is not known. In spite of the superior room temperature tensile strength (76,000 psi) obtained with

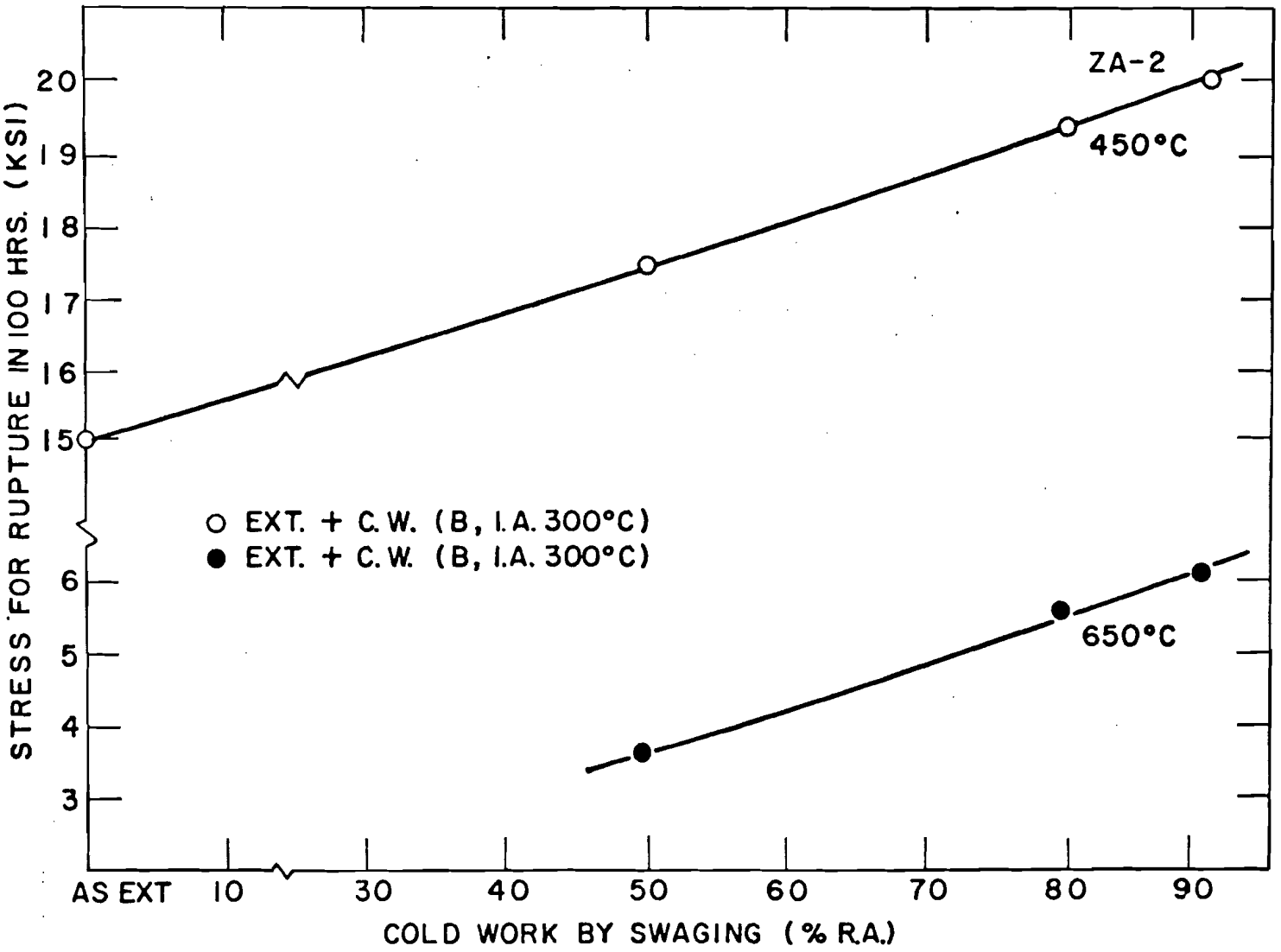

Figure 47. The effect of cold work (% R.A.) on the 100 hour stress-rupture life of ZA-2.

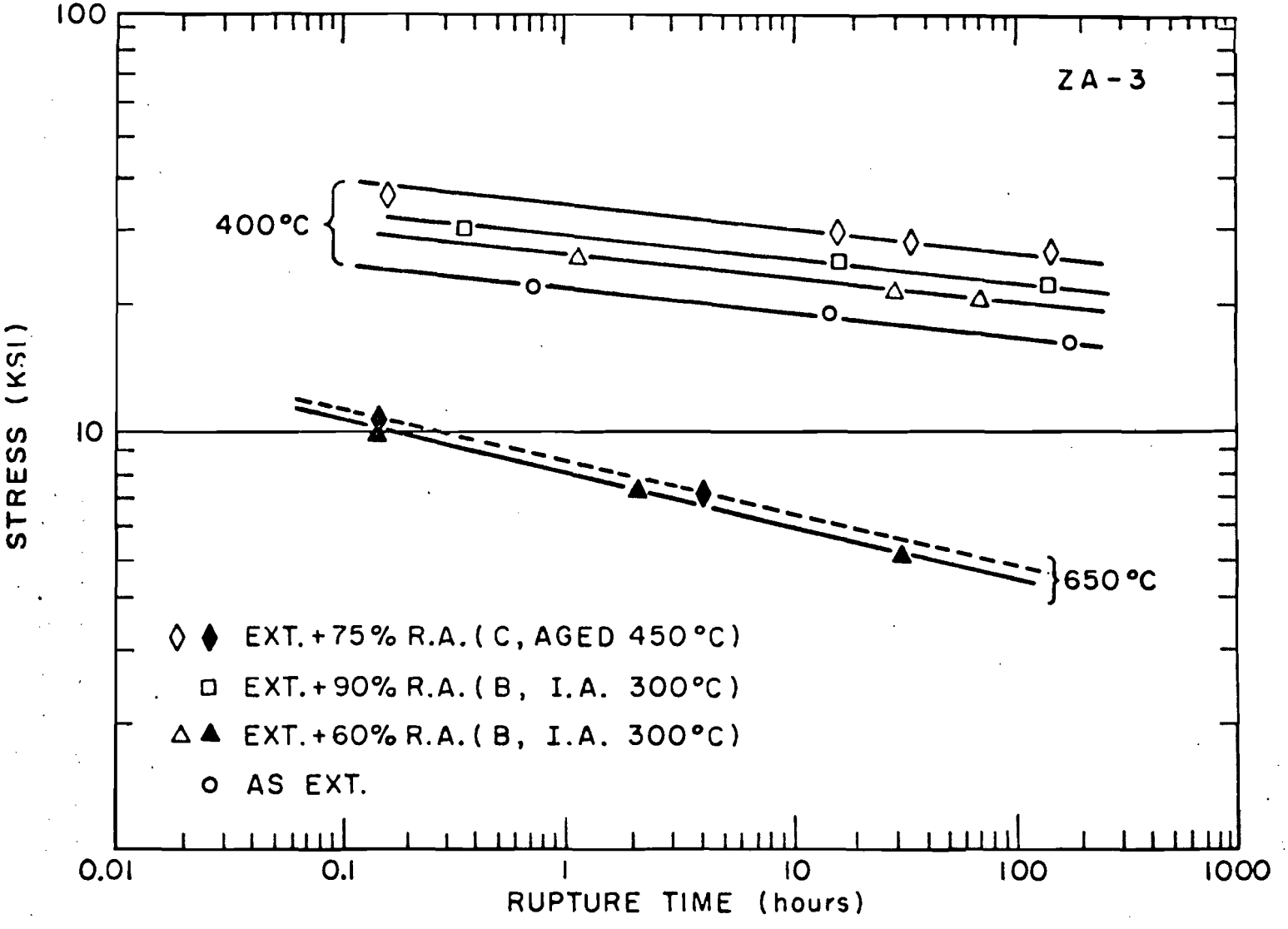

Figure 48. Log stress versus log rupture time plot for ZA-3.

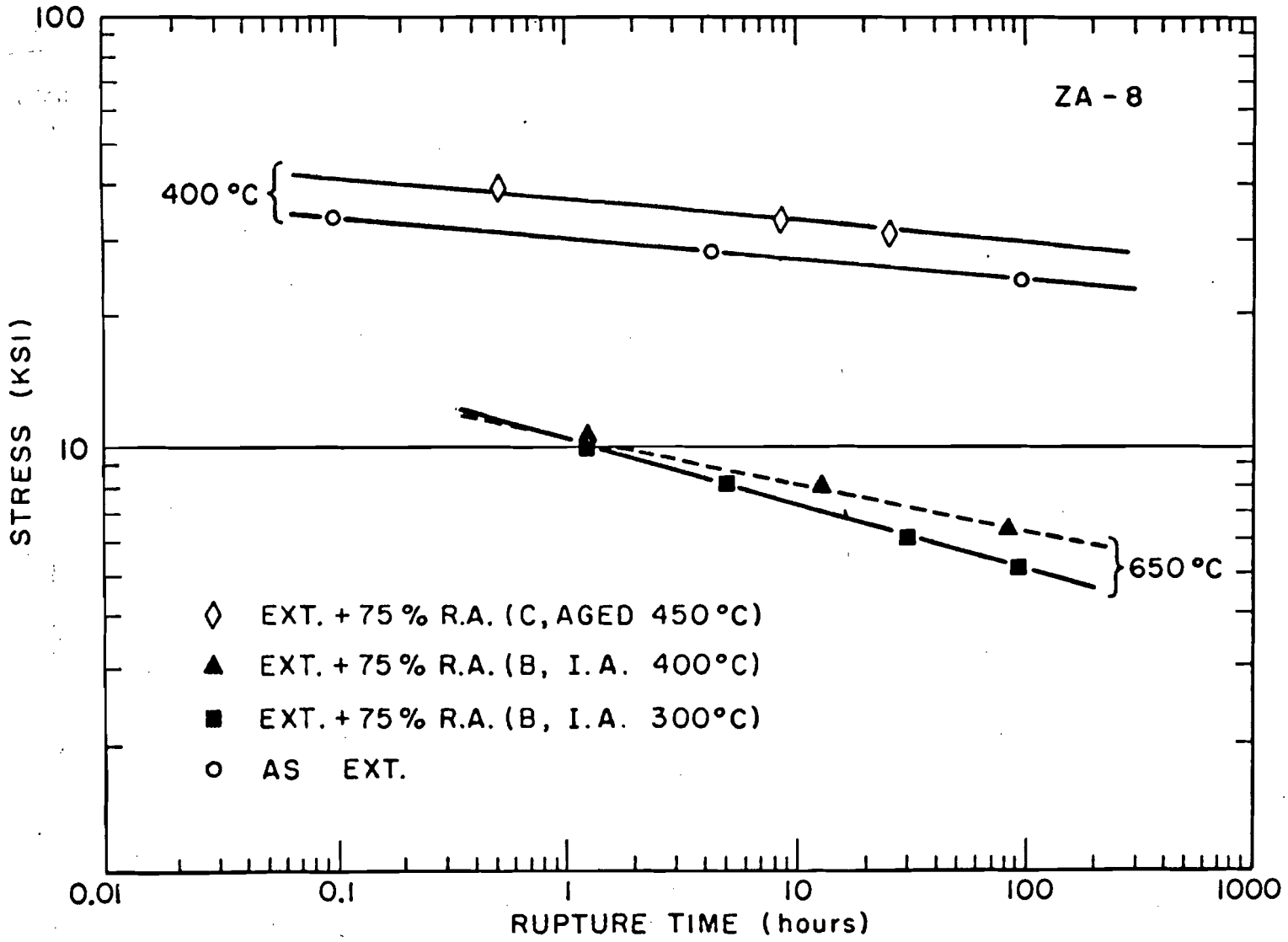

Figure 49. Log stress versus log rupture time plot for ZA-8.

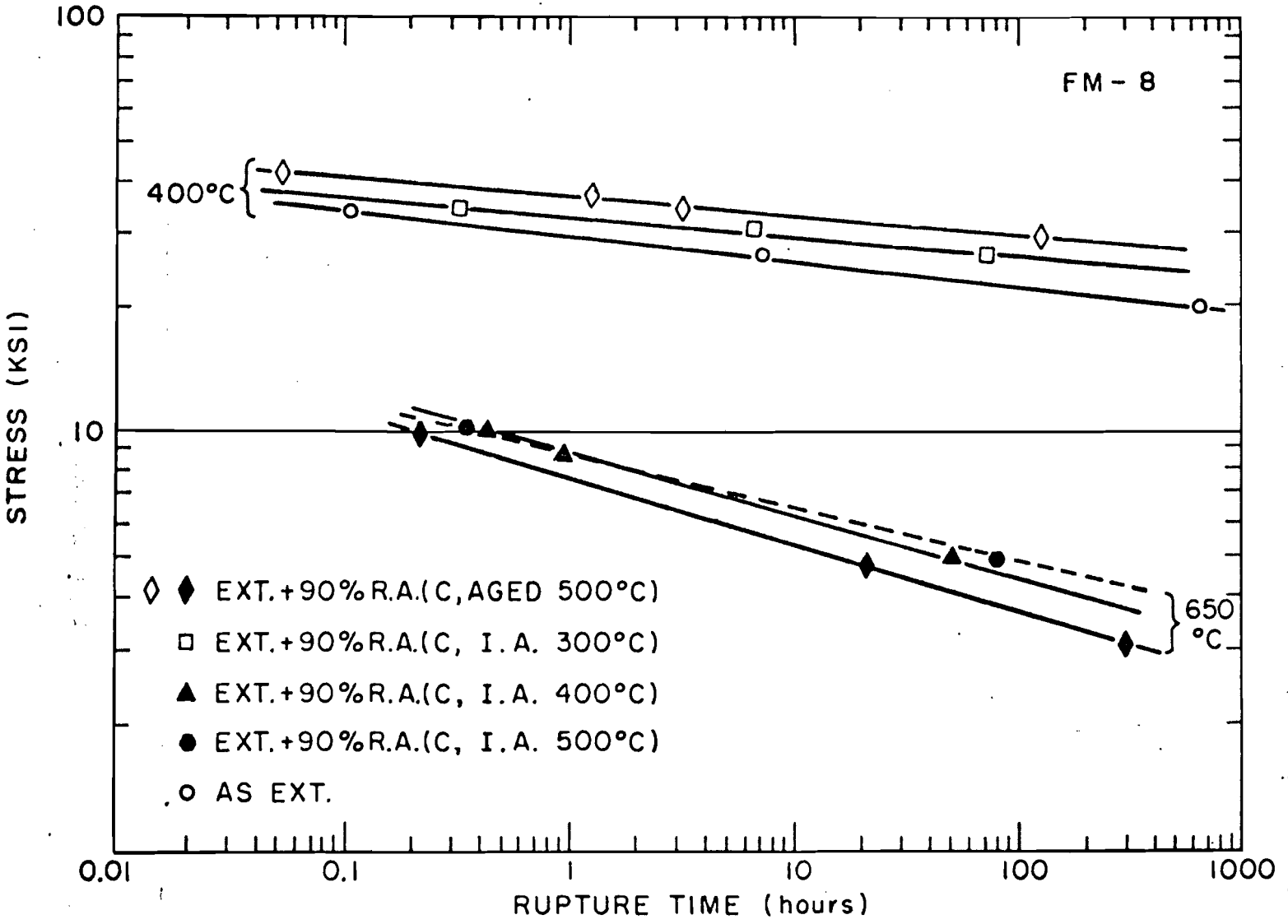

Figure 50. Log stress versus log rupture time plot for FM-8.

Table XVII

The Effect of I.A. Temperature on the 100 Hour Stress-Rupture Life of ZA-8 and FM-8

Alloy and Treatment	Stress (psi) for Rupture in 100 Hours	
FM-8	400°C	650°C
As Ext	22,000	--
Ext + 90% R.A. (F, I.A. 300°C)	25,500	4,050
Ext + 90% R.A. (F, I.A. 400°C)	26,000	4,200
Ext + 90% R.A. (F, I.A. 500°C)	--	4,950
Ext + 90% R.A. (C, Aged 500°C)	31,000	3,800
ZA-8		
As Ext	25,000	--
Ext + 75% R.A. (A, I.A. 20°C)	27,000	4,400
Ext + 75% R.A. (B, I.A. 300°C)	28,500	5,000
Ext + 75% R.A. (B, I.A. 400°C)	29,000	6,000
Ext + 75% R.A. (B, I.A. 500°C)	26,000	6,000
Ext + 75% R.A. (B, I.A. 600°C)	24,000	5,400

TMT B over TMT A (70,000 psi), TMT A resulted in superior strength (56,000 as compared to 52,000 psi) over B after a half hour exposure at 650°C. Although this partially explains the superior strength for short time rupture life of treatment A over B, no explanation can be found for the 10 hour case. As room temperature properties are also dependent on the dislocation substructure present, this strengthening obtained is unusual.

Electronmicroscopy studies did not reveal any positive correlation between substructure and properties in ZA-8. Owing to the pre-

sence of a network of massive clusters of ZrO_2 (Figure 16) it was prohibitively difficult to obtain any conclusive results from any of the structures observed. Several dislocation tangles and some localized cell formation were seen in almost all the TMTs listed in Table XVII (for ZA-8). Figure 52 for TMT B (I.A. 400°C) shows a typical structure. When an almost pure copper (with less than 0.03 wt. % Zr) rod was processed with a similar TMT A, well defined cell formation was observed (Figure 53).

The ternary Cu-Zr-Cr alloys with the combination of precipitation hardening and cold work, yield the best room temperature and stress-rupture properties. Figure 54 shows the tremendous increase in stress for a 100 hour rupture life obtained both at 400 and 650°C through precipitation hardening and cold work (C) as opposed to a cold work-anneal cycle (B). The stress required for rupture in 100 hours at 400°C for the 90% R.A. (B, I.A. 300°C) was found to be 21,000 psi, while precipitation combined with 75% R.A. (C) yielded a stress for 100 hour life of 38,500 psi, as compared to the as-extruded condition which yielded a stress of 14,800 psi. At 650°C, the 60% R.A. (B, I.A. 300°C) yielded a stress of 4,600 psi while treatment C resulted in a stress of 8,000 psi for a 100 hour rupture life. A maximum stress value of 9,200 psi for a 100 hour rupture life at 650°C was obtained through a three hour age at 500°C (Treatment D).

Although excellent stress-rupture strength values were obtained for ZAC-2(a) at 400°C, the alloy was found to be relatively unstable

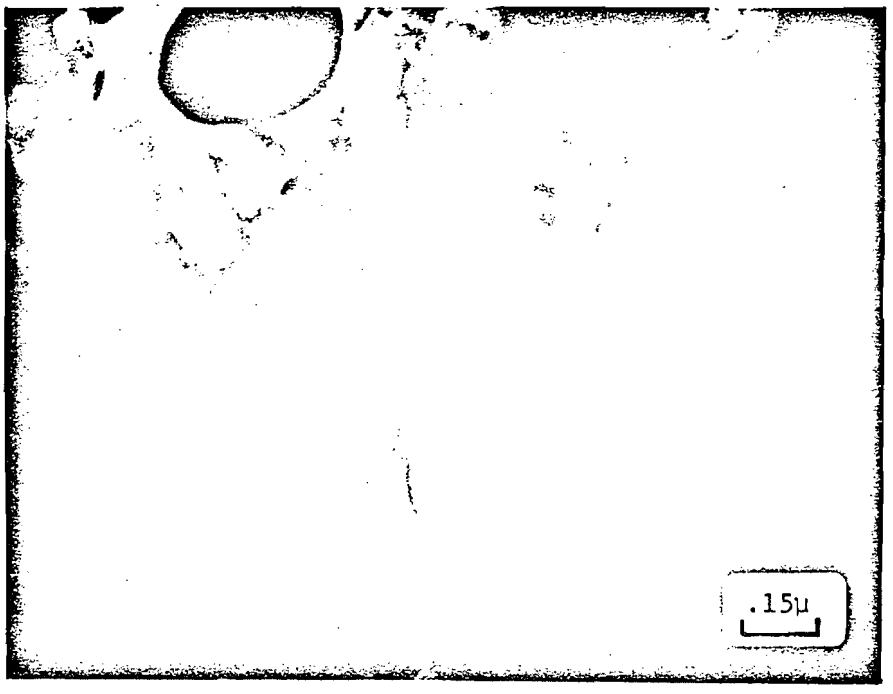

Figure 52. Transmission electron micrograph of ZA-8 in the Ext. + 75% R.A. (B, I.A. 400°C) condition.

Figure 53. Transmission electron micrograph showing the presence of cell structure (in Cu-0.03 wt. % Zr) after 75% R.A.

at 650°C (Figure 55). Table XVIII lists the stress for 100 hour rupture life obtained through the various TMTs investigated on ZAC-2(a). The almost continuous oxide film at the particle boundaries present in ZAC-2(a) (Figure 24b) is believed to be the major contributing factor to the low stress for 100 hour rupture life values obtained at 650°C. Although no conclusive evidence was obtained to confirm this, fracture surface studies did reveal particle separation at 650°C in ZAC-2(a). SEM studies on all the alloys revealed a typical dimpled ductile fracture at 400°C irrespective of the duration of the test (Figure 56). Although at 650°C very short life stress-rupture samples of ZAC-2(a) revealed a ductile type fracture surface (Figure 57a), all tests lasting over one hour duration had a fibrous appearance and particle separation, mainly along stringer boundaries (Figure 57b), was evident. SEM studies on ZAC-1 at 650°C, for a test lasting approximately the same duration as in Figure 57b, did not reveal any such signs of particle separation (Figure 58). Fine individual particles, homogenously distributed throughout the surface were clearly visible upon a closer examination of the fracture surface in Figure 57b. The identity of these particles (Figure 59) could not be determined. Optical metallography ascertained the presence of voids near the fracture surface and intergranular cracking throughout the specimen in all the alloys.

Preliminary stress-rupture tests on ZAC-2(b) and ZA-10(b) revealed no substantial effect of the initial coarse powder size on the properties of the wrought material. Generally these alloys were found to be

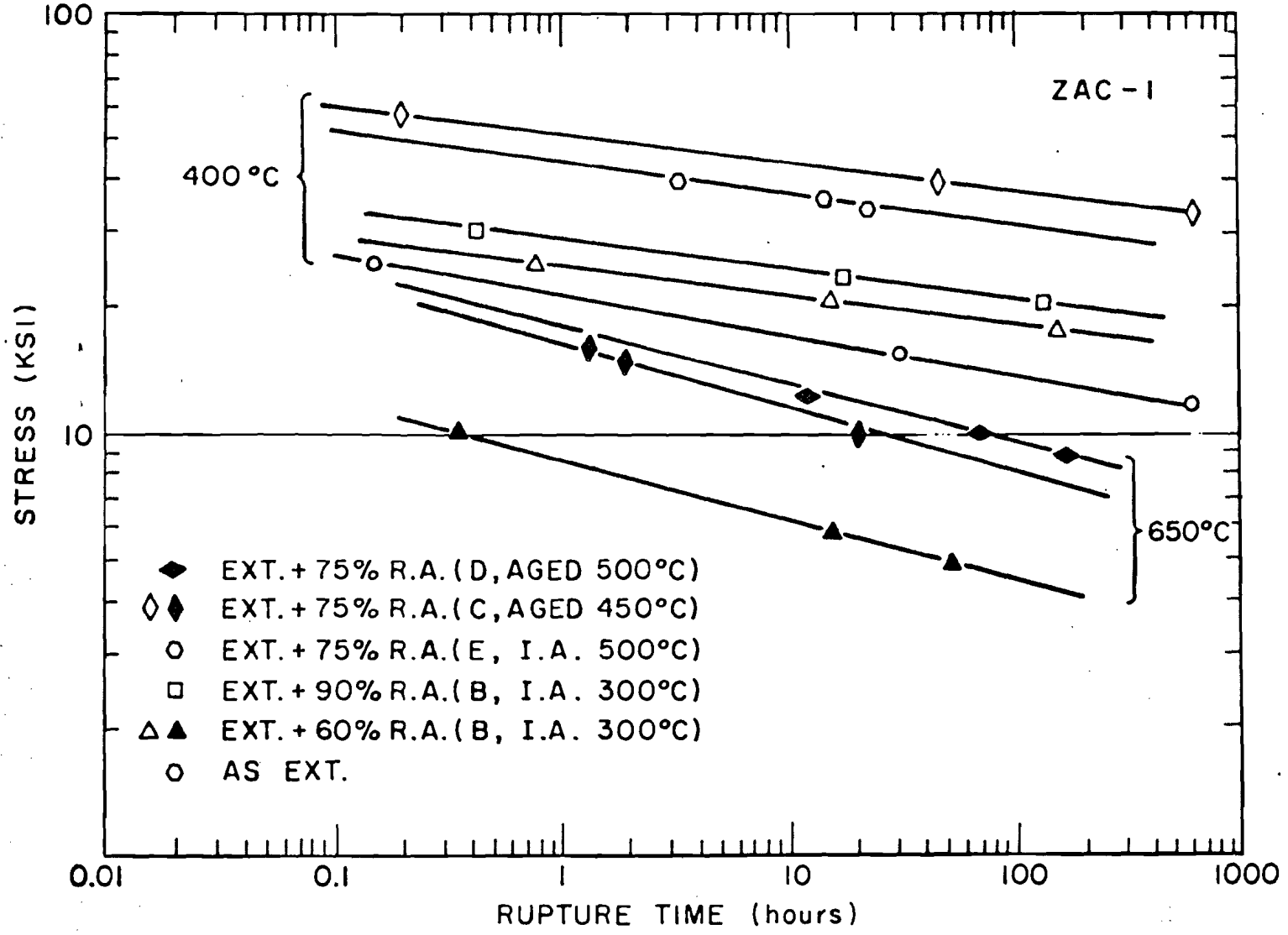

Figure 54. Log stress versus log rupture time plot for ZAC-1.

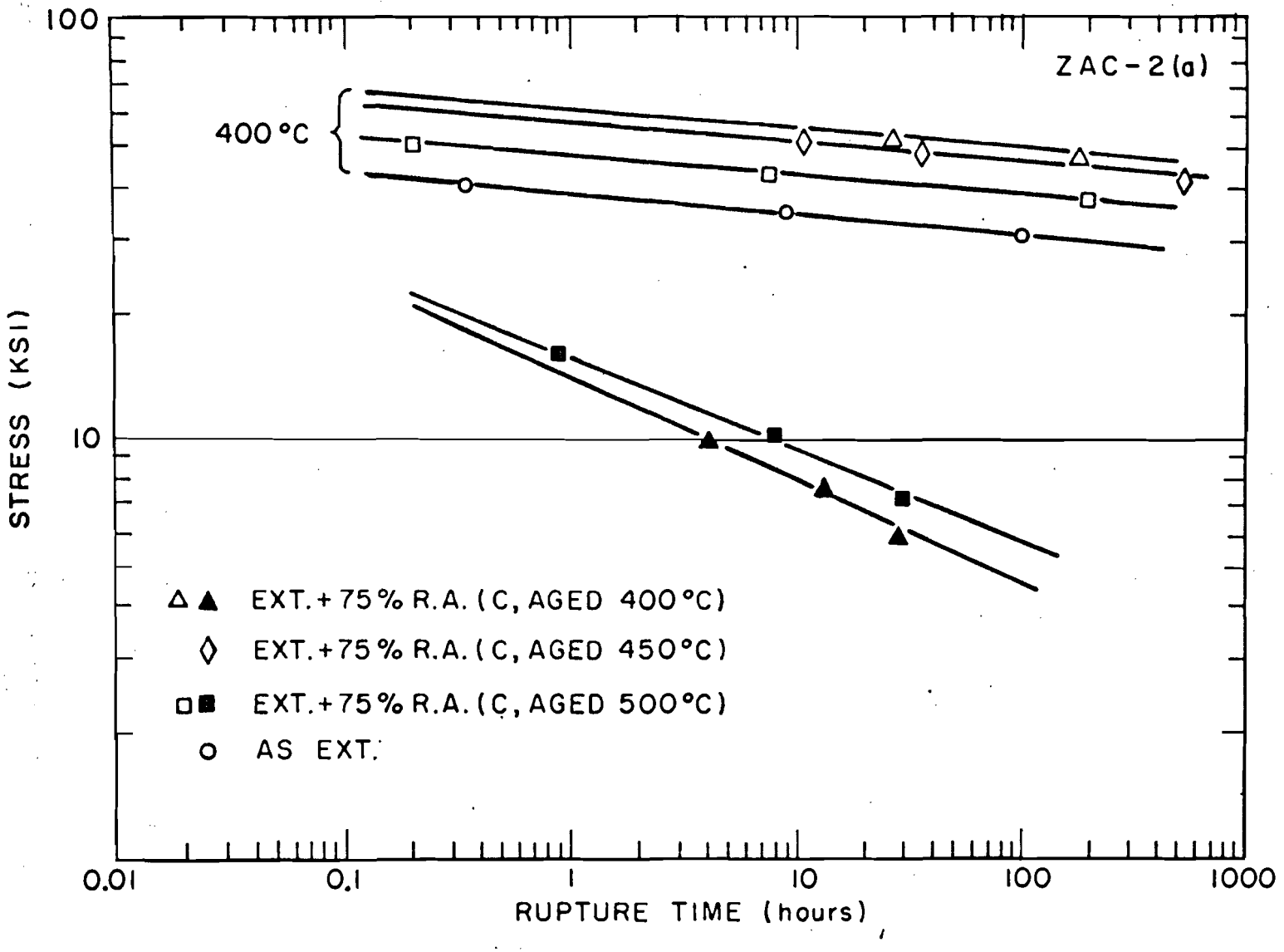

Figure 55. Log stress versus log rupture time plot for ZAC-2(a).

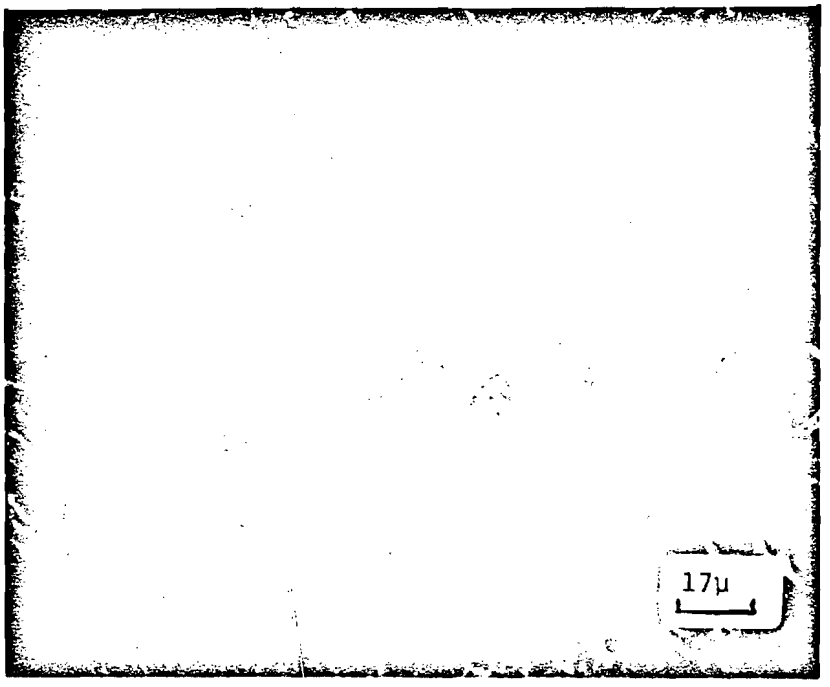

(a)

(b)

Figure 56. SEM fracture surfaces of alloys creep tested in the as-extruded condition.

(a) ZA-2 at 450°C (σ = 15,400 psi)
(b) ZAC-2(a) at 400°C (σ = 40,000 psi)

(a)

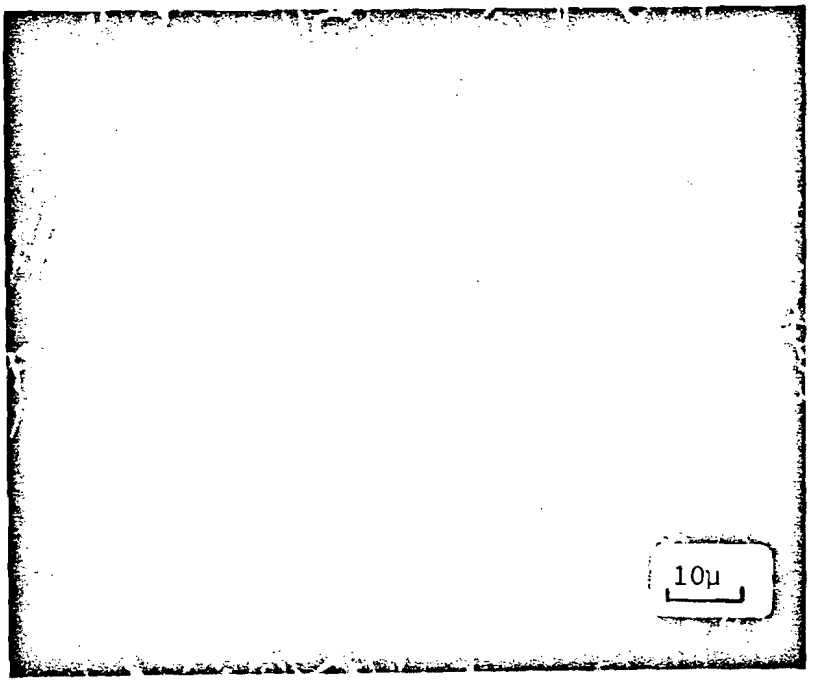

(b)

Figure 57. SEM photomicrographs of fracture surfaces of ZAC-2(a) creep tested at 650°C.

(a) Short duration (0.8 hrs.) test σ = 16,000 psi
(b) Long duration (10 hrs.) test σ = 10,000 psi

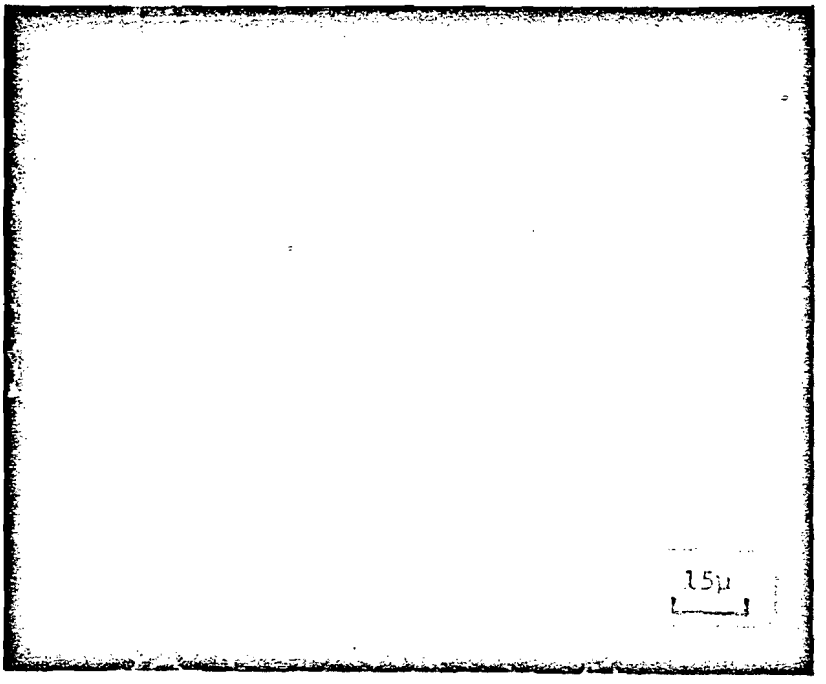

Figure 58. SEM fracture surface of ZAC-1 tested at 650°C (σ = 10,000 psi).

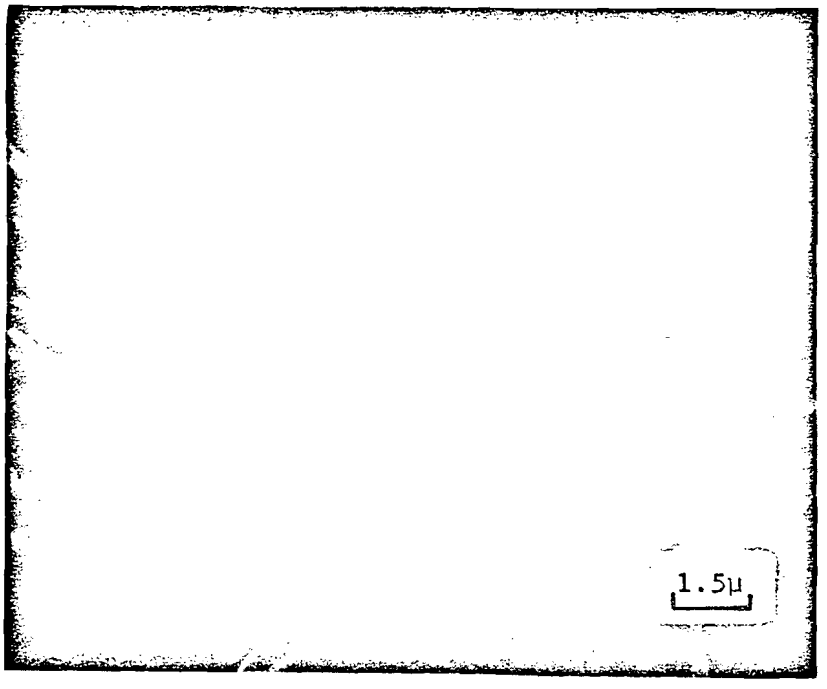

Figure 59. SEM fracture surface of ZAC-2(a) creep tested at 650°C (σ = 10,000 psi).

Table XVIII

Effect of TMT on 100 Hour Stress-Rupture Life of ZAC-2

Condition	Stress (psi) for Rupture in 100 Hours	
ZAC-2(a)	400°C	650°C
As Ext	29,500	--
Ext + 75% R.A. (C, Aged 400°C)	48,500	4,800
Ext + 75% R.A. (C, Aged 450°C)	45,000	5,200
Ext + 75% R.A. (C, Aged 500°C)	39,000	5,600
ZAC-2(b)		
As Ext	30,000	--
Ext + 75% R.A. (C, Aged 450°C)	46,000	4,000

a little stronger at 400°C while at 650°C the stress for 100 hour rupture life was relatively lower than their counterpart alloys extruded from finer sized powders (Table XVIII).

Stress values for 100 hour rupture life as a function of temperature for some of the alloys are compared with those of the conventionally ingot cast copper-zirconium alloys[31,85] in Figure 60. All the alloys were found to be significantly stronger in stress-rupture above 400°C than any ingot cast copper-zirconium alloys so far reported. Ductility measurements from stress-rupture tests showed considerable scatter (Appendix 6), but on the whole the ductility was found to be good. The average range in which most values fell was 2-10% elongation and 20-90% reduction of area. At 650°C, a decrease from approximately 80 to 30% reduction of area with increasing rupture life was observed in most cases. This was

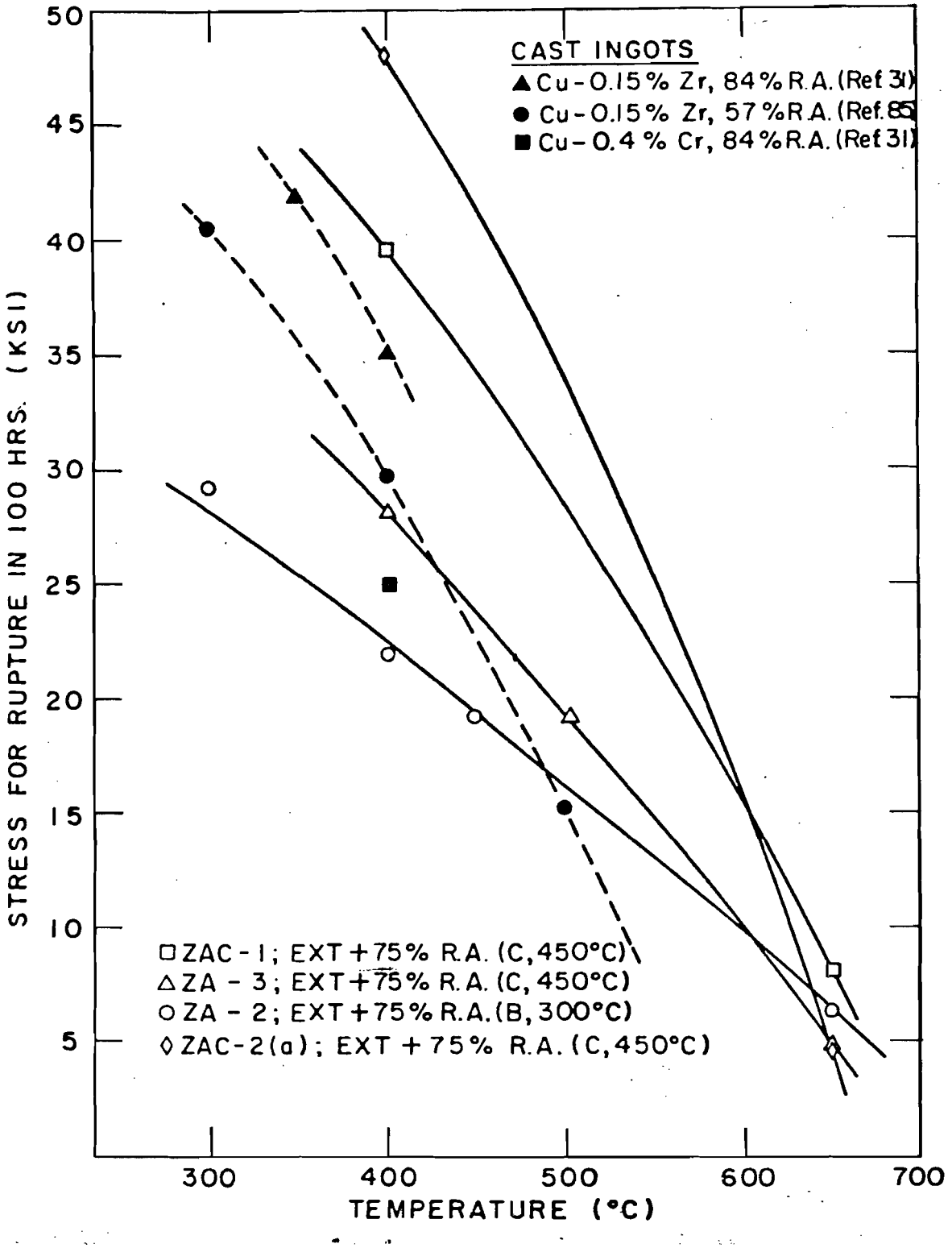

Figure 60. Stress for rupture in 100 hours versus test temperature.

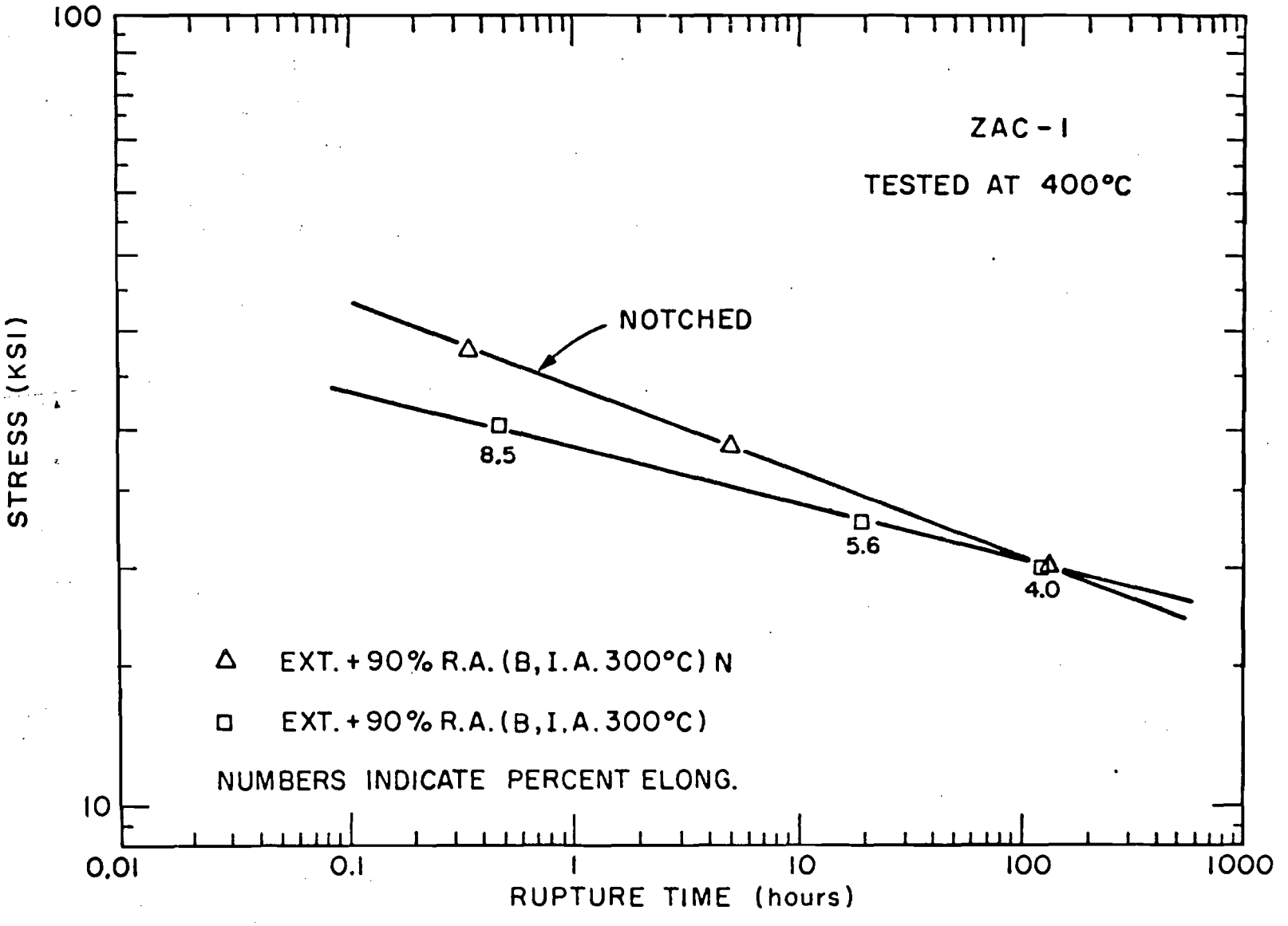

Figure 61. Comparison between stress-rupture life of notched (K_t approx. 38) and unnotched samples of ZAC-1 at 400°C.

attributed to extensive intergranular void formation in these samples.

Due to the well documented notch sensitivity effect obtained in copper-chromium alloys[32,87], the sensitivity of the ZAC series of alloys to the presence of a notch was investigated. Room temperature tensile tests (Table XIX) conclusively show the insensitivity of these alloys to notch weakening. In fact, substantially large amounts of notch strengthening was obtained, the strengthening level being proportional to the depth of the notch. The two notches used had K_t factors of approximately 3.8 and 5. The effect of a notch on the stress-rupture life of ZAC-1 at 400°C is shown in Figure 61. Similar observations were made by Gregory and Grant[92] on SAP.

As is evident from Table XIV, all the extruded alloys have excellent electrical conductivity values (% IACS). The effect of the various TMTs on the electrical conductivity of the copper-zirconium alloys was found to be small. For example, values of ZA-2 fell from 93.6% IACS in the as-extruded condition to 91.6% IACS after 90% R.A., using TMT (B, I.A. 300°C). In the case of ZA-8, all the various intermediate annealing temperatures (B, I.A. of 20, 300, 400, 500 and 600°C) only gave a variation of 3% IACS (Table XV). The electrical conductivity values of all the alloys were more drastically affected with the combination of solution anneal, cold work and aging cycles. All the electrical conductivity data are tabulated in Appendix 7.

Table XIX

Room Temperature Tensile Data of Notched* Alloys

Alloy & Condition	S.F. K_t	Y.S. (psi)	U.T.S. (psi)	Elong. (%)	R.A. (%)
ZA-2					
Ext + 80% R.A. (B, I.A. 300°C)	--	49,000	53,500	17.5	90.5
Ext + 80% R.A. (B, I.A. 300°C)	3.8	60,000	62,500	12.5	--
ZAC-1					
Ext + 90% R.A. (B, I.A. 300°C)	-	50,500	51,500	14.0	89.0
Ext + 90% R.A. (B, I.A. 300°C)	3.8	70,500	71,000	11.0	--
Ext + 90% R.A. (B, I.A. 300°C)	5.0	73,000	75,000	7.2	70.0
ZAC-2(a)					
Ext + 75% R.A. (C, Aged 450°C)	-	84,500	86,000	13.2	--
Ext + 75% R.A. (C, Aged 450°C)	3.8	89,000	92,000	8.5	55.0
Ext + 75% R.A. (C, Aged 450°C)	5.0	99,000	103,000	6.2	60.0

* 8-32 samples were machined to obtain a notch of 0.01 or 0.02" (these notches gave estimated strengthening factors (S.F.) of K_t 3.8 and 5.0 respectively) in depth into the original 0.10" gage diameter.

Dimensions were as follows:

Gage Length	0.50"
Gage Diameter	0.10"
Depth of Notch	0.01" or 0.02"
Root Radius	0.005"
Angle	48°

VII. DISCUSSION

It has been demonstrated that the potential for control of structure through rapid quenching of liquid Cu-Zr and Cu-Zr-Cr alloys is an ideal way of minimizing segregation, eliminating coarse secondary phases (Cu_3Zr and Cr) and achieving fine dendrite and grain size. Powders produced from steam and nitrogen atomization techniques were used in the present instance, with the nitrogen atomized powders yielding the best overall results due to a smaller level of oxidation of the zirconium. Owing to the conversion of some of the Zr to ZrO_2 during atomization and reduction, a combined effect of oxide dispersion and solid solution hardening was obtained in all the consolidated wrought alloys (Table VIII and XIII). Although the presence of ZrO_2 was beneficial to the high temperature stability of the nitrogen atomized alloys, its segregated distribution (Figure 10) in the steam atomized powders reduced both the room temperature and high temperature strength values and ductility of these alloys. Unlike the nitrogen atomized alloys, the extruded steam atomized alloys could not be cold worked to further enhance their properties; hence no further reference to these alloys will be made in this section.

Control of the size and distribution of the ZrO_2 formed during atomization is presently an unknown entity due to a lack of knowledge of the atomization kinetics. But, since present indications are that a relatively fine (less than 0.1μ) and homogenous distribution is obtained during atomization in nitrogen, this is of no major concern. Results obtained in this investigation and those on nickel-beryllium powders[55] indicate the

formation of relatively coarse (0.1 to 2μ) solute element oxides during reduction (Figure 16). Control over the selective oxidation of Zr to ZrO_2 during the reduction of Cu_2O (Chapter VI, B) could lead to substantial improvements in both room and high temperature strengths of these alloys. This could be achieved either with an appropriate short time, low temperature reduction cycle, or by the removal of surface Cu_2O through chemical solution or decomposition.

Positive identification between several of the particles present (Cu_3Zr or ZrO_2 in the ZA series and Cr, Cr_2Zr, Cu_3Zr or ZrO_2 in the ZAC series) in these alloys was impossible. Since the Bravais lattice structure of Cu_3Zr is still unresolved, selected area diffraction patterns (Appendix 3) on precipitates observed in splat cooled ZA-2 (Figure 6) could not be indexed. Electron diffraction and X-ray analyses positively revealed the presence of ZrO_2 in all the alloys. Since the relatively coarse (about 0.5μ) agglomerated particles of ZrO_2 formed during reduction (Figure 16) were opaque to the electron beam, it is assumed that the fine (less than 0.1μ) homogenously distributed ZrO_2 particles formed during atomization (Figure 23) are probably responsible for the diffraction spots obtained through electron diffraction of the matrix. Although elemental chromium was detected in all the Cu-Zr-Cr alloys, no positive identification of the presence of Cr_2Zr was obtained. It is possible that since Cr_2Zr is cubic, several of its diffraction spots which have identical "d" spacing as those of pure copper and ZrO_2 (Appendix 3), could have overlapped, preventing positive identification.

The problem of excessive non-uniform grain growth[29,30,31] obtained in cast Cu-Zr alloys upon exposure for over one half hour at temperatures above 900°C was non-existant in alloys made in this investigation. For example, a solution anneal at 980°C for 30 min. on ZAC-2(a) resulted in an average grain size of 8-10μ (initial grain size was 3-6μ). A measured grain size of 10-12μ was obtained after the solution annealed ZAC-2(a) was aged for 35 hours at 500°C. This extremely effective retardation of grain growth by the dispersion of ZrO_2 in these alloys is responsible for the excellent stability in room temperature hardness obtained on long time exposures at 500°C (Figure 31). Similar grain size stabilization effects were also observed in all the other alloys.

Annealing studies on as-extruded alloys (Figures 25, 26) demonstrated the superior stability above 600°C of the nitrogen atomized alloys compared to commercial ingot material. Since the amount of ZrO_2 obtained in the extruded alloy was proportional to the initial zirconium content of the master alloy (Table XIII), an increase in the softening temperature with increasing zirconium content was generally obtained (Figures 25,26). If one takes into consideration the formation of ZrO_2, suggestions by Saarivirta[2] that zirconium contents above 0.13 wt. % have no further effect on the softening temperature of Cu-Zr alloys are not valid for these alloys. Some correlation between stability, as measured by room temperature hardness versus annealing temperature, and stress values for 100 hour rupture life for the lower zirconium content alloys in the as-extruded condition (Appendix 6) is evident. Since the size and distribution of the

ZrO_2, whether in clusters (Figure 16), or around particle boundaries (Figure 24), affected the stress rupture properties: no such correlation was obtained for the higher zirconium content alloys. Due to differences in the levels of precipitation, as indicated by electrical conductivity data for ZAC-1 (82.6 % IACS) and ZAC-2(a) (89.2 % IACS), this trend between room temperature hardness and stress-rupture properties is rather obscure in the Cu-Zr-Cr alloys.

Thermomechanical treatments were necessary in both Cu-Zr and Cu-Zr-Cr alloys to optimize room and high temperature properties. The combined effects of a solution anneal, cold work and precipitation hardening generally yielded the best properties for both Cu-Zr and Cu-Zr-Cr alloys. The pronounced improvement in precipitation hardening (Figure 31) obtained by the addition of chromium to the Cu-Zr alloys resulted in alloys with the best overall properties.

A substantial increase in room temperature strength values was obtained through TMTs (Appendix 5) for all the alloys. The increase in tensile strength as a function of cold work is shown in Figure 37. In spite of various levels of strengthening obtained through different TMTs and degrees of cold work, a short time exposure (half hour) above 800°C resulted in almost identical room temperature tensile strength values in each respective alloy (Figures 39,40 and 41). This is caused by recrystallization of these alloys above 800°C, which eliminates the strengthening effects of the various TMTs: the stabilized grain size then determines the final room temperature strength values. A reasonable conclusion is

that any strengthening obtained through the TMTs studied (Table VI) is probably only effective, for prolonged use of these alloys, below 700°C.

The increase in stress-rupture life by TMT is largely due to the formation of stabilized dislocation networks and/or arrays which result in high levels of stored energy. Pinning of dislocations (networks, sub-grains or arrays) and grain-boundaries (Figure 23, 28) stabilizes the structures and results in improved creep-rupture strength. As is evident from Figures 46, 47 and 48, an increased amount of stored energy of cold work enhances creep-rupture properties; this is in agreement with the suggestions of Adachi and Grant[90]. The pronounced effect of intermediate annealing temperatures can be seen in Figure 51 and Table XVII. These results are consistant with the findings of Rasmussen and Grant[88] who suggest that the effective decrease in interparticle spacing with increasing cold work and the sweeping of dislocations into low angle boundaries by the annealing cycles (permitting further cold work) is the strengthening mechanism. They further indicate that not only the amount of stored energy but also its distribution is relevant in determining strengthening obtained through the TMT. Investigation on nickel alloys by Yin and Grant[91] show that the improvement in creep strength of pre-strained nickel is more dependent on the arrangement and density of pre-induced dislocations rather than sub-grain size. Hence, since the intermediate annealing temperature during a TMT determines the arrangement and density of dislocations obtained, it is a major consideration in determining the creep strength of a TMT material.

The dislocations introduced by a cold work cycle are subsequently rearranged during the intermediate (or final) annealing treatment. Progressive cold work, without intermediate annealing may result in high local strains leading to delamination along particle stringer boundaries. An intermediate annealing temperature of 300°C is too low to adequately rearrange the dislocations for maximum stored energy values (Figure 51). It is also evident from this figure that too high an intermediate annealing temperature (600°C) results in excessive dislocation arrangements and annihilation, effectively resulting in lower levels of stored energy. There is an optimum intermediate annealing temperature (which varies from alloy to alloy), depending on the composition of the alloy, at which dislocations are arranged in the lowest energy configuration, permitting optimum stored energy and creep properties.

Cu-Cr alloys are reputed[32,87] to possess poor toughness properties. In order to determine the effects of stress concentrations on the Cu-Cr-Zr alloys, notched room temperature tensile and creep-rupture tests were conducted. The introduction of a notch into a material can, by introducing triaxial stresses, increase or decrease the apparent strength. For strengthening to occur, the material must have sufficient ductility to accomodate the stress concentration caused by the presence of the notch. The amount of ductility required varies according to the notch geometry. Gregory and Grant[92], working with notched SAP alloys, showed an increase in stress-rupture strength when the elongation of the normal rupture samples lies above about 10%. Strengthening in ZAC-1 in stress-rupture was

obtained when smooth bar specimens had rupture ductilities above about 4% elongation (Figure 61). Room temperature tensile tests also revealed all the alloy to be insensitive to the presence of a notch (Table XIX).

VIII. CONCLUSIONS

Alloy production from rapidly quenched powders of Cu-Zr and Cu-Zr-Cr results in fine grained wrought structures with excellent mechanical properties. From investigations made on these alloys the following conclusions can be drawn:

1. Dendrite arm spacing correlates linearly with cooling rate (on log-log coordinates) for the Cu-Zr system.

2. In spite of complete solid solubility, (up to 5 wt. % Zr) indicated by X-ray diffraction, fine precipitates of Cu_3Zr exist in the matrix, throughout the composition spectrum.

3. The formation of localized clusters of ZrO_2 during steam atomization adversly affects the ductility, room temperature tensile strength and elevated temperature creep resistance of these alloys.

4. The formation of relatively coarse (0.5μ) ZrO_2 in clusters or as a continuous film on the surface of powder particles during reduction is detrimental to the creep resistance (above $0.5T_m$) of these alloys and should be avoided under all circumstances.

5. Fine (less than 0.1μ) and homogenously distributed ZrO_2 occuring during atomization greatly improves the high temperature stability of all these alloys. The presence of this ZrO_2 also effectively removed the problem of excessive non-uniform grain growth in these alloys upon exposure or re-exposure at elevated temperatures.

6. Pronounced solid solution strengthening effects, both at room and high temperatures, are obtained by the addition of chromium to the copper-

zirconium system: the latter alloys were found to have the best overall properties. These alloys were found to be significantly stonger in stress-rupture than any ingot cast Cu-Zr or Cu-Zr-Cr alloys so far reported.

7. For the range of cooling rates examined (10^3 to 10^4 °C per sec.) initial dendrite size of powders did not affect the final grain size of the wrought product, and both coarse (10^3 °C per sec.) and fine (10^4 °C per sec.) size range alloys yield comparable room and high temperature properties.

8. The resultant ductility values obtained in these alloys are superior to those of conventional ingot type materials; hot and cold plasticity of these alloys was excellent.

9. Thermomechanical treatments were necessary in all the alloys to optimize both room and high temperature properties. The combined effects of a solution anneal, cold work, age, and further cold work yield the best results.

10. The intermediate annealing temperature during a TMT was found to be a major contributor in determining the strength (room temperature tensile and elevated temperature creep-rupture) obtained, with optimum overall properties being obtained for a particular temperature. Although prolonged aging treatments between two swaging cycles in the ZAC series of alloys yielded superior stress-rupture properties, they adversely affected room temperature tensile strength values; hence a short (1 hour) aging treatment was found to be most effective.

11. The ZAC series of alloys was found not to be notch-sensitive in room temperature tension tests and 400°C creep-rupture tests up to 100 hours.

12. All alloys were found to have excellent electrical conductivity values. This was partly due to some conversion of Zr to ZrO_2 in the alloys.

IX. SUGGESTIONS FOR FURTHER WORK

1. Determination of the Bravais crystal structure of Cu_3Zr and a thorough examination of its precipitation kinetics.

2. A complete investigation of the kinetics of atomization techniques.

3. The relationships in these alloys among cold work, crystallographic texture and mechanical twinning (if any), and their combined and individual effects on strength and ductility.

4. A thermodynamic study and kinetics of the selective oxidation of ZrO_2 during the reduction of Cu_2O in these powders.

5. Detailed electron microscope studies on the effect of intermediate annealing temperature on substructure and its correlation with both room and high temperature properties.

6. A further study of the effect of chromium on the properties of copper-zirconium alloys. The use of higher levels of both chromium and zirconium.

7. The use of a similar technique to produce alloys using a number of other elements (hafnium, arsenic) as the third element with copper-zirconium.

X. BIBLIOGRAPHY

1) M. Hansen and K. Anderko: Constitution of Binary Alloys, McGraw-Hill, New York and London, 1958.

2) M.J. Saarivirta: Trans. AIME, 1960, vol. 218, p. 431.

3) V. Zwicker: Metall., 1962, vol. 16, p. 409.

4) W. Showak: Trans. AIME, 1962, vol. 224, p. 1297.

5) M.J. Donachie: J. Inst. Met., 1964, vol. 92, p. 180.

6) J.A. Belk: Private communications.

7) T.E. Allibone and Sykes: J. Inst. Met., 1928, vol. 39, p. 173.

8) A. Pogodin, T.S. Shumova and F.A. Kugutsheva: Compt. Tend. Acad. Sci., 1940, vol. 27, p. 670.

9) E. Raub and M. Engel: Metallk., 1948, vol. 39, p. 172.

10) M.V. Zakharov, M.V. Stepanova and V.M. Glazov: Metallovedenie i Obrabotaka Metallova, 1956, vol. 3, p. 23.

11) M.V. Zakharov, M.V. Stepanova and V.M. Glazov: Metallovedenie i Obrabotaka Metallova, 1957, vol. 3, p. 23.

12) K. Mizuno: Sumitomo Light Metal Tech. Rep., 1962, vol. 3, p. 55.

13) I. Kawakatsu, H. Suzuki and H. Kitano: J. Japan Inst. Metals, 1967, vol. 31, p. 1253.

14) R.F. Domagala, F.J. McPherson and M. Hansen: J. of Metals, 1953, vol. 5, p. 279.

15) G. Falkenhagen and W. Hofmann: Z Met., 1952, vol. 43, p. 69.

16) P. Duwex, R.H. Willens and W. Klement, Jr.: J. Appl. Phys., 1960, vol. 31, p. 1136.

17) P. Duwez: Fizika, 2 (Suppl. 2) 1.1 (1970)

18) P. Duwez: Trans. ASM, 1967, vol. 60, p. 607.

19) B.C. Giessen: Strengthening Mechanisms, Metals and Ceramics, ed. J.J. Burke, N.L. Reed, V. Weiss, Syracuse Univ. Press, Syracuse, New York, 1966.

20) R. Ray: Sc.D. Thesis, M.I.T., Cambridge, Mass., 1969.

21) A. Revolevschi: Private communications.

22) V.M. Martius: Progress in Metal. Physics, vol. 5, Pergamon Press, London, 1954.

23) T.F. Bower, H.D. Brody and M.C. Flemings: Trans. AIME, 1966, vol. 236, p. 624.

24) H. Matyja, B.C. Giessen and N.J. Grant: J. Inst. Metals, 1968, vol. 96, p. 30.

25) G.E. Ludin, D.J. McPherson and M. Hansen: J. Inst. Met., 1953, p. 273.

26) M.J. Saarivirta and A.E. Beck, Jr., U.S. Patent 2,842,438.

27) British Patent 838,981 (Nippert Electric Prod. Co.).

28) American Metal Climax Inc.: Technical Data on Amzirc, 1966.

29) J.P. Lynch: Wire and Wire Products, 1962, vol. 103, p. 1593.

30) J. Dooley, D.N. Hewett and N.B. Rutherford: C.D.A. Symposium, 1962.

31) M.J. Saarivirta and P.P. Taubenblat: Trans. AIME, 1960, vol. 218, p. 935.

32) W. Hodge: Trans. AIME, 1957, vol. 209, p. 408.

33) M.J. Saarivirta: Metal Ind., 1963, vol. 103, p. 685.

34) C.E. Sohl and R.J. DeAngelis: Technical Report No. 24-70-MET 11, Univ. of Kentucky, 1970.

35) M.L. Kronberg and F.H. Wilson: Trans. AIME, 1949, vol. 185, p. 501.

36) H. Suzuki, M. Kanno and I. Kawakatsu: J. Japan Inst. of Metals, 1969, vol. 33, p. 628.

37) Z. Henmi and T. Nagai: Trans. J.I.M., 1969, vol. 10, p. 305.

38) I. Tarora and T. Maruta: J. Japan Inst. Metals, 1961, vol. 25, p. 615.

39) H. Suzuki, I. Kawakatsu and H. Kitano: J. Japan Inst. of Metals, 1967, vol. 31, p. 342.

40) H. Suzuki, I. Kawakatsu, H. Kitano and A. Murase: J. Japan Inst. Metals, 1967, vol. 31, p.31.

41) J.C.M. Li: J. Applied Phys., 1962, vol. 33, p. 2958.

42) F. Bourelier and J. Montuelle: Mem. Sci. Rev. Met., 1968, vol. 65, p. 65.

43) K. Lucke and K. Detert: Acta. Met., 1957, vol. 5, p. 628.

44) W.C. Leslie, J.T. Michalack and F.W. Aul: Iron and its Dilute Solutions, Interscience Publ., 1963.

45) L.S. Darken: Trans. A.S.M., 1961, vol. 54, p. 600.

46) W. Jolly: J. Iron Steel Inst., 1967, vol. 205, p. 321.

47) P. Predecki, A.W. Mullendore and N.J. Grant: TMS-AIME, 1965, vol. 233, p. 1581.

48) R.C. Ruhl: Material Sci. & Eng., 1967, vol. 1, p. 313.

49) C.A. Hoffman and J.W. Weeton: NASA TN D-3527, 1966.

50) A. Taylor and B.J. Kagle: Crystallographic Data on Metal and Alloy Structures, Dover Publ., New York, 1963.

51) B.H. Alexander and F.N. Rhines: Trans. AIME, 1950, vol. 188, p. 1267.

52) B.D. Cullity: Elements of X-ray Diffraction, Addison-Wesley Publ., London, 1959.

53) J.E. Hilliard: Metal Progress, 1964, vol. 85, No. 5, p.99.

54) J.E. Hilliard: G.E. Res. Lab. Report, No. 62-RL-3133M, Schenectady, New York, 1962.

55) M.S. Grewal: Sc.D. Thesis, M.I.T., Cambridge, Mass., 1972

56) B. Chalmers: Principles of Solidification, John Wiley & Sons, New York, 1964.

57) P.G. Shewmon: Diffusion in Solids, McGraw-Hill, New York, 1963.

58) O. Preston: Sc.D. Thesis, M.I.T., Cambridge, Mass. (1958).

59) D.H. Roberts and N.A. Ratcliff: Metallurgica, 1964, vol. 70, p. 223.

60) D. Hardwick and W.J. McG Jegart: J. Inst. Metals, vol. 90, p. 17.

61) H.J. McQueen, W.A. Wong and J.J. Jonas: Acta Met., 1967, vol. 15, p. 586.

62) D. McLean: Mechanical Properties of Metals, John Wiley & Sons, New York, 1965.

63) P.G. Shewmon: Transformation in Metals, McGraw-Hill, New York, 1969.

64) W.R. Hibbard, Jr., F.D. Rosi, H.T. Clark, Jr., and R.I. O'Herron: Trans. AIME, 1948, vol. 175, p. 283.

65) W.R. Hibbard, Jr., and E.W. Hart: Trans. AIME, 1955, p. 283.

66) V.W. Köster and W. Knorr: Zeitschrift für Metallkunde, 1954, vol. 45, p. 350.

67) V.W. Grubl and R. Fischer: Zeitschrift für Metallkunde, 1955, vol. 46, p. 742.

68) V.C. Bungle, E.R. Honak and W. Nielsch: Zeitschrift für Metallkunde, 1953, vol. 44, p. 71.

69) R.O. Williams: Trans. ASM, 1960, vol. 52, p. 530.

70) V.A. Tracy and D.K. Worn: Powder Met., 1962, vol. 10, p. 34.

71) B.A. Wilcox, A.H. Clauer and W.B. Hutchinson: "Structural Stability and Mechanical Behaviour of Thermomechanicall Processed Dispersion Strengthened Nickle Alloys." NASA CR-72832.

72) M.V. Heimendahl and G. Thomas: Trans. AIME, 1964, vol. 230, p. 1520.

73) R.J. Towner: Trans. AIME, 1964, vol. 230, p. 505.

74) G.S. Doble and R.J. Quigg: Trans. AIME, 1965, vol. 233, p. 410.

75) R.W. Fraser and D.J.I. Evans: Dispersion Strengthening, Bolton Landing Conf., Gordan Breach Sci. Publ., New York, 1968.

76) G.S. Ansell: Oxide Dispersion Strengthening, Boltan Landing Conf., Gordan Breach Sci. Publ., New York, 1968.

77) A.T. English and G. Chin: Acta Met., 1965, vol. 13, p. 1013.

78) N. Brow: Trans. AIME, 1961, vol. 221, p. 236.

79) W.F. Hosford, Jr., and W.A. Backofen: Fundamentals of Deformation Processing, 9th Sagamore Conf., Syracuse Univ. Press, 1964.

80) G.E. Dieter, Jr.: Mechanical Metallurgy, McGraw-Hill, New York, 1961.

81) C. Barrett and T.B. Massalski: Structure of Metals, Third Edition, McGraw-Hill, New York, 1966.

82) O.D. Sherby and P.M. Burke: Mechanical Behaviour of Crystalline Solid at Elevated Temperature, Pergamon Press, London, 1968.

83) N. Jaffe and J.E. Dorn: Trans AIME, 1962, vol. 224, p. 1167.

84) J. Weertman: J. Applied Phys., 1957, vol. 28, p. 362.

85) Deformation and Fracture at Elevated Temperatures, ed., N.J. Grant and W. Mullendor, M.I.T. Press, Cambridge, Mass., 1965.

86) C.L. Bulow: Electro-Tech., 1963, vol. 71, p. 113.

87) D. Peckner: Materials in Design Eng., 1960, vol. 51, p. 16.

88) J.G. Rasmussen and N.J. Grant: Powder Met., 1965, vol. 8, No. 15, p. 92.

89) D. Brock: A Study on Ductile Fracture, Nederlandse Boekdruk Industne, S'-Hertogenbosch, 1971

90) M. Adachi and N.J. Grant: Trans. AIME, 1960, vol. 218, p. 881.

91) M.W. Yim and N.J. Grant: Trans. AIME, 1963, vol. 227, p. 868.

92) E. Gregory and N.J. Grant: Trans. AIME, 1954, vol. 6, p. 247.

93) J.W. Cahn: Acta Met., 1956, vol. 4, p. 449.

XI APPENDIX

Appendix 1

Reduction Data

Designation	As Rec. O_2 Wt. %	O_2 Wt. % of Reduced Powder	O_2 Wt. % in Wrought Alloy
IMT-1	0.21	0.19	0.19
IMT-2	0.35	0.30	0.30
IMT-3	0.47	0.43	0.43
IMT-4	0.67	0.56	0.56
ZA-2	0.03	0.02	0.03
ZA-3	0.04	0.06	0.03
ZA-8*	0.07	0.08	0.08
FM-8	0.11	0.11	0.11
ZA-10(a)	0.18	0.12	0.09
ZA-10(b)	0.18	0.11	0.08
ZAC-1	0.04	0.03	0.04
ZAC-2(a)	0.11	0.10	0.07
ZAC-2(b)	0.11	0.10	0.07

* ZA-8 reduced at 300°C for 6 hours, all others were reduced at 450°C for 10 hours.

Appendix 2

Compaction and Extrusion Data

Powder	Packing Density*
ZA-2	70.0**
ZA-3	70.0**
ZAC-1	70.0**
ZA-8	65.4
FM-8	61.0
ZA-10(a)	65.1
ZA-10(b)	48.6
ZAC-2(a)	58.2
ZAC-2(b)	49.0
IMT-1	51.2
IMT-2	57.4
IMT-3	54.3
IMT-4	59.0

* Powder compacting data relative to percent of theoretical density of pure copper (8.93 gms/cm^3).

** Assumed approx. densities after isostatic compaction.

Figure A-1 shows the effect of powder size on compaction density.

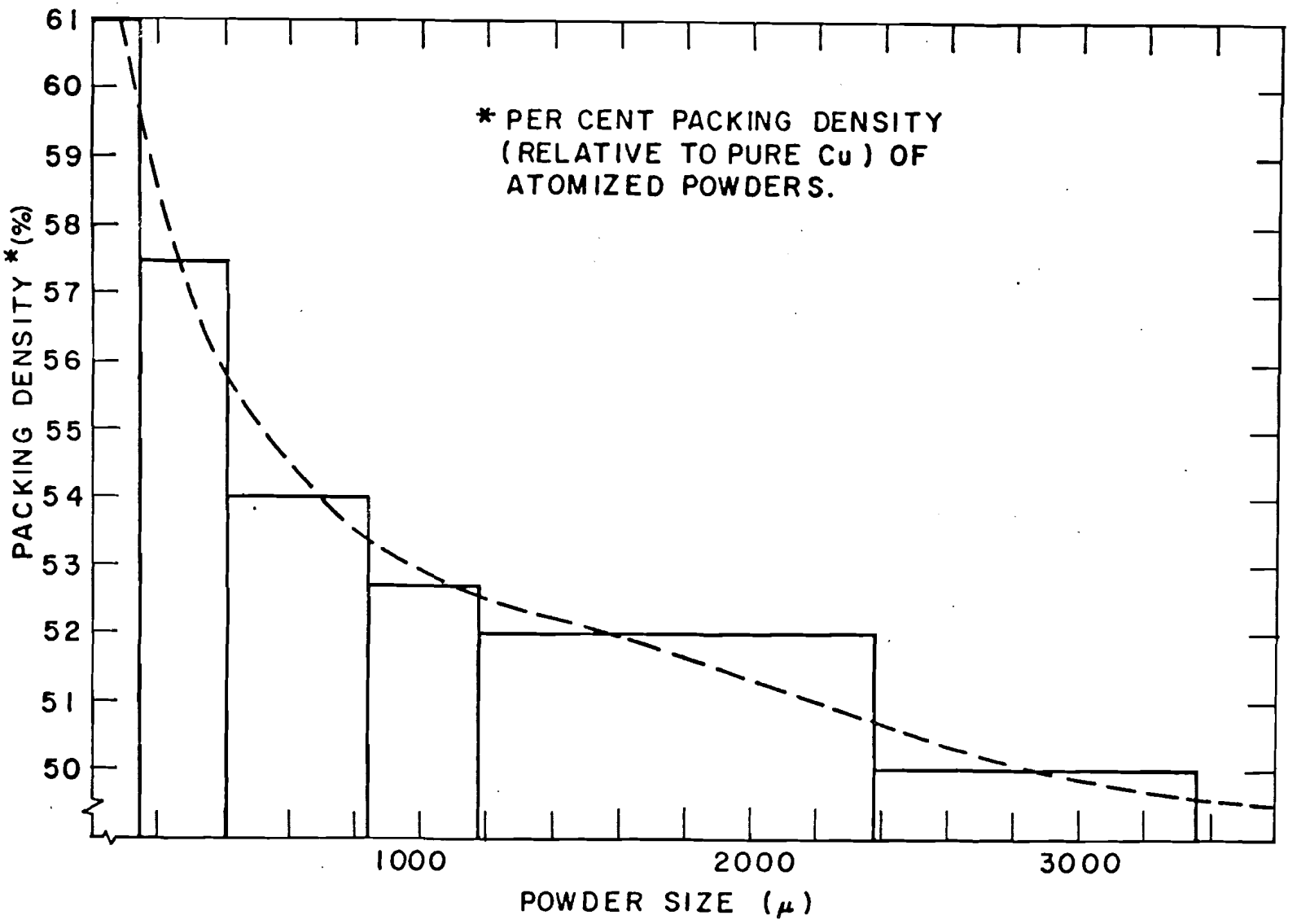

Figure A-1. Effect of powder size on packing density of atomatized powders (relative to pct. of theoretical density of pure copper 8.93 gms/cm^3.

Table IV

Hot Extrusion Data* and Final Alloy Composition

Steam Atomized Powders

Alloy	Ext. Temp.	Ext. Ratio	Die Size inch	Max. Upset Force (tons)	Max. Running Force (tons)	Zr Wt. %	O_2 Wt. %	Cu(bal) Wt. %
IMT-1	650	30:1	0.555	360	300	0.64	0.19	99.17
IMT-2	650	30:1	0.555	340	290	0.64	0.30	99.06
IMT-3	650	30:1	0.555	320	290	1.07	0.43	98.50
IMT-4	650	30:1	0.555	320	290	1.07	0.56	98.37

* A Ram speed of 100 inches per minute was used.

Table V

Hot Extrusion Data* and Final Alloy Compositions for

Nitrogen Atomized Powders

Alloy	Ext. Temp. (C)	Max. Upset Force (tons)	Max. Running Force (tons)	Ram Speed inch/min.	Zr Wt. %	Cr Wt. %	O_2 Wt. %	Cu(bal) Wt. %
ZA-2	600	360	270	140	0.20	-	0.03	99.77
ZA-3	650	350	325	100	0.37	-	0.03	99.60
ZA-8	650	400	355	30	0.80	-	0.08	99.17
FM-8	650	400	380	100	0.88	-	0.11	98.94
ZA-10(a)	650	450	400	30	0.90	-	0.09	99.02
ZA-10(b)	650	450	400	30	0.90	-	0.08	99.02
ZAC-1	650	350	325	100	0.10	0.32	0.04	99.54
ZAC-2(a)	650	420	370	30	0.23	0.33	0.07	99.37
ZAC-2(b)	650	450	400	30	0.23	0.33	0.07	99.37

* All extrusions (except for FM-8, which was extruded with a 30:1 ratio in a 0.555 inch die) were extruded through a 0.610 inch die to obtain a 25:1 ratio.

Appendix 3

Microscopy

A. Optical metallography.

Standard metallographic techniques were employed for polishing (through Linde B) for optical microscope examination. An acidic Ferric chloride etch of the following composition was used:

10 g. Ferric chloride
30 ml. Hydrochloric acid
120 ml. Water

Mean linear intercept measurements were made with a Hilliard circle[53,54] for grain size calculations. The mean linear intercept, $\bar{\ell}$, was calculated as

$$\bar{\ell} = \ell/Mn$$

where ℓ = total line length placed on the photograph, M = magnification, and n = number of boundaries intersected. Since this dimension does not measure the true diameter of the grain volume, as the plane of polish contains the full diameter of a few, if any, grains. Hence assuming uniform Kelvin polyhedra Cahn[93] obtained, the true face-to-face diameter as

$$d = 1.68\ \bar{\ell} = 1.68\ (\ell/Mn)$$

which was the relationship used for this investigation.

B. Electron Microscopy.

Thin wafers approximately 12-15 mils. thick, of the material to be examined, were sectioned using a silicon carbide blade. These wafers

were then ground and polished on both sides to obtain slices approximately 5mil. thick with a Linde B finish. Discs of 3mm diameter were then punched and lacquered with microstop around their periphery.

Final thinning was carried out in an Astromet apparatus (with submerged double jet) using the following electrolyte:

500 c.c. Phosphoric acid
500 c.c. Glycerin
125 c.c. Water

A voltage between 6 to 8 voltages was used, with the electrolyte maintained below 10°C. Thirty to forty minutes were usually required for perforation. Foils were examined at 100 KV on a JEM 7 unit.

Extensive election diffraction work revealed the presence of ZrO_2 in the alloys. The presence of elemental chromium was identified in the ZAC series of alloys. No positive identification of individual particles (Cu_3Zr, ZrO_2, Cr, Cr_2Zr) could be made. Selected area diffraction on splat cooled ZA-2 on precipilate particles revealed the presence of unidentifiable diffraction spot (Figure A-2). Figure A-3 shows a generalized diffraction pattern of ZAC-1. The camera constant was found to be approximately 24 (mm $\mathring{A}$) hence

$$d \times \overline{R} = 24$$

where d = spacing of various planes ($\mathring{A}$) and $\overline{R}$ = measured distance between Debye rings of the diffraction pattern. Calculations on the two patterns Figures A-2 and 3) are given below. A comparison is also made between the pattern of splat cooled ZA-2 and a typical pattern obtained on the wrought alloy.

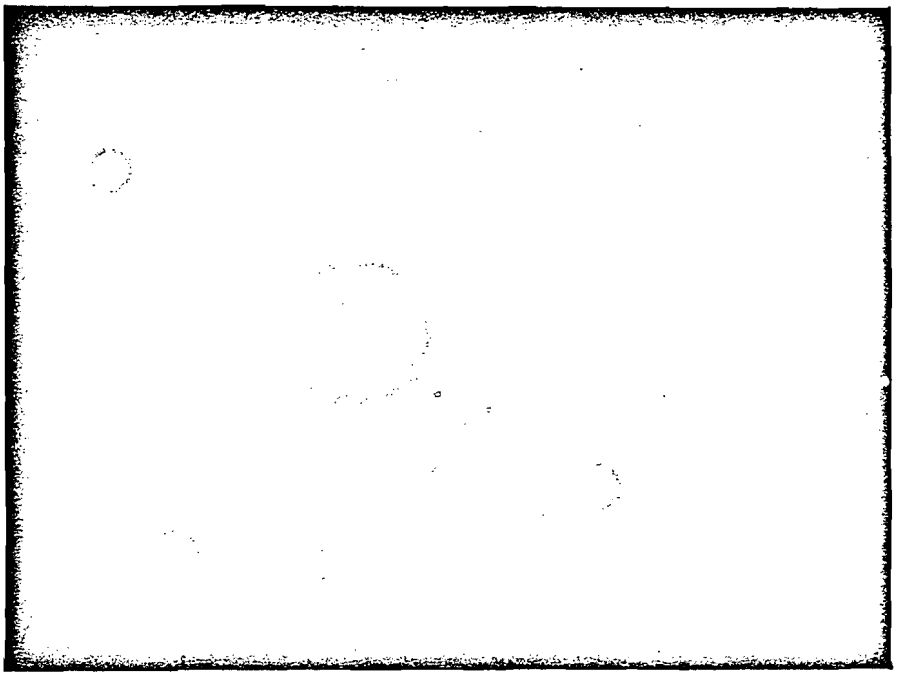

Figure A-2. Selected area diffraction pattern obtained of splat ZA-2.

Figure A-3. Diffraction pattern of ZAC-1 in the extruded condition.

Index Pattern of Splat Cooled ZA-2 (Figure A-2)

Line	$\overline{R}$(mm)	d(Å)	Identification
(1)	7.8	3.06	?
(2)	10.0	2.40	?
(3)	11.6	2.07	(111) Cu
(4)	13.4	1.79	(200) Cu or (220) ZrO_2
(5)	16.4	1.46	(222) ZrO_2
(6)	18.8	1.27	(220) Cu or (400) ZrO_2
(7)	22.1	1.09	(311) Cu
(8)	24.8	0.97	(333, 511) ZrO_2

A Typical Pattern Obtained on As-Extruded ZA-2

Line	$\overline{R}$(mm)	d(Å)	Identification
(1)	9.4	2.56	(200) ZrO_2
(2)	11.6	2.07	(111) Cu
(3)	13.3	1.80	(200) Cu or (220) ZrO_2
(4)	15.7	1.53	(311) ZrO_2
(5)	16.4	1.46	(222) ZrO_2
(6)	18.7	1.28	(220) Cu or (400) ZrO_2
(7)	21.6	1.10	(311) Cu
(8)	26.7	0.90	(400) Cu

A Typical Pattern Obtained on As-Extruded ZAC-1 (Figure A-3)

Line	$\overline{R}$(mm)	d(Å)	Identification
(1)	9.4	2.56	(200) ZrO_2 or (220) Cr_2Zr
(2)	11.6	2.07	(111) Cu or (222) Cr_2Zr
(3)	13.3	1.80	(200) Cu or (220) ZrO_2
(4)	18.8	1.27	(220) Cu or (400) ZrO_2 or (440) Cr_2Zr
(5)	20.3	1.18	(211) Cr
(6)	21.8	1.10	(311) Cu or (533) Cr_2Zr
(7)	23.1	1.04	(222) Cu or (444) Cr_2Zr
(8)	29.0	0.83	(222) Cr

Appendix 4

X-ray Analysis

Lattice parameters of some of the nitrogen atomized powders in the as-extruded condition. Subsequent decomposition studies up to 700°C on these powders showed no variations (within experiment error) in lattice parameters of these powders.

Powder	Calculated Lattice Parameter Å*
ZA-2	3.615
ZA-3	3.616
ZA-8	3.618
ZAC-1	3.619

* Estimated error of ± .002 Å

Appendix 5

Room Temperature Tensile Test Data

Alloy & Condition	0.2% Offset Y.S. (psi)	U.T.S. (psi)	Elong. (%)	R.A. (%)
IMT-1 (As-Ext)	26,000	38,500	31.6	55.2
IMT-2 (As-Ext)	25,000	35,000	32.0	71.0
IMT-3 (As-Ext)	45,000	47,500	23.3	30.0
IMT-4 (As-Ext)	28,000	37,000	25.4	31.2
ZA-2				
As-Ext	28,000	37,000	34.2	84.5
Ext + 30% R.A. (B, I.A. 300°C)	39,000	46,000	16.4	85.0
Ext + 50% R.A. (B, I.A. 300°C)	47,000	49,000	23.0	82.5
Ext + 80% R.A. (B, I.A. 300°C)	49,000	53,500	21.4	88.0
Ext + 90% R.A. (B, I.A. 300°C)	47,500	54,500	17.6	90.5
Ext + 90% R.A. (A, I.A. 20°C)	49,000	51,200	16.0	88.0
Ext + 75% R.A. (C, Aged 450°C)	56,000	57,000	16.4	90.5
Ext + 90% R.A. (C, Aged 450°C)	57,000	58,000	16.6	90.5
ZA-3				
As-Ext	25,000	37,000	34.0	88.0
Ext + 60% R.A. (B, I.A. 300°C)	42,500	55,250	22.3	86.5
Ext + 90% R.A. (B, I.A. 300°C)	56,000	59,000	14.0	90.5
Ext + 75% R.A. (C, Aged 450°C)	59,000	60,000	14.0	89.0
ZA-8				
As-Ext	47,000	60,500	30.5	65.5
Ext + 50% R.A. (A, I.A. 20°C)	67,500	69,000	13.5	68.0
Ext + 75% R.A. (A, I.A. 20°C)	63,500	68,000	15.5	70.0
Ext + 30% R.A. (B, I.A. 300°C)	52,500	62,000	13.6	65.0
Ext + 40% R.A. (B, I.A. 300°C)	60,500	63,500	13.8	78.0
Ext + 58% R.A. (B, I.A. 300°C)	61,500	66,500	17.4	74.0
Ext + 67% R.A. (B, I.A. 300°C)	64,000	70,000	13.6	81.0
Ext + 75% R.A. (B, I.A. 300°C)	69,000	76,000	18.0	78.0
Ext + 75% R.A. (B, I.A. 400°C)	63,000	68,000	18.8	74.0
Ext + 75% R.A. (B, I.A. 500°C)	61,000	67,000	19.0	78.0
Ext + 75% R.A. (B, I.A. 600°C)	59,000	66,000	20.2	76.0
Ext + 75% R.A. (B, I.A. 450°C)	64,000	69,500	20.0	65.0

Alloy & Condition	0.2% Offset Y.S. (psi)	U.T.S. (psi)	Elong. (%)	R.A. (%)
FM-8				
As-Ext	37,000	50,000	34.4	80.5
Ext + 90% R.A. (A, I.A. 20°C)	60,000	63,000	12.8	77.0
Ext + 90% R.A. (F, I.A. 300°C)	60,000	64,000	14.0	77.0
Ext + 90% R.A. (F, I.A. 400°C)	57,000	61,500	15.0	81.0
Ext + 90% R.A. (F, I.A. 500°C)	57,000	62,000	15.4	84.5
Ext + 90% R.A. (C, Aged 500°C)	57,500	61,000	13.0	84.5
ZA-10(a)				
As-Ext	34,000	51,000	34.0	53.8
Ext + 75% R.A. (C, Aged 450°C)	63,000	65,500	25.5	69.5
ZA-10(b)				
As-Ext	35,000	50,500	27.5	49.5
Ext + 75% R.A. (C, Aged 450°C)	70,500	71,800	10.5	55.2
ZAC-1				
As-Ext	35,000	37,000	22.6	86.5
Ext + 60% R.A. (B, I.A. 300°C)	42,000	44,500	21.2	84.5
Ext + 90% R.A. (B, I.A. 300°C)	50,500	51,500	14.0	89.0
Ext + 75% R.A. (C, Aged 450°C)	73,000	76,000	14.0	85.0
Ext + 75% R.A. (D, Aged 500°C)	63,000	66,000	14.6	85.0
Ext + 75% R.A. (E, I.A. 500°C)	63,000	71,200	17.8	
ZAC-2(a)				
As-Ext	46,500	60,500	21.0	68.0
Ext + 75% R.A. (C, Aged 400°C)	82,000	84,500	13.0	60.0
Ext + 75% R.A. (C, Aged 450°C)	84,000	86,500	13.2	70.0
Ext + 75% R.A. (C, Aged 500°C)	81,500	84,000	15.0	75.0
ZAC-2(b)				
As-Ext	46,000	62,500	20.0	59.5
Ext + 75% R.A. (C, Aged 450°C)	82,000	84,500	10.5	31.2

The Effect of Annealing Temperature on Room Temperature Tensile Properties

Alloy & Condition	Exposure Temp. (°C)	Y.S. (psi)	U.T.S. (psi)	Elong. (%)	R.A. (%)
ZA-2*					
Ext + 50% R.A. (B, I.A. 300°C)	400	39,600	45,000	26.0	87.0
Ext + 80% R.A. (B, I.A. 300°C)	400	39,000	47,000	22.0	92.0
Ext + 90% R.A. (B, I.A. 300°C)	400	42,500	46,000	18.8	90.1
Ext + 50% R.A. (B, I.A. 300°C)	600	34,500	39,000	30.0	92.0
Ext + 80% R.A. (B, I.A. 300°C)	600	34,500	37,200	27.0	93.1
Ext + 90% R.A. (B, I.A. 300°C)	600	33,000	38,000	23.2	91.2
Ext + 50% R.A. (B, I.A. 300°C)	800	24,300	36,000	34.4	92.2
Ext + 80% R.A. (B, I.A. 300°C)	800	23,500	35,000	34.0	94.0
Ext + 90% R.A. (B, I.A. 300°C)	800	23,000	34,500	32.0	92.0
ZA-3					
Ext + 75% R.A. (C, Aged 450°C)	350	49,000	52,600	16.2	87.2
Ext + 75% R.A. (C, Aged 450°C)	500	24,000	47,600	38.6	86.0
Ext + 75% R.A. (C, Aged 450°C)	600	23,000	47,000	40.5	86.0
Ext + 75% R.A. (C, Aged 450°C)	750	16,800	45,700	42.1	85.3
ZA-3*					
Ext + 75% R.A. (C, Aged 450°C)	280	46,000	50,500	18.5	87.0
Ext + 75% R.A. (C, Aged 450°C)	400	43,600	49,000	21.0	87.1
Ext + 75% R.A. (C, Aged 450°C)	600	19,200	41.500	34.8	87.0
Ext + 75% R.A. (C, Aged 450°C)	750	14,100	41,000	39.0	87.5
ZA-8					
Ext + 75% R.A. (B, I.A. 300°C)	350	55,100	65,500	18.0	74.0
Ext + 75% R.A. (B, I.A. 500°C)	350	54,000	63,000	20.2	78.0
Ext + 75% R.A. (B, I.A. 600°C)	350	51,200	60,300	25.2	80.0

Alloy & Condition	Exposure Temp. (°C)	Y.S. (psi)	U.T.S. (psi)	Elong. (%)	R.A. (%)
Ext + 75% R.A. (B, I.A. 300°C)	500	48,600	58,000	21.0	83.0
Ext + 75% R.A. (B, I.A. 300°C)	500	43,600	59,000	27.6	81.0
Ext + 75% R.A. (B, I.A. 300°C)	500	40,500	56,500	27.6	81.0
Ext + 75% R.A. (B, I.A. 300°C)	600	48.000	57,500	25.0	81.0
Ext + 75% R.A. (B, I.A. 500°C)	600	43,000	57,000	28.6	81.0
Ext + 75% R.A. (B, I.A. 600°C)	600	40,500	55,500	29.6	78.0
Ext + 75% R.A. (B, I.A. 300°C)	750	36,000	53,400	27.2	81.0
Ext + 75% R.A. (B, I.A. 500°C)	750	36,000	53,000	29.4	80.0
Ext + 75% R.A. (B, I.A. 600°C)	750	36,000	52,500	36.2	79.0
ZAC-1					
Ext + 75% R.A. (C, Aged 450°C)	350	73,000	78,000	16.0	65.0
Ext + 75% R.A. (C, Aged 450°C)	500	55,000	60,500	24.5	85.0
Ext + 75% R.A. (C, Aged 450°C)	600	44,000	55,000	38.0	87.0
Ext + 75% R.A. (C, Aged 450°C)	750	23,000	49,000	43.0	85.0
Ext + 75% R.A. (D, Aged 500°C)	350	62,800	70,500	20.4	87.0
Ext + 75% R.A. (D, Aged 500°C)	500	43,600	58,500	23.6	90.0
Ext + 75% R.A. (D, Aged 500°C)	600	41,000	52,600	25.0	92.0
Ext + 75% R.A. (D, Aged 500°C)	750	20,000	42,500	43.9	92.0
ZAC-1*					
Ext + 75% R.A. (C, Aged 450°C)	280	61,500	68,000	18.2	80.0
Ext + 75% R.A. (C, Aged 450°C)	400	59,000	67,000	18.6	82.0
Ext + 75% R.A. (C, Aged 450°C)	500	46,700	56,500	19.2	87.0
Ext + 75% R.A. (C, Aged 450°C)	600	42,500	52,700	22.0	86.0
Ext + 75% R.A. (C, Aged 450°C)	750	19,000	42,500	42.0	85.0
ZAC-2(a)					
Ext + 75% R.A. (C, Aged 450°C)	350	72,600	82,100	20.0	70.0
Ext + 75% R.A. (C, Aged 500°C)	350	71,500	81,000	17.0	70.0
Ext + 75% R.A. (C, Aged 450°C)	500	50,000	61,200	20.8	81.0
Ext + 75% R.A. (C, Aged 500°C)	500	47,500	60,000	20.2	78.0

Alloy & Condition	Exposure Temp. (°C)	Y.S. (psi)	U.T.S. (PSI)	Elong. (%)	R.A. (%)
Ext + 75% R.A. (C, Aged 450°C)	600	47,500	57,500	21.4	81.0
Ext + 75% R.A. (C, Aged 500°C)	600	47,000	57,000	20.0	74.0
Ext + 75% R.A. (C, Aged 450°C)	750	19,500	45,000	41.4	81.0
Ext + 75% R.A. (C, Aged 500°C)	750	18,600	44,800	41.2	78.0

* Signify's tests annealed for one hour at temperature, all other tests were annealed for one half hour.

Appendix 6

Stress Rupture Data

Alloy & Condition	Temp. (°C)	Stress (psi)	Rupture Time(hrs)	Elong. (%)	R.A. (%)
IMT-1	400°C	22,000	0.33	2.1	18.0
	400°C	20,000	2.78	16.5	30.0
	400°C	18,000	23.40	2.1	21.0
	400°C	17,000	58.40	15.0	21.0
IMT-2	400°C	20,000	0.32	7.5	59.0
	400°C	17,000	4.10	5.2	26.0
	400°C	14,500	78.40	6.0	34.0
IMT-3	400°C	23,000	0.67	2.3	11.0
	400°C	22,000	0.67	5.5	30.0
	400°C	20,000	33.00	2.5	17.0
	400°C	18,000	14.71	2.8	13.0
IMT-4	400°C	20,000	1.00	1.5	21.0
	400°C	17,000	27.50	1.1	8.0
	400°C	16,000	96.40	1.0	8.0
ZA-2					
As-Ext	450°C	20,000	0.07	22.6	78.0
As-Ext	450°C	18,500	0.70	28.4	70.0
As-Ext	450°C	16,000	9.00	25.8	78.0
As-Ext	450°C	15,400	170.00	--	--
Ext + 50% R.A. (B, I.A. 300°C)	450°C	25,000	0.31	26.5	74.0
Ext + 50% R.A. (B, I.A. 300°C)	450°C	22,200	2.40	27.6	75.5
Ext + 50% R.A. (B, I.A. 300°C)	450°C	20,000	7.70	5.8	70.0
Ext + 50% R.A. (B, I.A. 300°C)	450°C	18,000	23.40	--	--

Alloy & Condition	Temp. (°C)	Stress (psi)	Rupture Time(hrs)	Elong. (%)	R.A. (%)
Ext + 50% R.A. (B, I.A. 300°C)	650°C	10,000	0.07	41.0	81.5
Ext + 50% R.A. (B, I.A. 300°C)	650°C	5,000	5.00	22.2	12.2
Ext + 50% R.A. (B, I.A. 300°C)	650°C	4,000	33.60	10.7	10.7
Ext + 80% R.A. (B, I.A. 300°C)	450°C	25,000	0.05	4.1	90.0
Ext + 80% R.A. (B, I.A. 300°C)	450°C	22,000	1.07	2.8	87.0
Ext + 80% R.A. (B, I.A. 300°C)	450°C	21,000	2.18	4.7	81.0
Ext + 80% R.A. (B, I.A. 300°C)	450°C	20,000	8.80	3.9	80.0
Ext + 80% R.A. (B, I.A. 300°C)	650°C	12,000	0.10	4.5	90.0
Ext + 80% R.A. (B, I.A. 300°C)	650°C	10,000	1.33	7.9	78.0
Ext + 80% R.A. (B, I.A. 300°C)	650°C	7,600	6.50	2.9	50.0
Ext + 80% R.A. (B, I.A. 300°C)	650°C	6,900	15.00	1.8	44.0
Ext + 90% R.A. (B, I.A. 300°C)	450°C	26,000	0.40	4.3	90.0
Ext + 90% R.A. (B, I.A. 300°C)	450°C	23,000	4.00	3.6	85.0
Ext + 90% R.A. (B, I.A. 300°C)	450°C	20,000	41.00	7.3	87.0
Ext + 90% R.A. (B, I.A. 300°C)	300°C	45,000	0.02	3.2	89.0
Ext + 90% R.A. (B, I.A. 300°C)	300°C	35,000	2.40	9.6	90.0
Ext + 90% R.A. (B, I.A. 300°C)	300°C	31,000	40.63	2.7	93.0
Ext + 90% R.A. (B, I.A. 300°C)	400°C	30,000	0.30	4.3	87.0
Ext + 90% R.A. (B, I.A. 300°C)	400°C	25,000	9.15	3.1	87.0
Ext + 90% R.A. (B, I.A. 300°C)	400°C	22,000	64.50		
Ext + 90% R.A. (B, I.A. 300°C)	650°C	12,000	0.15	4.5	90.0
Ext + 90% R.A. (B, I.A. 300°C)	650°C	10,000	0.60	4.2	87.0
Ext + 90% R.A. (B, I.A. 300°C)	650°C	7,600	14.70	1.1	25.0
Ext + 90% R.A. (B, I.A. 300°C)	650°C	6,900	20.00	-	--
Ext + 90% R.A. (C, Aged 300°C)	400°C	35,000	0.75	5.2	94.0
Ext + 90% R.A. (C, Aged 300°C)	400°C	32,000	14.00	3.1	92.0
Ext + 90% R.A. (C, Aged 300°C)	400°C	29,500	71.50	3.9	92.0
Ext + 90% R.A. (C, Aged 300°C)	450°C	30,000	0.90	2.7	94.0
Ext + 90% R.A. (C, Aged 300°C)	450°C	27,000	5.70	2.7	94.0
Ext + 90% R.A. (C, Aged 300°C)	450°C	25,000	15.80	5.9	92.0
Ext + 90% R.A. (C, Aged 300°C)	450°C	20,000	322.00	2.5	92.0
Ext + 90% R.A. (C, Aged 300°C)	650°C	12,000	0.01	4.5	90.0
Ext + 90% R.A. (C, Aged 300°C)	650°C	11,500	0.35	3.5	96.0
Ext + 90% R.A. (C, Aged 300°C)	650°C	10,000	0.70	3.3	96.0
Ext + 90% R.A. (C, Aged 300°C)	650°C	6,000	34.00	2.3	18.0

Alloy & Condition	Temp. (°C)	Stress (psi)	Rupture Time(hrs)	Elong. (%)	R.A. (%)
ZA-3					
As-Ext.	400°C	22,000	0.70	9.9	93.0
As-Ext.	400°C	20,000	14.40	9.3	91.0
As-Ext.	400°C	17,000	162.50	9.4	97.0
Ext + 60% R.A. (B, I.A. 300°C)	400°C	27,000	1.20	9.6	91.0
Ext + 60% R.A. (B, I.A. 300°C)	400°C	22,000	29.40	9.8	90.0
Ext + 60% R.A. (B, I.A. 300°C)	400°C	21,000	66.70	10.5	90.0
Ext + 60% R.A. (B, I.A. 300°C)	650°C	10,000	1.54	20.0	95.0
Ext + 60% R.A. (B, I.A. 300°C)	650°C	7,000	2.00	--	34.0
Ext + 60% R.A. (B, I.A. 300°C)	650°C	5,000	31.00	5.8	26.0
Ext + 90% R.A. (B, I.A. 300°C)	400°C	30,000	0.33	7.3	92.0
Ext + 90% R.A. (B, I.A. 300°C)	400°C	25,000	16.74	7.2	92.0
Ext + 90% R.A. (B, I.A. 300°C)	400°C	22,000	138.00	0.5	92.0
Ext + 75% R.A. (C, Aged 300°C)	400°C	37,000	0.17	7.2	89.0
Ext + 75% R.A. (C, Aged 300°C)	400°C	30,000	18.00	5.6	85.0
Ext + 75% R.A. (C, Aged 300°C)	400°C	28,000	32.10	1.9	89.0
Ext + 75% R.A. (C, Aged 300°C)	400°C	27,000	148.90	1.8	85.0
Ext + 75% R.A. (C, Aged 300°C)	500°C	22,000	2.97	6.5	85.0
Ext + 75% R.A. (C, Aged 300°C)	500°C	19,000	85.00	5.9	--
Ext + 75% R.A. (C, Aged 300°C)	650°C	11,000	0.15	7.9	50.0
Ext + 75% R.A. (C, Aged 300°C)	650°C	7,000	4.00	5.8	32.0
ZA-8					
As-Ext	400°C	35,000	0.12	10.1	80.0
As-Ext	400°C	29,000	4.16	--	--
As-Ext	400°C	25,000	98.60	9.1	61.2
Ext + 50% R.A. (A, I.A. 20°C)	400°C	40,000	0.76	6.0	55.0
Ext + 50% R.A. (A, I.A. 20°C)	400°C	37,000	10.00	5.1	38.0
Ext + 75% R.A. (A, I.A. 20°C)	400°C	37,000	0.47	29.0	87.0
Ext + 75% R.A. (A, I.A. 20°C)	400°C	30,000	19.35	25.0	87.0
Ext + 75% R.A. (A, I.A. 20°C)	650°C	9,600	4.50	26.0	30.0
Ext + 75% R.A. (A, I.A. 20°C)	650°C	5,000	60.80	24.0	25.0

Alloy & Condition	Temp (°C)	Stress (psi)	Rupture Time (hrs)	Elong. (%)	R.A. (%)
Ext + 75% R.A. (B, I.A. 300°C)	400°C	37,000	0.58	-	--
Ext + 75% R.A. (B, I.A. 300°C)	400°C	35,000	17.00	7.7	38.0
Ext + 75% R.A. (B, I.A. 300°C)	400°C	30,000	36.20	6.9	81.0
Ext + 75% R.A. (B, I.A. 300°C)	650°C	8,000	5.36	8.8	55.0
Ext + 75% R.A. (B, I.A. 300°C)	650°C	6,000	31.80	4.2	44.0
Ext + 75% R.A. (B, I.A. 300°C)	650°C	5,000	92.00	3.7	38.0
Ext + 75% R.A. (B, I.A. 400°C)	400°C	40,000	0.22	7.1	87.0
Ext + 75% R.A. (B, I.A. 400°C)	400°C	30,000	54.50	6.0	81.0
Ext + 75% R.A. (B, I.A. 400°C)	650°C	10,000	1.20	7.2	85.0
Ext + 75% R.A. (B, I.A. 400°C)	650°C	8,000	11.00	5.1	81.0
Ext + 75% R.A. (B, I.A. 400°C)	650°C	7,000	11.50	4.7	32.0
Ext + 75% R.A. (B, I.A. 400°C)	650°C	6,000	78.20	4.6	44.0
Ext + 75% R.A. (B, I.A. 500°C)	400°C	35,000	0.47	7.0	85.0
Ext + 75% R.A. (B, I.A. 500°C)	400°C	30,000	8.70	8.0	85.0
Ext + 75% R.A. (B, I.A. 500°C)	650°C	8,000	10.20	6.9	60.0
Ext + 75% R.A. (B, I.A. 500°C)	650°C	7,000	25.20	6.5	44.0
Ext + 75% R.A. (B, I.A. 600°C)	400°C	30,000	2.34	8.6	85.0
Ext + 75% R.A. (B, I.A. 600°C)	400°C	26,000	33.40	7.5	87.0
Ext + 75% R.A. (B, I.A. 600°C)	650°C	8,000	5.00	7.3	81.0
Ext + 75% R.A. (B, I.A. 600°C)	650°C	6,000	56.20	-	38.0
Ext + 75% R.A. (B, I.A. 600°C)	650°C	5,000	167.20	-	--
Ext + 75% R.A. (C, Aged 450°C)	400°C	40,000	0.51	6.7	81.0
Ext + 75% R.A. (C, Aged 450°C)	400°C	35,000	8.35	5.3	77.8
Ext + 75% R.A. (C, Aged 450°C)	400°C	32,000	15.87	1.7	77.8
Ext + 75% R.A. (C, Aged 450°C)	400°C	31,000	21.65	10.0	85.0
Ext + 75% R.A. (C, Aged 450°C)	650°C	10,000	0.34	13.0	55.0
Ext + 75% R.A. (C, Aged 450°C)	650°C	6,000	1.64	12.3	50.0
FM-8					
As-Ext	400°C	35,000	0.10	8.5	88.0
As-Ext	400°C	27,000	5.86	6.5	55.0
As-Ext	400°C	20,000	653.50	4.0	53.0

Alloy & Condition	Temp. (°C)	Stress (psi)	Rupture Time(hrs)	Elong. (%)	R.A. (%)
Ext + 90% R.A. (F, I.A. 300°C)	400°C	35,000	0.34	6.0	85.0
Ext + 90% R.A. (F, I.A. 300°C)	400°C	30,000	5.84	5.3	85.0
Ext + 90% R.A. (F, I.A. 300°C)	400°C	26,000	63.40	4.6	77.0
Ext + 90% R.A. (F, I.A. 300°C)	650°C	10,000	0.50	7.0	77.0
Ext + 90% R.A. (F, I.A. 300°C)	650°C	5,000	30.00	-	--
Ext + 90% R.A. (F, I.A. 400°C)	400°C	35,000	1.00		
Ext + 90% R.A. (F, I.A. 400°C)	400°C	30,000	6.00	4.9	85.0
Ext + 90% R.A. (F, I.A. 400°C)	400°C	27,000	60.00	6.5	85.0
Ext + 90% R.A. (F, I.A. 400°C)	650°C	10,000	0.43	5.8	81.0
Ext + 90% R.A. (F, I.A. 400°C)	650°C	8,700	0.95	8.4	77.0
Ext + 90% R.A. (F, I.A. 400°C)	650°C	5,000	44.50	4.5	38.0
Ext + 90% R.A. (C, Aged 500°C)	400°C	48,000	0.05	4.7	85.0
Ext + 90% R.A. (C, Aged 500°C)	400°C	37,000	1.20	4.5	85.0
Ext + 90% R.A. (C, Aged 500°C)	400°C	35,000	3.00	5.0	85.0
Ext + 90% R.A. (C, Aged 500°C)	400°C	30,000	115.00	3.8	85.0
Ext + 90% R.A. (C, Aged 500°C)	650°C	10,000	0.20	7.0	77.0
Ext + 90% R.A. (C, Aged 500°C)	650°C	5,000	20.20	4.3	38.0
Ext + 90% R.A. (C, Aged 500°C)	650°C	3,200	270.80	-	--
Ext + 90% R.A. (F, I.A. 500°C)	650°C	10,000	0.36	6.3	57.0
Ext + 90% R.A. (F, I.A. 500°C)	650°C	5,000	79.50		
ZA-10(a)					
As-Ext	400°C	40,000	0.34	8.0	70.0
As-Ext	400°C	25,000	8.50	9.5	70.0
As-Ext	400°C	23,000	62.50	16.3	68.0
As-Ext	650°C	10,000	0.26	6.3	68.0
ZA-10(b)					
As-Ext	400°C	25,000	7.54	10.5	31.8
As-Ext	400°C	23,000	153.00	5.6	39.0
As-Ext	650°C	10,000	0.21	10.5	31.8

Alloy & Condition	Temp. (°C)	Stress (psi)	Rupture Time(hrs)	Elong. (%)	R.A. (%)
ZAC-1					
As-Ext	400°C	27,000	0.13	9.5	80.0
As-Ext	400°C	17,000	30.00	10.2	65.0
As-Ext	400°C	12,000	523.50	29.0	30.0
Ext + 60% R.A. (B, I.A. 300°C)	400°C	27,000	0.71	7.1	91.0
Ext + 60% R.A. (B, I.A. 300°C)	400°C	22,000	16.45	8.4	80.0
Ext + 60% R.A. (B, I.A. 300°C)	400°C	18,000	147.50	3.5	93.0
Ext + 60% R.A. (B, I.A. 300°C)	650°C	10,000	0.35	8.9	50.0
Ext + 60% R.A. (B, I.A. 300°C)	650°C	6,200	12.00	5.2	21.0
Ext + 60% R.A. (B, I.A. 300°C)	650°C	5,000	52.50	2.9	17.0
Ext + 90% R.A. (B, I.A. 300°C)	400°C	30,000	0.43	3.6	78.0
Ext + 90% R.A. (B, I.A. 300°C)	400°C	23,000	18.60	3.2	90.0
Ext + 90% R.A. (B, I.A. 300°C)	400°C	20,000	119.80	4.9	90.0
Ext + 90% R.A. (C, Aged 450°C)	400°C	60,000	0.20	3.0	81.0
Ext + 90% R.A. (C, Aged 450°C)	400°C	40,000	51.30	3.3	44.0
Ext + 90% R.A. (C, Aged 450°C)	400°C	33,000	530.00	2.1	11.0
Ext + 90% R.A. (C, Aged 450°C)	650°C	16,500	1.30	2.7	25.0
Ext + 90% R.A. (C, Aged 450°C)	650°C	15,000	2.00	2.0	31.0
Ext + 90% R.A. (C, Aged 450°C)	650°C	10,000	17.85	5.1	32.0
Ext + 75% R.A. (D, Aged 500°C)	400°C	40,000	52.00	4.3	18.0
Ext + 75% R.A. (D, Aged 500°C)	650°C	12,500	11.35	1.5	25.0
Ext + 75% R.A. (D, Aged 500°C)	650°C	10,000	45.00	1.5	18.0
Ext + 75% R.A. (D, Aged 500°C)	650°C	9,000	110.50	1.0	18.0
Ext + 75% R.A. (E, I.A. 500°C)	400°C	40,000	3.90	6.8	85.0
Ext + 75% R.A. (E, I.A. 500°C)	400°C	37,000	10.50		
Ext + 75% R.A. (E, I.A. 500°C)	400°C	35,000	20.00	3.7	18.0
Ext + 75% R.A. (E, I.A. 500°C)	650°C	10,000	23.20	2.7	18.0
ZAC-2(a)					
As-Ext	400°C	40,000	0.33	8.0	70.0
As-Ext	400°C	35,000	8.50	9.5	70.0
As-Ext	400°C	30,000	94.00	2.3	21.0

Alloy & Condition	Temp. (°C)	Stress (psi)	Rupture Time(hrs)	Elong. (%)	R.A. (%)
Ext + 75% R.A. (C, Aged 400°C)	400°C	50,000	26.95	2.8	50.0
Ext + 75% R.A. (C, Aged 400°C)	400°C	45,000	174.00	2.5	25.0
Ext + 75% R.A. (C, Aged 400°C)	650°C	10,000	4.63	2.4	11.0
Ext + 75% R.A. (C, Aged 400°C)	650°C	7,800	13.90	-	--
Ext + 75% R.A. (C, Aged 400°C)	650°C	6,000	30.80	2.0	11.0
Ext + 75% R.A. (C, Aged 450°C)	400°C	50,000	11.72	1.3	65.0
Ext + 75% R.A. (C, Aged 450°C)	400°C	47,000	36.40	1.3	60.4
Ext + 75% R.A. (C, Aged 450°C)	400°C	40,000	52.50	-	3.1
Ext + 75% R.A. (C, Aged 450°C)	650°C	16,200	0.89	9.9	11.0
Ext + 75% R.A. (C, Aged 450°C)	650°C	10,000	9.10	-	--
Ext + 75% R.A. (C, Aged 450°C)	650°C	6,000	70.00	-	--
Ext + 75% R.A. (C, Aged 500°C)	400°C	50,000	0.20	5.0	70.0
Ext + 75% R.A. (C, Aged 500°C)	400°C	42,000	7.25	5.1	74.0
Ext + 75% R.A. (C, Aged 500°C)	400°C	37,000	195.20	4.6	38.0
Ext + 75% R.A. (C, Aged 500°C)	650°C	16,200	0.70	2.8	18.0
Ext + 75% R.A. (C, Aged 500°C)	650°C	10,000	8.35	3.3	25.0
Ext + 75% R.A. (C, Aged 500°C)	650°C	7,000	30.00	2.4	18.0
ZAC-2(b)					
As-Ext	400°C	35,000	2.23	3.6	13.0
As-Ext	400°C	30,000	100.00	3.1	26.0
As-Ext	400°C	29,000	300.00	(Test discontinued)	
Ext + 75% R.A. (C, Aged 450°C)	400°C	50,000	13.30	3.3	50.0
Ext + 75% R.A. (C, Aged 450°C)	400°C	47,000	32.0	2.1	38.0
Ext + 75% R.A. (C, Aged 450°C)	650°C	10,000	3.6	3.6	25.8
Ext + 75% R.A. (C, Aged 450°C)	650°C	7,000	10.0	3.9	25.0
Ext + 75% R.A. (C, Aged 450°C)	650°C	5,000	30.0	-	--

Appendix 7

Electrical Conductivity Data

Alloy & Condition	Electrical Condition (% IACS)
ZA-2	
As-Ext	93.6
Ext + 50% R.A. (B, I.A. 300°C)	93.1
Ext + 80% R.A. (B, I.A. 300°C)	92.6
Ext + 90% R.A. (A, I.A. 20°C)	91.2
Ext + 90% R.A. (B, I.A. 300°C)	91.6
Ext + 90% R.A. (C, Aged 450°C)	88.1
ZA-3	
As-Ext	92.0
Ext + 90% R.A. (B, I.A. 300°C)	89.6
ZA-8	
As-Ext	91.2
Ext + 75% R.A. (A, I.A. 20°C)	88.1
Ext + 75% R.A. (B, I.A. 300°C)	88.5
Ext + 75% R.A. (B, I.A. 400°C)	88.9
Ext + 75% R.A. (B, I.A. 500°C)	90.5
Ext + 75% R.A. (B, I.A. 600°C)	88.4
FM-8	
As-Ext	90.6
Ext + 90% R.A. (A, I.A. 20°C)	88.0
Ext + 90% R.A. (F, I.A. 300°C)	86.5
Ext + 90% R.A. (F, I.A. 400°C)	87.6
Ext + 90% R.A. (F, I.A. 500°C)	89.2
Ext + 90% R.A. (C, Aged 500°C)	80.5
ZA-10(a)	
As-Ext	92.0

Alloy & Condition	Electrical Condition (% IACS)
ZA-10(b)	
As-Ext	92.5
ZAC-1	
As-Ext	82.6
Ext + 60% R.A. (B, I.A. 300°C)	80.9
Ext + 90% R.A. (B, I.A. 300°C)	80.1
Ext + 75% R.A. (C, Aged 450°C)	85.0
Ext + 75% R.A. (D, I.A. 500°C)	85.8
ZAC-2(a)	
As-Ext	90.6
Ext + 75% R.A. (C, Aged 400°C)	79.2
Ext + 75% R.A. (C, Aged 450°C)	81.2
Ext + 75% R.A. (C, Aged 500°C)	85.4
ZAC-2(b)	
As-Ext	91.4

BIOGRAPHICAL NOTE

The author was born in Lahore (now Pakistan) in 1944. From 1961 to 1965 he attended the University of Wisconsin (Madison) from where he graduated with a B.Sc. in Metallurgy in 1965. He then attended the University of Michigan (Ann Arbor) where he received an M.Sc. in Metallurgy in 1966. Before returning to graduate studies at M.I.T. in 1968, he worked as a research scientist at the National Physical Laboratory (New Delhi, India).